Analysis of Fluid-Solid Interaction Contributing to Thermal Fatigue in T-Junction Pipes of Nuclear Power Reactors using STAR-CCM+

A Thesis Submitted to the Department of Nuclear Engineering
University of Ghana

By

SOLOMON BELLO
(10586821)
(B.Eng. Electrical Electronics Engineering, 2008)

In Partial Fulfillment of the Requirements for the Award of Master of Philosophy

in

Nuclear Science and Technology

July, 2017

DECLARATION

This thesis is the result of research work undertaken by Solomon Bello in the Department of Nuclear Engineering, University of Ghana, under the supervision of Dr. Seth Kofi Debrah and Dr. Vincent Agbodemegbe.

SOLOMON BELLO

Date:

SETH KOFI DEBRAH, PhD.
(Principal Supervisor)

Date:

VINCENT YAO AGBODEMEGBE, PhD.
(Co-Supervisor)

Date:

ABSTRACT

The focus of this project is on the investigation of phenomena causing degradation of specific zones of piping considering high temperature single-phase mixing in the location of T-Junction in Nuclear power plants. At these locations, thermal stratification and/or turbulent mixing are capable of generating damage-inducing thermal fluctuations of appropriate frequency and amplitude. Fluctuating stresses imposed on this section of the piping system are possible grounds of thermal fatigue failures in piping systems of nuclear power plants resulting into leakages of coolant. These stresses are produced mainly because of the temperature fluctuations that exist in regions where cold and hot streams are vigorously mixed together. A classic scenario for such mixing appears in turbulent flow via a T-junction.

In this study, the purpose will be to perform a 3-D Simulation of fluid-Solid Interaction at a mixing Joint. Two different simulations of thermal mixing in T-junction of a nuclear power plant will be considered and perform thermal analyses of parameters leading to structure degradation. Pipe dimensions and flow parameters such as wall thickness and high operating temperatures difference are modeled and corresponding fluid-solid interaction's effect on wall thickness is investigated by using STAR-CCM+ Code for the simulations, where which fluid-flow calculations will be carried out. Thereafter, the flows inlet temperature will be interchange and another simulation conducted with same parameters so as to determine the effect in a different possible scenario. The flow characteristics and the temperatures in the pipe wall downstream are obtained using this Computational Fluid Dynamics. Simulations result and validation outputs with T-Junction experiment carried out at the FSI Test Facility, University of Stuttgart and

contributions of the various investigated parameters contributing to thermal fatigue were presented.

ACKNOWLEDGEMENT

I give thanks to God Almighty for the privilege of this opportunity at such a time as this and the grace to successfully complete this program in good health. To Him alone is all my praise.

I like to sincerely thank the management of Nigeria Atomic Energy Commission (NAEC) for nominating me for this program, the International Atomic Energy Agency (IAEA) for sponsorship and to CD Adapco, for providing a reduced cost licence for the STAR-CCM+. I feel honored, thank you very much.

My profound gratitude goes to my supervisors; Dr. Seth Kofi Debrah and Dr. Vincent Agbodemgbe both of the Department of Nuclear Engineering for their time spent in guiding me all through the period of this work and for knowledge imparted. Your great inputs made the research a success, I am immensely grateful. Not forgetting Professor E.H.K. Akaho (former DG, GAEC) for fatherly advice and encouragement in ensuring that I remain focus, Professor Danso (former HOD, Nuclear Engineering), Dr. Denis Adortey (International Programme Coordinator), and to everyone at the Department for the cordial relationship that ensue a good working relationship, I appreciate you all.

To my colleagues and friends, thank you for the moral support and time spent together, you made my stay easier and fun with more lessons learnt.

This wouldn't be complete without appreciating my mum for her fervent prayers, ***Mum, ma'aku avo ete'tere***. Finally, to her Royal Majesty, my adorable wife, your unconditional love and perseverance has kept our love union stronger and we are sure souring higher. Your beauty is sure born from within. ***Aya'mee,*** **I LOVE YOU.**

DEDICATION

To my darling wife Daina and beloved son Nethan for subjecting you to my absence during the pursuit of this noble cause.

NOMENCLATURE

D_m	Diameter of main line	[m]
D_b	Diameter of branch line	[m]
V_{branch}	Branch Fluid Velocity	[m/s]
V_{main}	Main Pipe Fluid Velocity	[m/s]
lte	Thermal Equilibrium	[-]
lhe	Hydraulic Equilibrium	[-]
$0.5D_m$	0.5 x Diameter of Main inlet	[m]
$1D_m$	1 x Diameter of Main inlet	[m]
$2D_m$	2 x Diameter of Main inlet	[m]
$3D_m$	3 x Diameter of Main inlet	[m]
$4D_m$	4 x Diameter of Main inlet	[m]
$5D_m$	5 x Diameter of Main inlet	[m]
$6D_m$	6 x Diameter of Main inlet	[m]
$7D_m$	7 x Diameter of Main inlet	[m]
TI	Turbulent Intensity	[-]
T_{main}	Temperature of flow in Main Line	[^oC]
T_{branch}	Temperature of flow in branch line	[^oC]
T^*_{rms}	Root Mean Square Temperature	[-]
Cp	Specific heat capacity	[J/kgK]
K	Thermal conductivity	[W/mK] T

LIST OF GREEK SYMBOLS

$\boldsymbol{\rho}$	Density	[kg/m^3]
μ	Turbulent Viscosity	[Pa.s]
β	Coefficient of Thermal Expansion	[K^{-1}]
ε	Turbulence dissipation	[m^2/s^3]
k	Turbulence Kinetic Energy	[m$^{2/}$s^2]
ω	Specific Dissipation	[s-1]

LIST OF TABLES

LIST OF FIGURES

LIST OF ACRONYMS

BWR	Boiling Water Reactor
CFD	Computational Fluid Mechanics
DES	Direct Eddy Simulation
DNS	Direct Numerical Simulation
EC	European Commission
ECCSs	Emergency Core Cooling Systems
EPRI	Electric Power Research Institute
EVM	Eddy Viscosity Model
FSI	Fluid Solid Interaction
FEM	Finite Element Method
HCF	High Cyclic Fatigue
HCTF	High Cyclic Temperature Fluctuation
HPI	High Pressure Injection
LES	Large Eddy Simulation
LCF	Low Cycle Fatigue
LOCA	loss of coolant
LMFBRs	Liquid metal fast breeder reactor
MPA	Material Testing Institute
MRP	Materials Reliability Project
NESC	Network for Evaluation of Structural Components
NLEVM	Non Linear Eddy Viscosity Model
NPP	Nuclear Power Plant

NRS	Nuclear Reactor Safety
PISO	Pressure Implicit with Split Operator
PIV	Particle Image Velocimetre
PSD	Power spectral densities
PWR	Pressurized Water Reactor
RANS	Reynolds Averaged Navier-Stokes Simulation
Re	Reynolds number
RHR	Residual Heat Removal
RMS	Root Mean Square
RSTM	Reynolds Stress Transport Models
SAS	Scale Adaptive Simulation
SOC	Second Order Closure
THERFAT	THERmal FATigue
TKE	Turbulence Kinetic Energy
WALE	Wall Adaptive Local Eddy Viscosity
3D-CAD	3 Dimensional Computer Aided Design

TABLE OF CONTENTS

CHAPTER ONE

INTRODUCTION

1.0 Background

Thermal fatigue is dilapidation machinery that is induced on the main piping network of a Nuclear Power Plant (NPP). Thus, it is said to be a severe safety issue and is perceived as one of the dominant factors on the ageing and Plant life management of Nuclear Power Plants (NPP's) [1].

The high cycle temperature fluctuations close to piping walls are as a result of mixing of low and high temperature fluid flowing in the pipe. The temperature fluctuation leads to stress fluctuations that acts on the piping structure and is one of the possible sources of thermal fatigue.

Nakamura in 2015 [2] further pointed out that temperature fluctuation caused by fluid mixing at T-junctions generates thermal stress which upon exceeding fatigue limit leads to pipe cracking. Prawoto in 2013 [3] suggested that a material subjected to stresses in a cyclic pattern will suffer from fatigue cracking when the induced stress is lower than the ultimate tensile stress of the material. This implies that the failure of materials occur at a stress level below its nominal strength.

Other possible phenomena that can lead to failure of piping materials are Thermal stratification, Thermal striping, and turbulent mixing.

1.1 Thermal Stratification

The thermally stratified single-phase liquid flows are identified to be the culprit of thermal fatigue by manifesting high amplitude thermal fluctuations by means of two distinct mechanisms. The first, sometimes referred to as global stratification loading, is the result of a typically low frequency time-dependent stratified layer height resulting in high amplitude thermal fluctuations and a variable bending moment in the pipeline. The second mechanism leading to potentially damaging stress reversals in a pipe are instabilities in the stratified layer itself [4]

1.2 Thermal Striping

Temperature fluctuations observed at interfaces between two non-isothermal components or mixing T-junction components in heat transport systems is referred to as thermal stripping [5]. This suggests that heat is readily transferred to the material, thereby subjecting it to a repetitive cycle of temperature fluctuations that could potentially lead to fatigue and crack initiation. Thermal fluctuation becomes prominent and is observed more frequently when the temperature increases and decreases. Such temperature differentials can produce stresses high enough to cause fatigue failure in pipes, thereby limiting its lifespan.

1.3 Turbulent mixing

Turbulence flow is a flow system in fluid dynamics described by chaotic variations in flow velocity and pressure. It is different from laminar flow system, which arises when fluid flows in parallel layers, and there is no disturbance between those layers. [6]

Turbulent mixing is generally experienced when two or more streams meet and exit together via a single conduit driven by extreme kinetic energy in portions of a fluid stream, which overcomes the fluid's viscosity damping effect. Due to this, low viscosity fluids are more susceptible to turbulence, but more problematic in highly viscous fluids. Generally, unsteady vortices appearing in many sizes interact with each other in turbulence flow which subsequently leads to increase in drag due to friction effects. Thus, the energy needed to needed to pump fluid through a pipe, for instance. A dimensionless constant termed the Reynolds number is used to predict the onset of turbulence. This number is the calculation of the stability between kinetic energy and viscous damping in flow of fluid. The interaction within turbulence generates a very complicated situation. As described by Richard Feynman, turbulence has remained the most vital unsolved problem of classical physics. [7]

The above phenomena are all vital safety concern in nuclear plant thermal-hydraulic systems, as it can result to unanticipated failure of the pipe material as shown in figure 1.1

Figure 1.1: Thermal fatigue failure [8]

This kind of failure shown above caused by thermal fatigue occurs outside of the nuclear core area, which naturally consists of piping arrangements such as T-junctions, leakage valves and elbows. Precisely, the mixing T-junctions of the residual heat removal systems in the structure of reactors are perceived to be the most prone to thermal striping [9].

1.4 NPPs Piping Materials and its Fatigue Limits.

Fatigue limit are terms used to describe the property of materials, that is, the amplitude or range of cyclic stress which can be induced to the material without failing [1].

NPPs piping materials are all outside of the core and hence, absorption of neutrons is not the case of concern. The Mechanical properties, corrosion resistance,cost and safety of the material are the vital features in choosing alloys for these applications. Based on these, Stainless steels and alloy steels are major materials used.

Stainless steel is strong, very corrosion resistant and has a wide range of mechanical properties depending on the composition. Chromium has been the most significant

alloying element found in all stainless steel. Some also have substantial amounts of nickel. The quantity of chromium and the presence or absence of nickel determines the type of crystal structure (and therefore, material properties). [10]. Two major types of stainless steel: Martensitic and Austenitic are mostly use:

1.4.1 Martensitic stainless steels

Martensitic stainless steels also known as heat treatable or 400 Series contain variable carbon content with less than 14% Cr carbon content. Martensite is formed from these steels by a rapid cooling down from a high temperature. Martensite is a non-equilibrium crystal structure in steels with a good physical properties, very hard, strong and brittle. The steels are tempered so as to relieve brittleness, enabling a well-controlled putrefaction of some of the Martensite to equilibrium crystal structures. Before heat treatment is applied, Martensitic steels can be welded and are easily fabricated and machined.

1.4.2: Austenitic stainless

Austenitic stainless steels are also referred to as 300 Series or 18-8 stainless, this class of stainless steel contains nickel and chromium, they are non-heat treatable and contain low carbon less than 0.15%. Corrosion resistance are provided by the chromium while nickel performs the stability of the austenite crystal structure that exists only above 700-800°C.

Austenite has certain properties that are not found in the normal room temperature crystal structures of steels. Thus, It is neither non-magnetic nor show a ductile brittle transition temperature. The excellent corrosion resistance of this stainless steel also serves as a factor in its selection. [10] ***(See Appendix I)*** for Mechanical properties and fatigue limit of stainless steels.

Thermal fatigue is a unique case of fatigue produced not by thermal loadings and not outward mechanical loadings thus ensuing in stress-generating thermal expansion and contraction in the material. Figure 1.2 shows thermal fatigue in a 14mm thick A316L stainless steel.

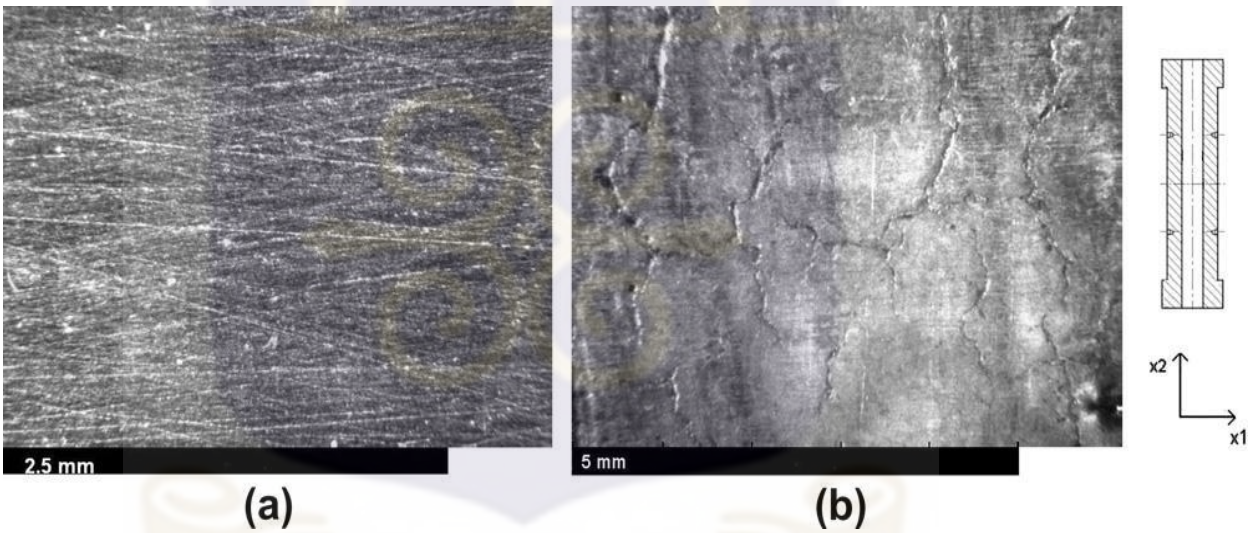

Figure 1.2 A 316L stainless steel sample, 14 mm thick (a)before and (b)after 55,600 quench cycles with ΔT = 275 K, showing a crack network formed due to thermal fatigue [11].

This is a safety linked issue in primary pipework structures of nuclear power plants, Principally, as a result of the life extension of existing reactors and in the design of a next generation reactor, such safety issue need address.

High cycle thermal fatigue and thermal striping was the center of the international community in the 1980‘s and 90‘s owing to cracks that had happened in NPP pressurizer surge lines owed to thermal stratification. Prior to that, in the context of liquid metal and molten salt reactors, the problem was confirmed as an impending risk as early as the mid 1970‘s due to the potentially heat transfer coefficients and high temperature gradients of the moderators [12]. Major investigation on thermal fatigue and thermal striping in T-Junctions of fast reactor as it connected to mechanical codes was covered in the IAEA TECDOC 1381” [13]

1.5 T-Junctions

The 90-degree intersections between pipes of varying sizes in the coolant piping networks of commercial PWR and BWR reactors are referred to as T-junctions (the nomenclature also referred to Mixing-Tee, T-type junction and T-pipe among others.) as shown in figure 1.3

Figure 1.3: Typical T-Junctions that exist in Nuclear Power Plants.

The obvious candidates in NPP's piping system that are susceptible to thermal fatigue are for example T-junctions where fluids with differing temperatures mix together, leaking check valves that produce a blend of fluids with different temperatures downstream, the injection nozzles that could undergo high thermal stresses every time they go into service and the leaking elbow. [14]

T-junctions that are liable to high fluid temperature difference appeared to be situated in the Residual Heat Removal (RHR), High Pressure Injection (HPI), feed water makeup, and Emergency Core Cooling Systems (ECCS) of Light Water Reactors (LWRs) as shown in figure 1.4

Figure 1.4: Mixing Joints in Piping Network

Some T-Junctions can exist openly at the cold or hot leg of the Reactor Cooling Systems (RCS) in Pressurize Water Reactors (PWRs) where slight branch lines bring about the auxiliary systems. T-junction mixing is of interest in the context of thermal fatigue

because it placed in a location where hot and cold streams are regularly meeting, in a supposed joining or confluence

It is for this reason that T-junctions have been the epicentre of High Cyclic Temperature Fluctuation (HCTF) research in the field of nuclear engineering. The prevalent exhibition of such mixing in LWRs is the event of turbulence, hotter stream usually confronting the T-junction in the horizontal pipe encountered a second, normally lower temperature flow coming from the branch line. Given these boundary conditions, wide selections of mixing scenarios are possible.

1.6 Research Problem

Unstable stresses inducing on the piping system is the main cause of thermal fatigue.

This has remained a very prevailing problem and the consequences are usually very grave extending from structural damage to a total shut-down as occurred with the French PWR Civaux in 1998 [15], Japanese PWR Tsuruga-2 in 1999 [15] and Tomari-2 in 2003[15]. Also, 65 leaks, 64 non-through-wall cracks, and 3 structural failure events where recorded of which thermal fatigue is said to be the root cause. [16]

Thus, thermal fatigue is considered to be a severe safety concern and is perceived as one of the greatest influential factors on the ageing and plant life management of NPPs [1]. Understanding these phenomena and the development of evaluation methods is essential to ensure safety and continuous operation of Nuclear Power Systems [17]

This study therefore seeks to investigate these potential phenomena contributing to thermal fatigue of a nuclear power reactor via STAR-CCM+ CFD Simulations using experimental statistics with interest on wall thickness.

1.7 Research Justification

Nuclear thermal hydraulics is a substantial part of reactor safety thus, the properties of materials used in a nuclear reactor fluid transfer is of major importance considering the safety of the NPP operation and possible lifetime extension. It is thus essential to certify the integrity of such material. Since intense heat is produced in a nuclear reactor pressure vessel and this heat must be remove effectively and transfer to another section of the plant for optimum power output, a major component such as the piping system which serves as a medium for such heat removal and coolant transfer must have its integrity maintained.

During the reactor active lifetime, many factors lead to degradation of the inner wall of this pipe which with time leads to wearing out and eventual cracks and final breakages. Major accident such as radioactive contaminated fluid leaking out to the environment and loss of coolant (LOCA) occur. This may lead to severe damages, resulting in partial or in some cases total loss of investment together with loss of life.

Thus the accurate knowledge of parameters and various degree of thermal load of the materials that contribute and subsequently leads to such material's failure is very much necessary and required.

1.8 Research Objective

The aim of this study is focused on performing a 3-D Simulation of fluid-solid interaction at a mixing joint considering two different orientations of fluid inlets temperature in T-junction and perform a thermal analyses of parameters leading to structure degradation.

1.8.1 Specific Objectives

To achieve the aim of this research the following operations was carried out;

- Review an experimental work from the FSI test facility in the University of Stuttgart and perform sensitivity analysis of turbulence models for the experimental results.
- Perform simulation and visualization of fluid-solid interaction with varying temperatures so as to analyse thermal stress using STAR-CCM+ computational tools.
- Investigate the phenomena of cross-flow mixing in main flow and analyse its effects on wall thickness.
- Analyse main parameters leading to degradation of structure at the mixing area of the T-Junction such as the mean temperature fluctuations at various locations along the tube, pressure drop, turbulence kinetic energy, Thermal Conductivity and the Velocity Fields downstream the T-junction.

1.9 Scope of the Study

To Ensure accurate analysis that portrays the experimental result, this study will apply specific models in STAR-CCM+ to perform thermal stress analysis from the investigation of temperature fluctuations, distribution of mean and turbulent flow fields of T-junction geometry modeled with consideration to wall thickness and flow parameters of T-Junction in nuclear reactors.

In this study, two simulations will be carried out both with data from an experimental study with a much higher outlet temperature of 280 ^{0}C to do a comparative analyses with the experimental result so as to validate the the model ussed, This will be accompanied by a second simulation where inlets fluid temperatures are interchange to reflect another possible scenario. In-depth analyses of the thermal loads that will leads to stress generation contributing to thermal fatigue were presented.

STAR-CCM+ will be utilize for this study. The study will comprise investigation of fluid flow interaction and fluid-Solid Interactions in the Mixing Joints (T-Junction).

1.10 Structure of Thesis

This work is presented in five (5) Chapters. The first Chapter (Chapter 1) states the background to the research study. It explains the most suitable Piping Material and its properties, then went on to describes the various types of mixing joints that exist in NPP piping systems and their strategic locations. The problem statement and justification of the research were also presented while outlining the objectives and limitation.

Chapter 2 reviewed some of the cited cross flow mixing and turbulent penetration investigations in T-junctions. The mechanism of thermal fatigue failure and processes of

thermal fatigue analysis were highlighted. Connection between thermal fatigue and thermal mixing with parameters influencing them were also discussed before concluding with the recent technique for predicting thermal fatigue.

Chapter 3 explains the simulations methodology used in the research presenting the most suitable approach to provide the best results that replicates the experimental work carried out. The CFD were presented stating the various eguation employed to solve the flow problem such as the transport equation and the turbulence models. Further in this Chapter, scenario of flow characteristics was simulated for detailed analysis.

Chapter 4 is an extensive analysis of the results as a whole revealing effects of each of the investigated parameters based on which, a conclusion was established and recommendation presented in the last Chapter (Chapter 5).

CHAPTER TWO

LITERATURE REVIEW

2.0 INTRODUCTION

Temperature fluctuations close to the wall boundary are intensely attenuated, resulting to huge error in wall temperature fluctuation estimates when likened to the experiments by Pasutto et al [18] in the standard wall function based on Large Eddy Simulation (LES) in a T-junction. Employing the wall-function based LES approach; Howard and Pasutto (2009) [19] also pointed out the importance of assessing how accurate the wall modelling approaches are. The Westin et al and Nakamura and Oumaya Direct Eddy Simulation (DES) also stated the same question about the precision of near-wall modeling. Based on these observations modeling the near-wall is a very significant and serious facet that affects the precision of any CFD prediction.[20, 21]

The field of research encompassing the problem of thermal fatigue in the location of T-junctions in nuclear power plant (NPP) piping has been active for a number of decades. Therefore, it enjoys a tremendous wealth of published experimental and theoretical results, many of which are referenced in this thesis and consolidated in the remainder of this chapter. Prior to delving into a detailed work I like to convey to readers some of the notable experimental and simulation work done in cross flow mixing and review of the scenario, knowledge and understanding of which can offer an appreciated overview of the history and present state of affairs in the research community.

2.1 Thermal Fatigue Failure Mechanism

Thermal loads and cracking failure mechanism at mixing zone of hot and cold fluids can be disintegrated into elemental processes as indicated in Figure 2.1

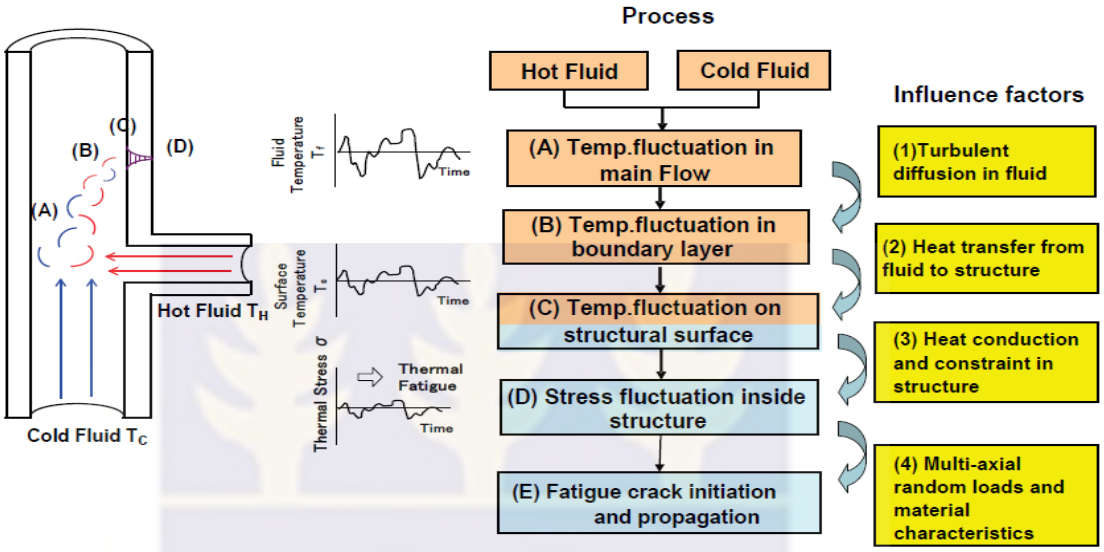

Figure 2.1: Thermal load and cracking mechanism at a mixing zone of hot and cold fluids [21]

Mechanisms at mixing zones of hot and cold fluids shown in the Figure 2.1 as proposed by Nakamura et al [21] can beare described as follows;

A. Vortices generate temperature fluctuations in the main flow

B. Fluctuation propagates to the boundary layer of flow

C. The fluctuations in the layer is transferred to the structure surface

D. Fluctuations on the surface then propagate through the pipe wall by heat conduction and generate thermal stress by the constraint of pipe structure.

E. The recurrence of thermal stress instigates high cycle fatigue cracking.

2.2 Thermal Fatigue/Thermal Mixing

Because of the lack of accurate prediction methods for assessing HCTF induced by non-isothermal streams mixing, various studies attempter to define such methods.

This HCTF phenomena has been widely studied using computations, [22,23,24,25,26] and experimental testing. Reports of some investigations on T-junctions thermal fatigue was reviewed and summarized.

No experiments have accurately replicated the key phenomena leading to thermal cracking at BWR conditions. This holds particularly true for fatigue cracks in control rods. To address this issue, experiments described in Angele et al. 2011 and Tinoco et al. 2009, [27] were conducted in a test section reproducing the annular volume around the stems. Water temperatures were sampled at 50 Hz using 0.13-mm thermocouples. These probes were positioned 1mm from the faces of the inner and outer tubes (that is, in the water domain) at many azimuthal and axial measurement positions. However, these experiments were conducted at low temperatures and pressures, far from those encountered in BWRs.

2.2.1 Cross-Flow Mixing

Cross-flow mixing has been intensively researched in academia and industry, typically at low temperatures. since 1980. In cross-flow mixing (shown in Figure 2.2) velocity ratios are such that turbulent mixing occurs virtually entirely in the mixing pipe of the T-junction.

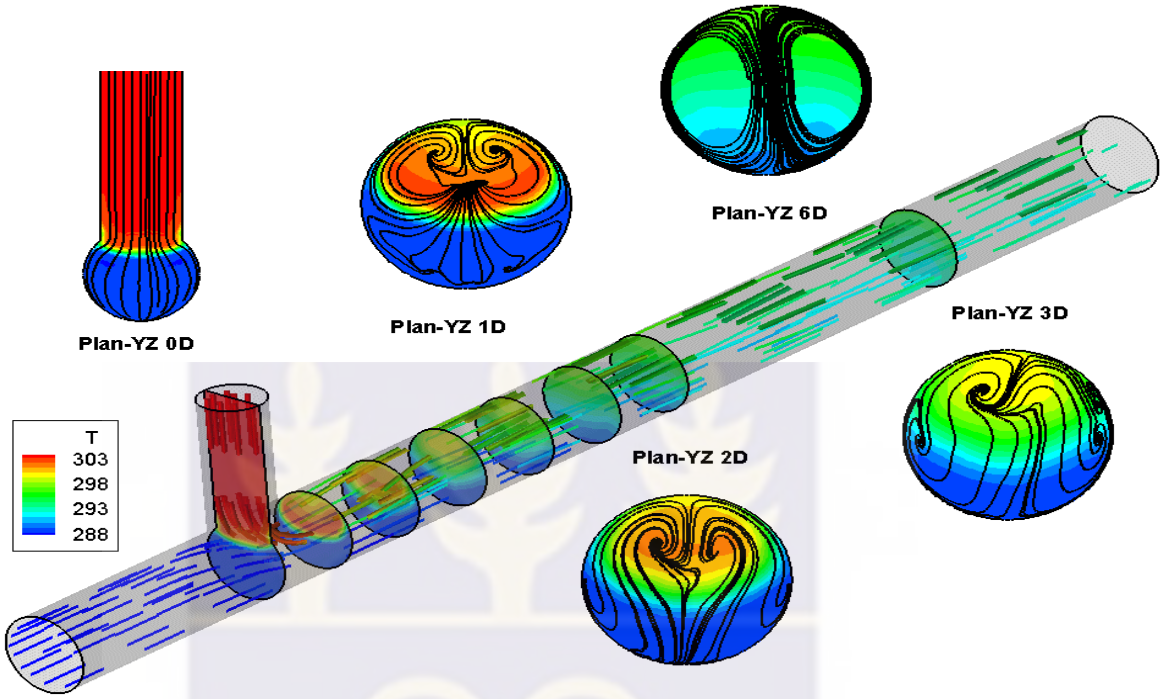

Figure 2.2 Cross-flow mixing in a T-junction.[28].

This category of mixing was outlined more in research publications centered on the momentum ratio of the entering stream, Table 2.2. The branch may be oriented horizontally or vertically.

For clearer understanding of action taking place at the mixing joints of T-Junction during mixing, Figure 2.3 shows the dissected T-junction revealing the main interaction in the area susceptible to Thermal Fatigue

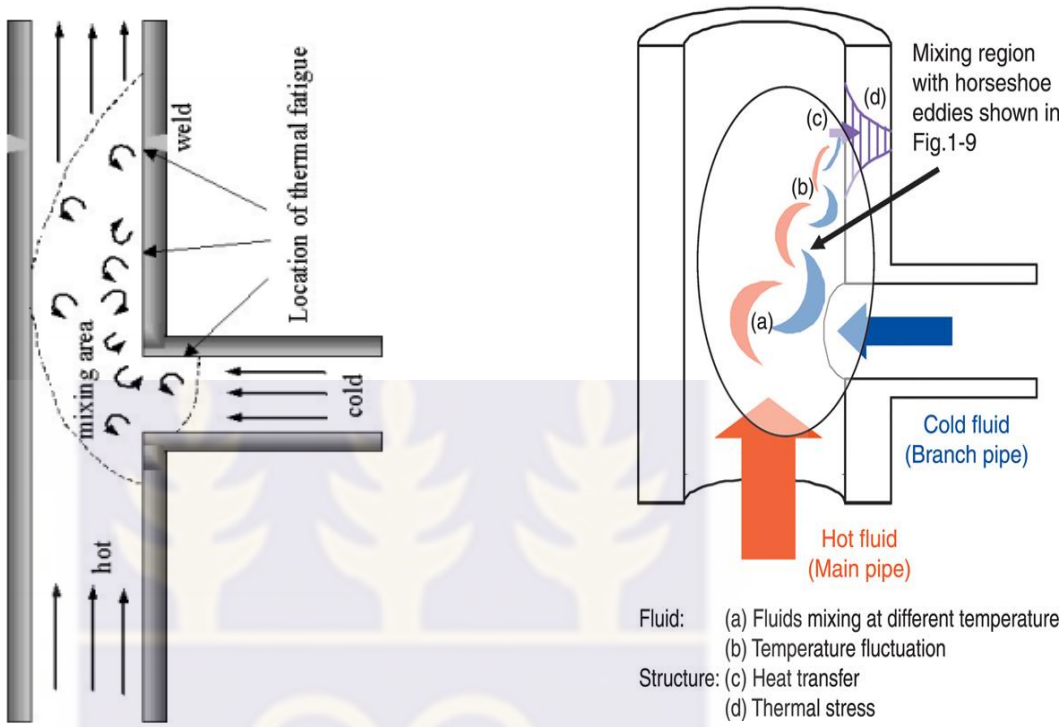

Figure 2.3 Dissected T-junction showing the main interaction in the area susceptible to Thermal Fatigue. [29]

Depending on the inertia of the branch flow, An impinging jet results in branch line flow which impacts the far wall of the T-junction (relative to the branch). The deflecting jet results in mixing more or less in the center of the mixing pipe, while a wall jet does not contain enough inertia to escape far from the wall of the mixing pipe. A sketch of each jet type is presented in Figure 2.4. Each jet type may produce characteristic frequencies downstream of the junction in both temperature and velocity fields as a result of large scale vortices formed due to vortex shedding of the main flow obstructed by the branch flow, including a Karman vortex street or hairpin vortices.

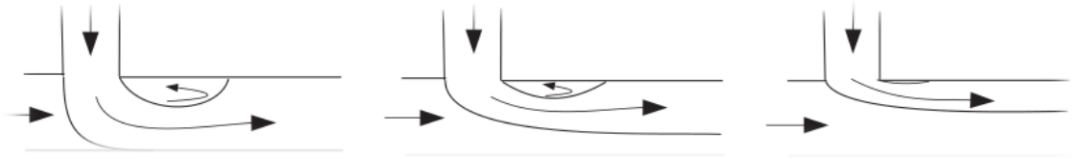

(a) Impinging jet, *(b) Deflecting jet* *(c) Wall jet,*

Figure 2.4 Flow behaviors figure adapted from Sakowit [30].

Table 2.1 Categorization of jet types in cross-flow T-junction mixing based on Kamide [31].

Jet Type	**Momentum Ratio**
Wall jet	Pr > 1.35
Deflecting jet	0.35 < pr < 1.35
Impinging jet	Pr < 0.35

2.2.1.1 Cross-flow Mixing Cases

Summarized below are some major cross flow related simulation of thermal Mixing case reported.

It was recognized by the OECD NEA that thermal fatigue, the result of T-junction mixing represents a nuclear reactor safety problem for which CFD analysis brings real benefits [32]. Computational fluid dynamics have historically played a significant role in research and development related to NPPs, especially in the field of reactor safety [33,34,35]. With the steady decrease in cost of ever greater computing power it has recently become

practical and popular, in previous years, to simulate single phase T-junction mixing with time resolved large eddy simulations (LES). Studies on a wide range of parameters have been simulated including investigations into the effect of T-junction geometry [36,37,38], turbulence or subgrid-scale (SGS) model [39, 40], structure of the mesh [39], time step [41], and conjugate heat transfer [42, 43].

The fatigue failure at Civaux 1 was simulated using the CAST3M code developed by the CEA [14, 44]. Two geometries were simulated, one which includes two additional upstream bends in the branch pipe of the T-junction in question, see Figure 2.5. The thermal-hydraulic and mechanical analysis indicated a concerning reality; it found that in the simulation of the T-junction where only one upstream bend in the branch line was resolved (Figure 2.5 left), there was no substantial thermal or mechanical load discovered at the position of the experienced failure. When the upstream bends were added in the computation grid (Figure 2.5 right), however, the findings change dramatically: Large-scale instability of bigger amplitude was found. This gave rise to pulses which were characterized by the occurrence of substantial thermal fluctuations‖ [14].

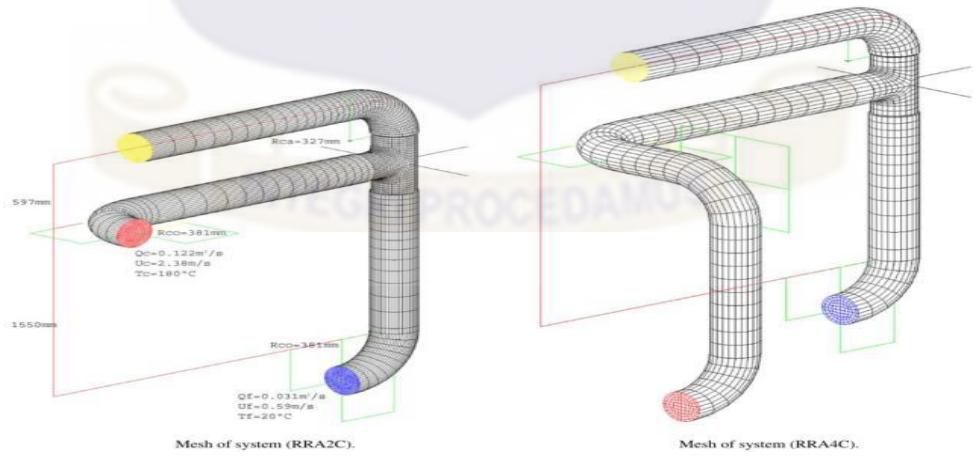

Figure 2.5: Mesh of T-junction from Civaux 1 NPP, figure adapted from Chapuliot[14]

In recent years, the T-junction research community has been focusing primarily on CFD validation of cross flow mixing cases. The OECD NEA CFD benchmarking activity centered on the cross flow T-junction mixing experiments at Vattenfall in Sweden was completed and analyzed [28, 45] as shown in figure 2.6. The results were limited to the fluid dynamic aspects of the flow and did not include conjugate heat transfer with the wall. In terms of the top scoring simulations in the benchmark exercise, LES claimed the top 9 of 29 positions and reproduced the average and RMS value of the flow variables with good accuracy some individual submissions to the benchmark have been independently published [39, 46, 47]. It was observed that the mesh plays significant role, even for highly refined meshes. Just having the largest number of cells does not guarantee strong results. Furthermore, the issue of peaks in the power spectra of the thermocouple signal and PIV data was seen as an important test of the codes‘ ability to reproduce the flow for the purpose of a thermal fatigue analysis, in this regard the results were underwhelming.

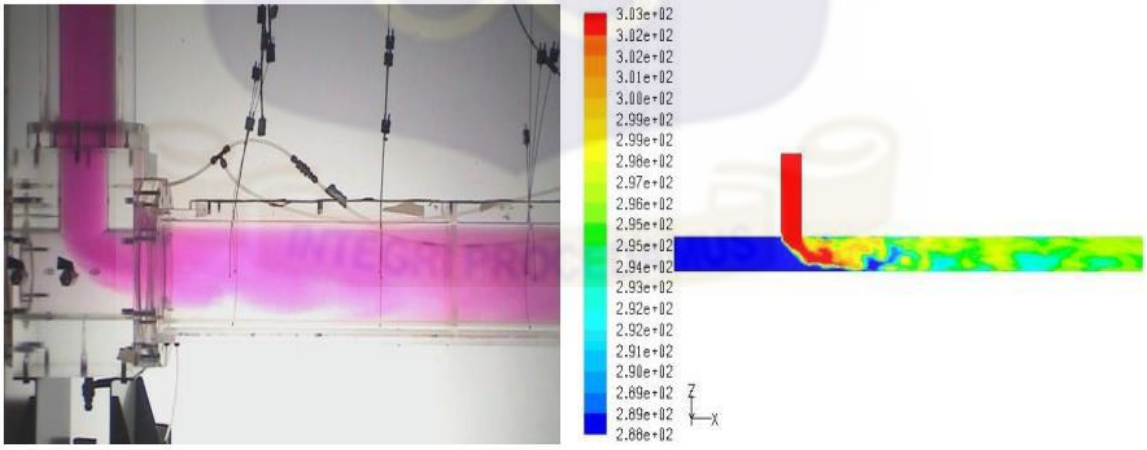

Figure 2.6 Side-by-side comparison of cross-flow T-junction mixing [48]

Another Simulation of cross flow mixing of T-Junction thermal fatigue is the CFD simulation of fluctuating heat transfer at CEA in France by the international consortium working with eleven partners on the Modelling of T-junction Heat transfer (MOTHER) project [49]. Once again cross-flow mixing is the topic of concern. The project is managed by Vattenfall, Sweden, but carried out at the laboratories of CEA in France, the result displayed in figure 2.7. The primary goal of the project, which encompasses both experimental and simulation activities, is the validation of CFD for fluctuating heat transfer. The international community approaches a validated CFD suite for the cross-flow mixing issue, still to be shown, however, is whether such simulations are capable of accurately reproducing turbulent mixing in more complex geometries (such as those including upstream or downstream bends), at large ΔT, or the wide variety of mixing scenarios possible in T-junctions based on velocity ratio (such as turbulent penetration).

Advanced simulation work is already being conducted on reactor condition streams and geometries. These include LES simulations, some with conjugate heat transfer, at the IKE at the University of Stuttgart with direct comparisons to experimental data from their T-junction facility [50,51,52,53].

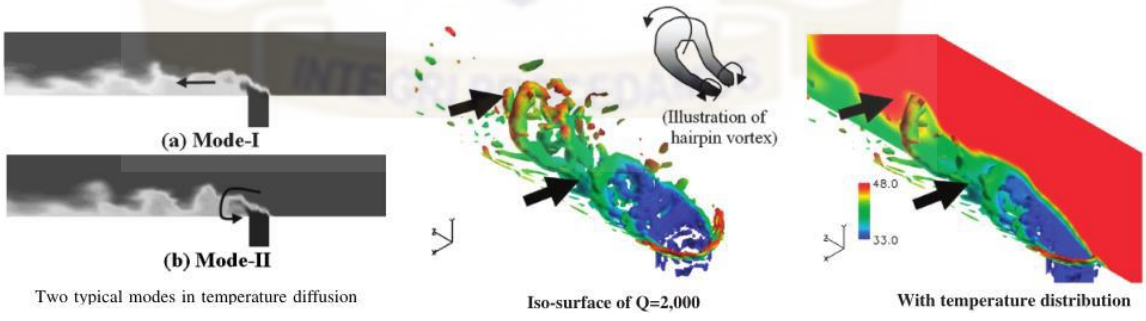

Figure 2.7 LES simulation results showing temperature fluctuation distribution Tanaka (2010) [54].

In Japan, CFD benchmarking efforts pursued in both private and public spheres utilize experimental results from the WATLON facility. Results from that facility were compared with in-house codes of the Japan Nuclear Cycle Development Institute, DINUS-3 and AQUA, as well as the LES-based code MUGTHES of the JAEA [54]. Although early simulations were not successful in reproducing accurately the temperature fluctuations or their spectra, more recent efforts have proven to show good agreement and have thereby advanced the understanding of the flow mechanisms. For example results from the MUGTHES code have indicated that in the case of a wall jet, mutual interaction between the Karman vortex street and so-called hairpin-vortexes are the dominant temperature-fluctuation-inducing phenomena. However, the results remain sensitive to the Smagorinsky constant, with values below some threshold failing to reproduce hairpin vortices [54].

Qian and Kasahara, also in Japan, have for the past five years delved into the mixing downstream of T-junctions as a means of predicting thermal loading. In a series of high quality LES simulations of the WATLON cases, the most recent appearing in the first quarter of 2015, the authors have investigated effects of SGS models, an important step prior to coupling such codes with an FEM simulation. Their work includes detailed studies of the effect of numerical schemes for convective term of the energy equation in the LES SGS turbulence model [25,26,27]. Furthermore, at the Institute of Nuclear Safety System in Japan, a number of simulation results have been published. These include DES and LES sensitivity studies of results testing Smagorinsky constant and temperature diffusion schemes, as well as Finite Element Method (FEM) with boundary conditions based on CFD results [56, 57].

The Fluid-Structure Interaction at thermal Mixing events conducted by X. Schuler et al were carried out with the newly constructed FSI test facility at MPA which permits single-phase flow experiments of water in typical power plant piping diameters (DN40 and DN80) at high temperatures (maximum 280 °C) and pressure (maximum 75 bar). The data base for numerical modeling of thermal flow mixing was from the experimental results which serve as validation by means of thermo-fluid dynamics simulations applying CFD procedures and performed by IKE and also for modeling of thermal and mechanical loads of the piping structure by structural mechanics simulations with FEM methods which are implemented by MPA". The useful measurement techniques and the entire test facility was described, e. g. the novel near-wall LED-induced fluorescence procedure for non-intrusive flow temperature measurements. [29]

A T-Junction Experiment conducted at FSI test facility in University of Stuttgart was run at temperatures up to 256°C (measured by XTM3) and pressures of about 8 MPa. A PID controller was used to regulate the Resistance heating pads along the length of the main line inlet run; this is done with reference thermocouples positioned in between the outer walls of the conduit and the mats. The circulating working fluid was continually being heated along the main pipe at a typical rate of 40 K/hour. Whereas, the cold stream flowing from the branch pipe at room temperature never stops, in such a way that the thermal fluctuation is continuously taking place but reduces downstream at the T-junction.

At high main flow temperatures, there exist great thermal stresses in the facility as a result of stratification in the flow results which injects a bending movement in the pipeline that was not fastened. [58] The studied of this activity has been carried out in

FEM simulations considering the temperature profiles from LES.[29]

Two separate simulations were carried out considering the main flow temperatures of Tm = 120 and 280ºC. First was at 120ºC, before the arrival of cold flow. Then the upstream flow at 280ºC thus the flow then rising considerably in such a way that downstream is no longer horizontal to gravity but slightly sloped. The ability of this phenomenon in posing as an influence on mixing behavior at the T-junction cannot be barred.

The Coupled CFD-FEM strategy to predict thermal fatigue in mixing tees of Nuclear Reactors by Hannink et al was another work reviewed, The demonstration case that is discussed in this research was based on an experimental setup with a temperature difference of 15 °C between the hot stream and the cold stream. The experimental setup was designed to certify the CFD model [58, 59]. However, the temperature difference of 15 °C is not adequate to induce thermal fatigue. In this work, the temperature difference between the cold flow and the hot stream was therefore increased. This leads to stress fluctuations in the pipe wall. For the CFD analysis, an experimentally validated CFD model was used. Coupling between the FEM model and the CFD model was established by a user written interface. It was demonstrated that temperature data is transferred properly between both models.

Based on the stresses calculated in FEM, fatigue assessment was carried out according to Pressure Vessel Code and ASME Boiler [60].

The key issue connected with the life management and extension of nuclear power plants is High-cycle thermal fatigue rising from turbulent mixing of non-isothermal flows. The induced thermal loads and damage are not fully understood yet.

With the aim of acquiring extensive data sets for the validation of codes modeling

thermal mixing at reactor conditions, thermocouples recorded temperature time series at the inner wall of a vertical annular volume where turbulent mixing occurred in the Experimental Analysis of Thermal Mixing at Reactor Conditions by Mattia Bergagio, 2016. There, a stream at either 333K or 423K flowed upwards and mixed with two streams at 549K. Pressure was set at 72 × 105 Pa.

The annular volume was produced between two coaxial stainless-steel tubes. The thermocouples could only cover shield limited areas of the mixing region, thus the inner tube to which they were soldered was raised, lowered, and rotated around its axis, to extend the measurement region both axially and azimuthally.

Trends, which appeared from the variation of the experimental boundary conditions were deducted from the inner-surface temperature time series collected. An estimator evaluating intensity and inhomogeneity of the mixing process in the annulus was also computed. In addition, a frequency analysis of the de-trended inner-surface temperature time series was performed. In the cases examined, frequencies between 0.03 Hz and 0.10 Hz were noticed in the sub-region where mixing inhomogeneity peaked.

The uncertainty affecting such measurements was then estimated.

Furthermore, an initial assessment of the radial heat flux at the inner surface was conducted.

Between the thermal fatigue valuation methods the one-dimensional (1D) approach, also referred to as through wall approach was found, where accounts of fluid temperature are expected at a point next to the pipe boundary.

Thermal, mechanical and fatigue analyses are conducted for the tube wall supposing that the distribution of tube wall temperatures only differs along the tube wall thickness. In

this way, safe life prediction for the specific component is attempted. In this paper, the 1D approach was expanded to two-dimensional (2D), in view of a field with spatially and temporally fluctuating temperatures in the flow near the tube wall. The heat transfer equations are resolved using finite difference method. Results from 1D and 2D methods are compared.

The 2D results show appreciable temperature gradients in the axial trend which can exceed 90% of the temperature gradients in the radial (wall thickness) direction. The thermal fatigue load is proportional to the temperature gradients, or in other words, related to the existing temperature differences within the material. The temperature differences fluctuations in the material during the analysis generate changes in the stresses and strains fields which, in fact, develop the fatigue phenomena.

Introducing the fluid axial temperature dependence creates temperature differences in axial dimension which will contribute to fatigue in the same measure as radial temperature differences do. It was noticed; high values tend to decrease the material temperature fluctuations. The axial temperature differences generate axial thermal strains which will contribute to the creation of thermal stresses.

High values of the spatial fluid frequency then appear to be such conditions for which the onset of a new dimension to the thermal fatigue issues may be of concern due to obvious fatigue significance. Further work remains to be done in order to validate if such conditions are physically meaningful, i.e. if there are fluid-mixing flow conditions that can generate them.

Large Eddy simulations for thermal fatigue predictions in a T-Junction: Wall-function or wall-resolve based les? by Jayaraju et al were carried out in T-junction to investigate the

viability of wall-functions in precisely envisaging the thermal fluctuations that is being induced on the pipe walls. The WALE sub-grid-scale model engaged in the LES solver is validated by carrying out OECD/NEA T-Junction benchmark test-case. Reynolds number scaling is performed so as to reduce the computational costs, while still preserving the important flow features. The equivalent RMS components were constantly under-estimated close to the wall boundaries while the wall-function based simulation showed good agreement with the wall-resolved tactic for the bulk velocity and temperature fields. The same was true for the heat-flux RMS fluctuations. [61]

It is thus resolved that any comparison in the bulk contours is not an assurance for any kind of resemblance in the wall heat flux behavior.

Generally, there is clear confirmation in both the experiments and CFD assumptions for both mean and RMS quantities. It was concluded that based on the results that the extrapolative abilities of the LES solver of STAR-CCM+ is very good.

The applied numeric of thermo-fluid dynamic calculations of thermal mixing flows in Thermo-Fluid Dynamics – CFD simulations by IKE are based on large-eddy simulation (LES) which solves large scale turbulence directly, and therefore no special turbulence model is required. The main advantages of LES are that the general turbulence structure of thermal mixing flows can be mapped with an adequate approximation and small scale turbulence below the grid filter width has not be resolved because it is assumed to be nearly isotropic, and therefore simple algebraic functions, e. g. for the mixing length, can be used. Furthermore, in context of structural mechanics analysis of thermal fatigue the heat transfer interaction between the thermal mixing flow and the solid is of essential importance and hence has to be especially regarded in thermo-fluid dynamics simulations.

2.2.2 Turbulent Penetration

Another type of mixing scenario was reviewed so as to explain the differences, turbulent penetration in T-junctions is a mixing scenario which has also contributed to component failure due to thermal fatigue in commercial NPPs [62]. The phenomena, resulting from a T-junction branch line with zero velocity (a _dead leg‘) or weak in-flow or out-flow (e.g. in a leaking valve scenario), is a multifaceted one once described in a publication by a researcher at EdF as, ―a complex and somewhat amazing hydraulic behavior‖ [63]. Turbulent stream from the main pipe interacts with a laminar flow in the branch line resulting numerous mixing frequencies and large amplitude scalar fluctuations localized at different axial and circumferential positions depending on a number of factors. These factors include, but are not limited to, velocity ratio between the branch stream and main flow, main flow Reynolds number, junction geometry, and fluid densities. Turbulent

penetration may be the result of a leaking value from a branch line in. Flow structures which play a major role in cross-flow mixing, such as Karman vortex streets or hairpin vortices are not present in the case of turbulent penetration.

Due to the importance of the turbulent isothermal and thermal mixing phenomena for turbulent, thermal mixing, thermal striping and thermal fatigue problems in nuclear power plant, investigations was carried out in two different test case circumstances in the Simulation of turbulent and thermal mixing in T-junctions using URANS and scale-resolving turbulence models in ANSYS CFX" [57**]**. First scenario as proposes by ETHZ, Prasser et el [64] consist of turbulent mixing of two equal flows temperature in a T-junction of 5mm pipes in the horizontal plane and thereby eliminating any resistance effects. The second test case is based on the Vattenfall test facility with the temperature difference of 15K mixes in a T-junction in vertical plane, instigating thermal striping phenomena. While the turbulent mixing in the ETHZ test case could be replicated in good quantitative agreement with data, the outcomes of LES-like simulations were not yet fully substantial in terms of the attained accuracy in evaluation to the large-scale turbulence structure growth was well reproduced in the simulations.

A Turbulent penetration at LKE T-junction facility by Zboray [64] was performed at the T-junction facility of Walker (2009) [1] which was enhanced for cross-flow mixing tests at velocity ratios close to unity. The boundary conditions of these tests, in terms of turbulent penetration, were therefore limited to the onset of turbulent penetration. A new T-junction Test facility shown in figure 2.8 was designed and instrumented for the case of weak branch in-flow with a high degree of geometrical flexibility, allowing for various branch diameters, sensor positioning, and T-junction geometry.

The facility operates under adiabatic conditions at atmospheric pressure. It is comprised of an acrylic glass 90 degree T-junction and inlet run sections fed by flexible PVC hose and PVC-U piping. Each branch comprises a honeycomb section at the start of the acrylic inlet sections for flow conditioning. Two high-density polyethylene feed tanks of 750 l volume each separately supply the junction with tap water (approx. 150 µS/cm) in the main pipe and deionized water (approx. 3 µS/cm) in the branch line such that electoconductive measurement techniques, specifically WMSs, can distinguish mixing at the T-junction. A waste tank of 1000 l volume acts as a sump for the working fluid.

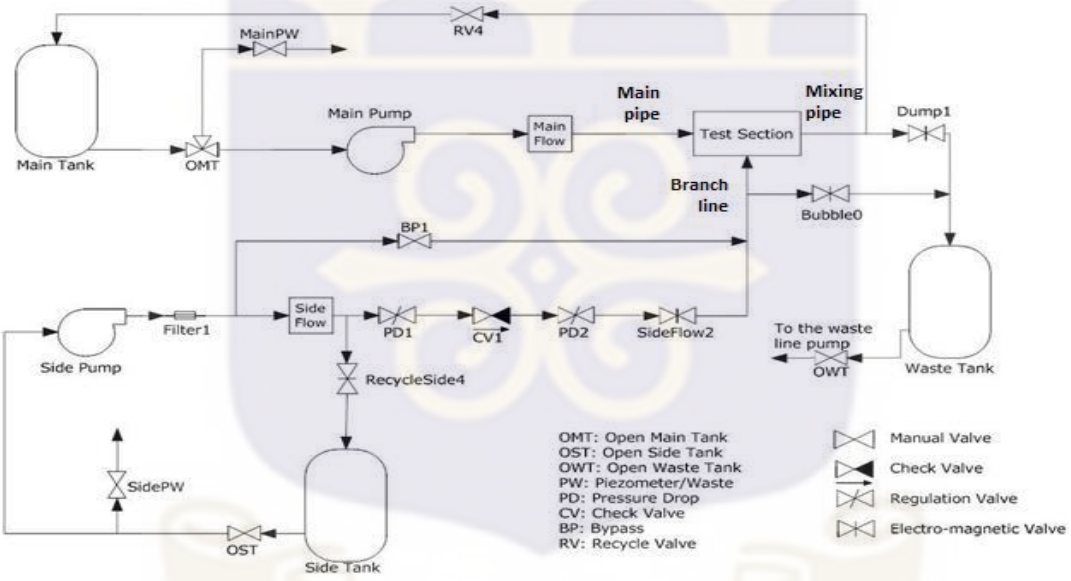

Figure 2.8: LKE T-junction Experimental Facility

The experimental procedure is essentially steady for all measurements at the facility. The experiment starts when the SideFlow2 valve is opened (RecycleSide4 is then closed), bringing deionized water into the branch pipe.17 The branch line flow rate is kept high so as to completely flush tap water from the auxiliary piping and the branch itself. The main

flow is kept low during this flushing procedure. At this point the PID controller is activated and seeks the set point flow rate in the vertical branch. As the branch flow rate reduces to the set point, the main flow PID controller is also activated and the velocity in the horizontal main pipe increases to its respective set point. As the flow rates approach the values for the given experiment, turbulent penetration begins.

Most recently, simulations have been performed in search of long-period fluid temperature fluctuations (St < 0.2) [65].

A systematic exploration of the performance of turbulent penetration under different flow conditions and geometries is crucial in adding to the limited experimental data and essentially nonexistent simulation results available with regards to mixing in T-junctions at high velocity ratios.

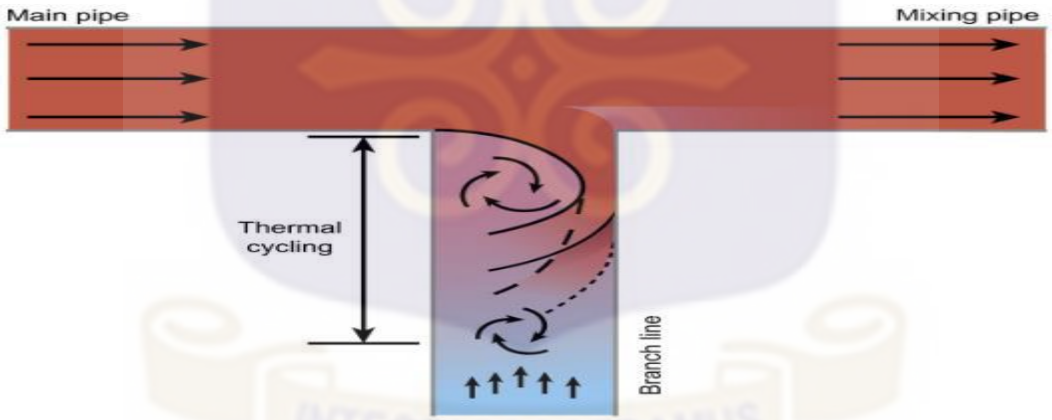

Figure 2.9: Schematic of the onset of turbulent penetration in a T-junction with equal branch diameters.[62]

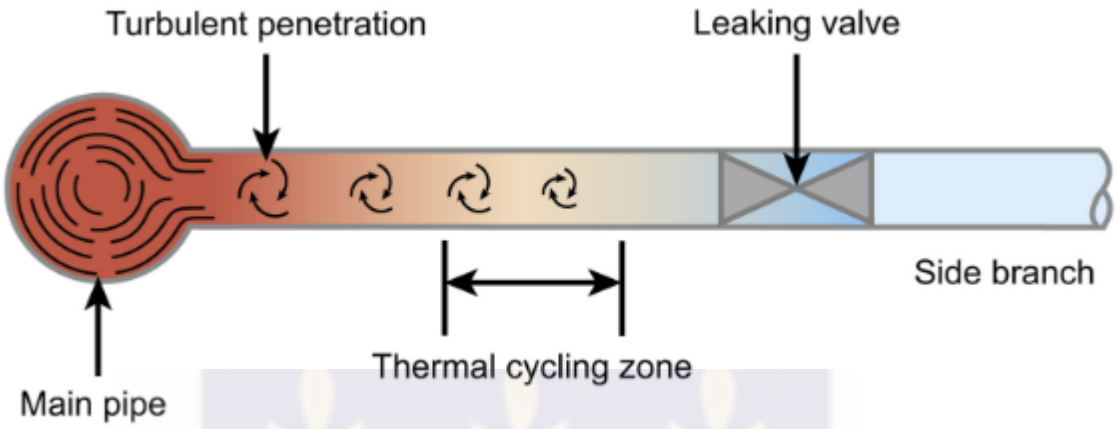

Figure 2.10: Turbulent penetration in a T-junction with unequal branch diameters. IAEA TECDOC 1361 [62].

2.2.3 Turbulent penetration and how it differs from cross-flow mixing

Turbulent penetration in T-junctions is a flow configuration categorically different than cross-flow mixing. Although, in the event of turbulent penetration, mixing between branch and main flows continues in the mixing channel downward of the T-junction, its character is unlike mixing at the same location at velocity ratios near unity (i.e. cross-flow mixing). To varying degrees on a spectrum between the dead-leg case and that of velocity ratios near the inception of turbulent penetration, the turbulent penetration in the vertical branch line makes flow at the downstream of the T-junction _ pre-mixed.

The consequence being that in the mixing pipe, large amplitude scalar fluctuations are unlikely, if not impossible, and hence the region of interest will no longer be the mixing pipe with regards to thermal fatigue.

Simultaneous measurements by WMSs in the branch line and mixing pipe at the same non-dimensional positions were analyzed. Figure 2.11 (left) shows comparison between

the scalar fluctuation contour in the branch line and mixing pipe, both one diameter from the T-junction at a velocity ratio of 33.3 where the main tap water run is normalized to 1 and the deionized branch flow to 0 (sharp-edged T-junction, *Dm* = 50 mm *Db* = 50 mm).

Maximum scalar fluctuations existing in the mixing pipe at this position are approximately half of that found at an equal distance into the branch line. A normalized PSD from two near-wall positions in both the branch line and mixing pipe are plotted in Figure 2.11 (right).

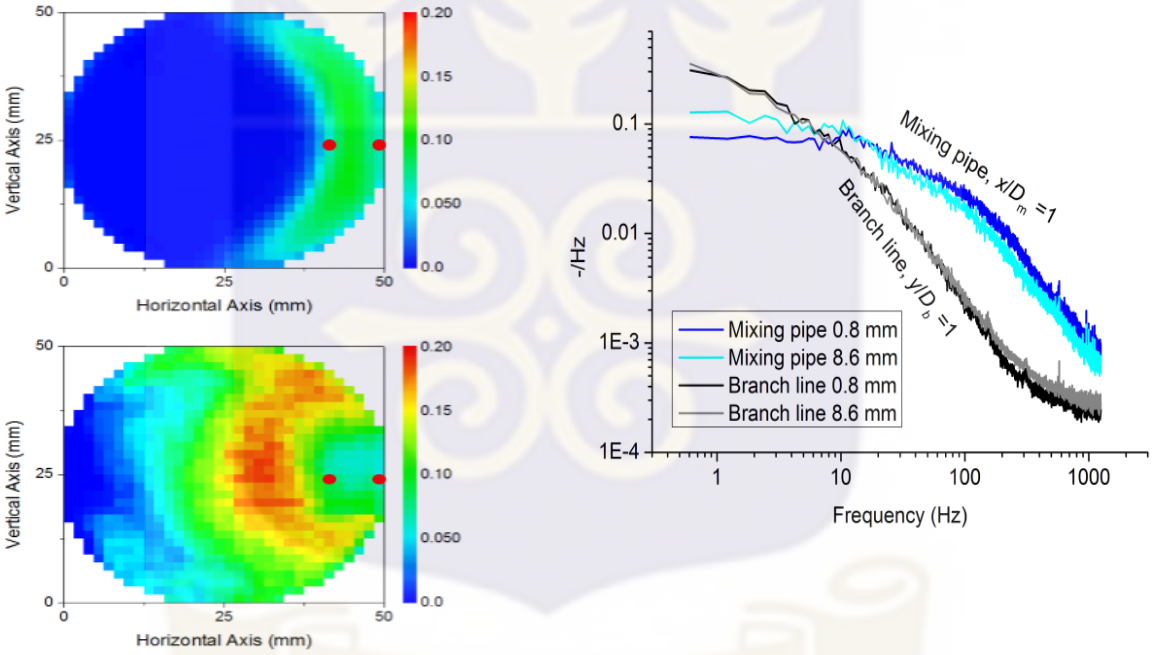

Figure 2.11 (left) RMS of the scalar in the mixing pipe at x = 1.0Dm (top) and the branch line at y = 1.0Db (bottom). (Right) PSD of scalar fluctuations near the wall (mm values represent distance from the wall) indicated by red dots in contours on left, Ur = 33.3

Scalar fluctuations in the mixing pipe at x =1.0Dm are categorized by high frequencies and low amplitudes; while in the branch line, damped high frequencies result in low frequencies (< 10 Hz) contributing far more to the scalar RMS, relative to the same location in the mixing branch.

Turbulent penetration results in the flow exiting the T-junction through the mixing pipe in what could be described, in the terminology of cross-flow T-junction mixing, as a weak wall jet. Upon exiting the branch line the fluid is accelerated down the mixing pipe in a concentrated, crescent shaped near-wall region, seen in Figure 2.11 (left, top), and likely dictated by the turbulent velocity contour in the main flow. Fluctuations are notable for their high frequency and low amplitude nature visible already before a more detailed spectral analysis. Meanwhile, in the branch, pulsations of main flow (i.e. turbulent penetration), some with amplitudes of 50% of the scalar, are visible on a much larger characteristic time scale.

2.3 Thermal loading

Turbulent mixing of waters with difference in temperature is depicted by fast and extremely uneven fluid motions. These fluctuations will surge the energy transfer rate to the solid as load. The fluid motion in turbulence occurs on several length and is associated with random fluctuations thus usually portrays the fluid movement very difficult to define in detail. The small volume of liquid in irregular motion which occurs for a short time before losing its characteristics is termed Eddies. The temperature fluctuations close to the pipe surface can be of the order of several HZ.

2.3.1 Thermal Fatigue

Researchers have been working for decades with regards to understanding and resolving fatigue problems related to several spheres of thermal hydraulics and reactor management and thus, the subject thermal fatigue has become of great interest for several years. Thermal fatigue is a phenomenon that occurs frequently in thermal hydraulics systems such as reheat systems, turbines, emergency core cooling systems (ECCS) of nuclear power plants (NPP) and as such should to be studied to comprehend the mechanisms behind the phenomenon. The understanding of these phenomena and the development of evaluation methods of thermal fatigue are imperative from the perspective of design, operation and safety of the plants. It is a significant factor in ageing management of nuclear power plant [66]. Thermal fatigue mechanisms need to be monitored to ensure safety and constant operation of nuclear power systems [67]. Roos et al., [68] considered thermal fatigue as an essential safety issue in primary piping system of nuclear power plants. The degradation mechanism of thermal fatigue is induced by temperature fluctuations that result from mixing hot and cold flows. Ayhan and Sökmen [24] suggested that these fluctuations occur when a fluid meeting at different temperatures arrives at the pipe wall before reaching thermal equilibrium.

2.3.2 Parameters Influencing Thermal Fatigue

Thermal fatigue is reliant on both mean and turbulent flow parameters such as; temperature, velocity, turbulent kinetic energy and turbulent dissipation rate.

Flow velocity is a vector field quantity used to express the motion of continuum. Mean vertical and horizontal velocity distributions give information about hydraulic conditions

of flow. Ayhan & Sökmen [34] stated that heat transfer area increases as the velocity of branch inlet flow increase due to rapid mixing. Thermal mixing therefore takes place at a relatively short distance after meeting of streams on increasing velocity. Hence after the T-Junction, the fully developed condition is disturbed.

Stress and stress intensity factors are analysed under fluid temperature fluctuations. The magnitude of temperature fluctuations gives information about the extent of thermal load and subsequently, the thermal fatigue related failure [34]

In turbulent flow, the mean kinetic energy linked with eddies is known as Turbulent kinetic energy (TKE). Methods of resolving TKE is reliant on the turbulence model used. TKE is a fundamental flow property required for fluid turbulence modeling.

2.3.3 Temperature Variation Induced Fatigue

Possible phenomena that can occur as a result of temperature fluctuations include; thermal stripping, thermal stratification, turbulent mixing, and thermal fatigue. Temperature fluctuations observed at interfaces between two non-isothermal components or mixing T-junction components in heat transport systems is referred to as thermal stripping [5]. This suggests that heat is readily transferred to the material, thereby subjecting it to a repetitive cycle of temperature fluctuations that could potentially lead to fatigue and crack initiation. Thermal fluctuation becomes prominent and is observed more frequently when the temperature increases and decreases. Such temperature differentials can produce stresses high enough to cause fatigue failure in pipes, thereby limiting its lifespan. Since materials function usefully at different temperatures, different materials have different fatigue limit. Tensile and compressive stress may be triggered by

limiting thermal expansion. This situation occurs in complex piping systems such as welded joints, elbows, and T-junctions which are commonly found in nuclear power plant.

2.3.4 Computational Tools and Recent techniques for Thermal Hydraulic Analyses

CFD has appeared to be an active tool used to compute flow in a module and thereby predict thermal load by studying the thermal fatigue phenomena. Several alternative modelling strategies have been developed. Early Researchers in the field, Westin et al.[20] and Manera et al.[69] were emphatic about the fact that, the most extensively used Reynolds Averaged Navier-Stokes (RANS) procedure reveals challenges in predicting precisely turbulent mixing in T-junctions.

Recent studies have moved to an intermediate approach and more advanced numerical tools like the Detached Eddy Simulation (DES) and Large Eddy Simulation (LES). Majority of the researches which involve LES simulations, wall functions have been used. LES aims at resolving all large scales in the flow domain. Only small (dissipative) structures are modelled by the sub-grid scales eddy viscosity. One merit of LES is that only a small part of the flow is modelled, whereas greatest part of the turbulence is the outcome of the numerical solution of the unsteady-state, three dimensional Navier-Stokes equations. LES has a drawback in that its computationally more costly than the RANS approach.

To define thermal load in mixing T-junction, it is thus important to use LES since the RANS method does not offer sufficient detailed information. Though, thermal

stratification glitches in elbows can still be assessed accurately with RANS. For accuracy in any CFD analysis of thermal fatigue, it is imperative that the thermal fluctuations on the walls of the mixing joints be correctly predicted.

The status of LES CFD for Nuclear Reactor Safety (NRS) Analysis has been reviewed by Kerntechnik (2011) where it has been stated that, provided best practices are observed, LES predicts bulk thermal mixing with good accuracy. Jayaraju et al., [8] performed LES on a T-Junction to examine the possibility of wall functions to accurately predict thermal fluctuations induced on pipe walls. The model used in the LES solver was validated by the OECD/NEA T-junction benchmark test case. There was a good agreement of wall function centered simulation with the wall resolved approach for the bulk temperature and velocity field. Equivalent root mean square (RMS) components were constantly under estimated close to the wall boundaries. LES with very fine meshes to capture turbulent eddies near the wall or direct numerical simulation may show good result however their calculation time and power are unrealistic.

Temperature fluctuations are imposed as thermal loads in the FEM-model of the structure. The coupled CFD-FEM presented by Hannink et al., [70] was established by user written interface between FLUENT and ANSYS to determine the stresses induced in the pipe. Temperatures from the CFD simulation was used as thermal loads in the FEM analysis using the FEM program ANSYS. The stress calculation was computed for the portion of the pipe in the mixing section which is important for the fatigue analysis. The stress calculation was performed with a time step of 0.020 s and for a total simulation time of 2.5 s. The temperature fluctuation in the structure for the simulation period varied between -11.8 °C and 11.4 °C. The stress intensity distribution was similar to that of the

temperature since they are both connected by a linear relation. Based on the stresses determined in FEM, a fatigue analysis was carried out which was referenced to ASME Boiler and Pressure Vessel Code [60]. The need to study thermal fatigue assessment of piping system's T-Junction connections using CFD models was pointed out [71]. An example is Fluid Structure Interaction (FSI), which was used in Hannink et al analysis. Though common fatigue related problems are understood and organized by plant instrumentation at fatigue predisposed locations, incidents that specify that certain T-Junction piping system connections are susceptible to temperature mixing effects are not well detected by common thermocouple instrumentations. Hence the need to use numerical analysis and algorithms in computing problems associated with fluid flow in a component and further predicting the thermal load.

Numerical simulations of thermal fatigue in a mixing T-junctions have been studied, where the Phoenix Tee configuration was evaluated through thermal hydraulic simulations using both RANS and LES methodology. [72]

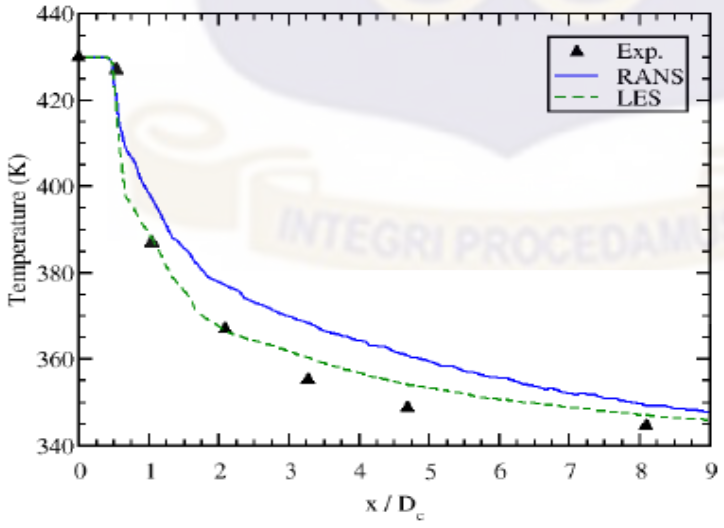

Figure 2.12: Mean temperature at wall past the hot injection pipe [72]

The simulation was performed using Fluent coupled between liquid and solid heat equation on mesh with 4.8 million tetrahedral prism cells. Flow rate of 800 kgs-1 and Reynolds number (Re) of 6x106 was used for the main cold sodium inlets of 610 K temperature and flow rate of 7 kgs-1 and Re of 5x105 was used for the second hot branch inlet at temperature of 700 K. The behavior of the hot jet within the main branch was well captured by both RANS and LES simulations. The mean temperature profiles at the wall past the hot injection pipe was well represented by the calculations with a very close agreement with the LES calculations as shown in Figure 2.12:

It was concluded that, the simulation calculations was able to correctly reproduce the main features of the turbulent mixing of two flows in a Tee junction of the Phoenix reactor and it demonstrates the ability of turbulent streams simulations to give valuable information for the evaluation of the thermal fatigue risk.

Thermal stress in mixing junction was reviewed using Fluid Structure Interaction (FSI) [47]. The study was carried out using FSI analysis and the temperature distribution at different zone determined using thermal hydraulic system analysis. Two bodies were created for the analysis; a solid body that is the pipe created in modeling software and a second body which is the fluid flowing through the pipe. The meshed model was transferred into CFD software and the inlet and velocity constraint were imposed and the model was then solved for the transient analysis. Based on temperature transient in the piping walls obtained from the CFD computations, the thermal stress was calculated. The pipe geometry model created is transferred into the structural analysis. The pipe was meshed using structural meshing and the transfer of the thermal results from the CFD computation was done through FSI analysis mapping of nodes and elements. The results

was directly imported and imposed on the pipe body. The corresponding stress analysis and the response features of the T-junction exposed to the mixing effects investigated were found maximum at the joint contact.

The effect of branch pipe diameter in thermal mixing of a T-junction pipe has also been studied. [24]. They studied the need to characterize temperature fluctuation in order to estimate the lifetime of pipe material. Several experiments and computational study conducted showed the most likely distance that thermal fatigue can occur in the two main pipe diameters after mixing downstream after mixing. The study described the effects of branch pipe when the main pipe was constant in the geometry. Calculations were performed using different pipe diameters with the same flow rate conditions. The hot branch hydraulic diameter was changed, whilst the mass flow rate and the cold branch hydraulic diameter was held constant. Analysis was done to determine the effects of these conditions on the frequency and magnitude of the temperature fluctuations. Comparative analysis was done for all cases. Detailed analysis was performed based on a previous work which showed the most probable distance of the two main diameters of 20 m at downstream after the junction where thermal fatigue occurs. LES turbulence model was chosen for turbulence calculation with filtered Navier-Stokes equation being used to solve the turbulence in Large Eddy Simulation (LES) as unsteady turbulent approach.

2.4 Damage cases in Nuclear Power Plants

Mixing of coolant causing high cycle thermal fatigue has been liable for thirteen (40) through-wall cracks in the main track of commercial PWRs in NPPs from 1982 to 1998, as displayed in Figure 2.13.

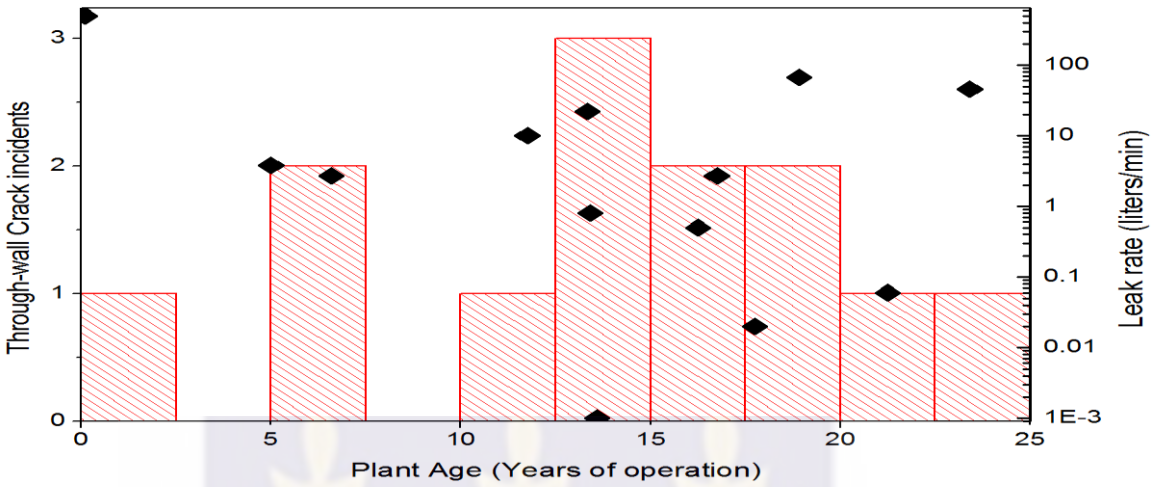

Figure 2.13: "Through-wall crack incidents (red bars), leak rates (black diamonds) vs. NPP age between 1982 and 1998 as compiled by the IAEA in TECDOC 1361 [72]".

Thermal fatigue was proposed from historic data not to be purely a lifetime management problem, with several accidents happening early in the 30, 40 or 60 years of envisioned plant lifetime. Dahlberg [73] in the final report of the European Commission Network for Evaluating Structural Components thermal fatigue project concludes.

In several instances thermal fatigue damage has advanced within little times, even less than a year. Therefore the popular grouping of thermal fatigue as an ageing procedure suggesting that its probability intensify gradually with time is conceivably misrepresented.

Only in 1998 accident at the recently established Civaux 1 NPP8, where a 180 mm long through-wall crack in EN 1.4307 (ANSI 304L) SS of a T-junction in the RHRS resulted in major leakage of coolant at the rate of 500 l/min, that attention was drawn to High Circlic Temperature Flunctuation due to turbulent mixing downstream of T-junctions by researchers and assessment procedure determined [4, 11, 72]. In the instance of the

Civaux accident (a _new phenomena‘ at the time) an inadequate knowledge of positions in the pipe system where turbulent mixing could portray large amplitude temperature fluctuations at critical frequencies meant that the piping network was not of a safe design for the particular operating conditions [62]”.

A widespread technique for determining critical frequencies for hollow cylinders specifies that the most damaging high cycle fluctuation frequencies for typical NPP stainless steels is around 0.1 to 10 Hz [73,74,75] compare to low cycle fatigue (LCF) which is nowadays acceptably understood and sufficiently controllable by instrumentation and monitoring systems, the HCF has significant investigation demands with respect to reliable and accurate information about frequencies and amplitude of temperature fluctuations in order to understand and describe adequately its mechanism which is implicitly needed for reasonable predictions of HCF for lifetime estimations of component parts.

Though, high cycle temperature fluctuations related with turbulent mixing cannot be effectively detected by common thermocouple instrumentations but for a proper evaluation of thermal fatigue, numerical simulations are necessary.

2.5 Estimators of thermal mixing

When intensity, inhomogeneity, and efficiency of mixing of non-isothermal water streams have to be inferred from large datasets, regardless of whether they contain experimental or simulation data, deriving significant indicators and developing algorithms to correctly interpret such data seem to be intricate tasks. As an example, in

Angele *et al.* [44] these datasets resulted from experiments, Reynolds-Averaged Navier-Stokes (U-RANS) and Scale-Adaptive Simulations (SAS) of non-isothermal water streams mixing in an annulus. The temperatures in these datasets were normalized.

Their average and RMS values were also determined, at many axial and azimuthal measurement positions. Power spectral densities (PSD) of experimental and SAS temperatures were then derived, to demonstrate that the most prominent spectral components emerge at low frequencies ($f < 0.5$ Hz), typical of thermal fatigue.

The mixing quality in a T-junction was assessed by three estimators, all found from the passive scalar modeling the mixing process.[30] First, a uniformity index *UI* was calculated as the weighted difference between the time-averaged concentration of the passive scalar and its mean value over a cross section of the computational domain. The RMS value of passive scalar was then computed, to account for the variation of this scalar with time. After that, the integral time scale of the fluctuations of the passive scalar was evaluated, to estimate the longest time over which they are correlated.

An estimator referred to as composite mixing indicator was calculated as the integral mean value in time of the cell-average dimensionless fluid temperature over its standard deviation; that is, over its level of homogenization inside the mixer[47]. The higher the composite mixing indicator, the better the thermal mixing. A quantity termed "temperature scalar dissipation indicator" was then introduced to measure the production and destruction of the temperature gradient.

Other researchers explored mixing parameters gaging micro- and macro mixing. As an example, in Koop and Browand [76], a parameter called "mixedness" was computed to assess the amount of micro mixing.

CHAPTER THREE

METHODOLOGY

3.1 Introduction

The step by step approaches adopted to achieve the research objectives spelled out in chapter one is presented in this Chapter. The sketches of geometries that portrays the experimental T-Junction were designed and the mesh model and physics models explained in sections 3.3.3 and 3.3.4 were applied and the geometries for this study presented. This research work was accomplished by performing numerical simulation using STAR-CCM+ based on an experimentation performed in the FSI test facility at the University of Stuttgart, thereafter a second simulation that involve interchanging both streams inlet temperatures in both lines so as to investigate a different possible scenarios. Although experimental work was not carried out in this research, but a study of the FSI experiment was reported first, so as to validate results of the simulation by CFD analysis. Upon successful validation, Analysis of both cases was then carried out both in the fluid and in the Structure/Wall Thickness of the Mixing Pipe.

Thus, the methodology shall be reported in three phases:

Phase 1 - THE EXPERIMENTAL REVIEW

Phase 2 - SIMULATION 1 (Case 1_Validation)

Phase 3 - SIMULATION 2 (Case 2_Analysis)

3.2 PHASE 1

3.2.1 Experimental Setup of FSI test facility.

The facility is shown schematically in Figure 3.1 along with the properties of the working fluid (deionized water with EC between 5 and 10 μS/cm at 20°C) and flow conditions. The main pipe has inner diameter *Dmain,* = 71.8 mm with hot water flowing at a constant mass flow rate of 0.4 kg/s (turbulent flow) comes in contact to a perpendicular, horizontal branch pipe with an inner diameter *Dbranch* = 38.9 mm carrying cold water of room temperature flowing at a rate of 0.1 kg/s coming into contact with the hot water.

The flow is then split downstream of the T-junction in accordance to the mass flow rate ratio and returned back to the T-junction; the stream headed to the branch line first passes through a heat exchanger. The mass flow rate ratio at the T-junction is such that at a low $\Delta T = Tm - Tb$ a wall-jet type flow pattern is manifest downstream of the T-junction at these flow rates. At higher ΔT, the cold branch line mixes weakly with the hotter, lighter flow, it rapidly sinks to the bottom of the downstream mixing pipe of the T-junction. More details of the behavior of the fluid at the facility beyond what was covered or articulated in this piece is explained in the submission of Kuschewski [49, 50]

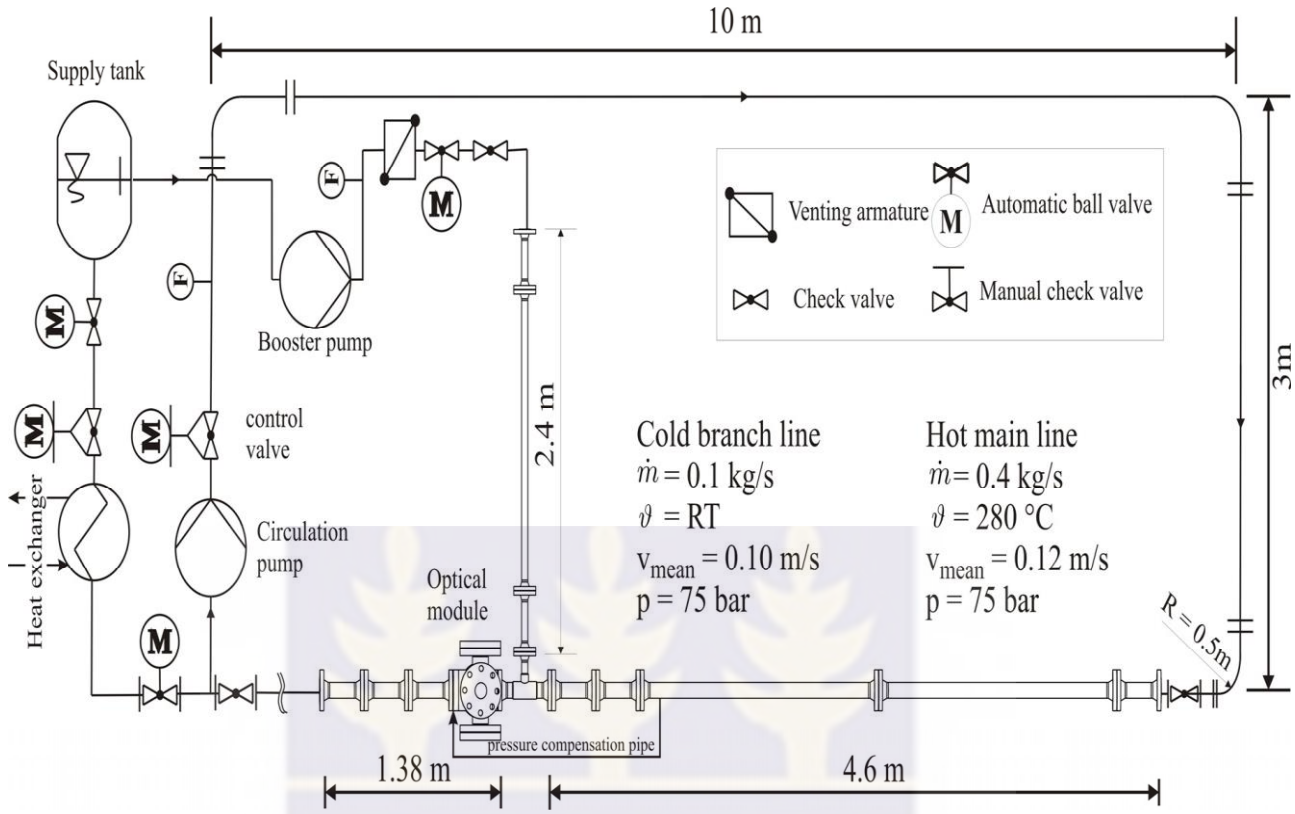

Figure 3.1 Piping and instrumentation diagram of the test facility at the University of Stuttgart [50]

3.2.2 Test Facility Operational Pattern

The Fluid-Structure-Interaction (FSI) test facility is a closed flow loop T-junction set-up which is installed at the Material Testing Institute (MPA), University of Stuttgart. As shown in Figure 3.2, it comprises a closed water loop with a three stage membrane booster pump and a circulation pump.

The cold injection line (DN40, ID 38.9 mm) is fed directly with the pressurized water (ambient temperature, 75 bar) from the supply tank. The water for the hot injection line (DN80, ID 71.8 mm) is heated up via ceramic resistance heating which are attached to the outer pipe surface. The maximum water temperature is 280 °C. Both injection lines have lengths of more than 50 diameters and include rectifiers. The water flows are combined in a horizontally aligned sharp edge 90° T-junction and mix in the outlet line

(DN80, ID 71.8 mm) with a length of 4.6 m. The T-junction is surrounded by different interchangeable modules connected by means of flanges. One module of the main line is equipped with thermocouples TC (see Appendix), and for the main and branch line an individual optical module is available to enable an optical access to the fluid flow. Figure 3.2 shows a view of the entire FSI test loop and a magnified cut-out including the T-branch and the thermocouple module. The experimental result is displayed in ***Appendix IV***.

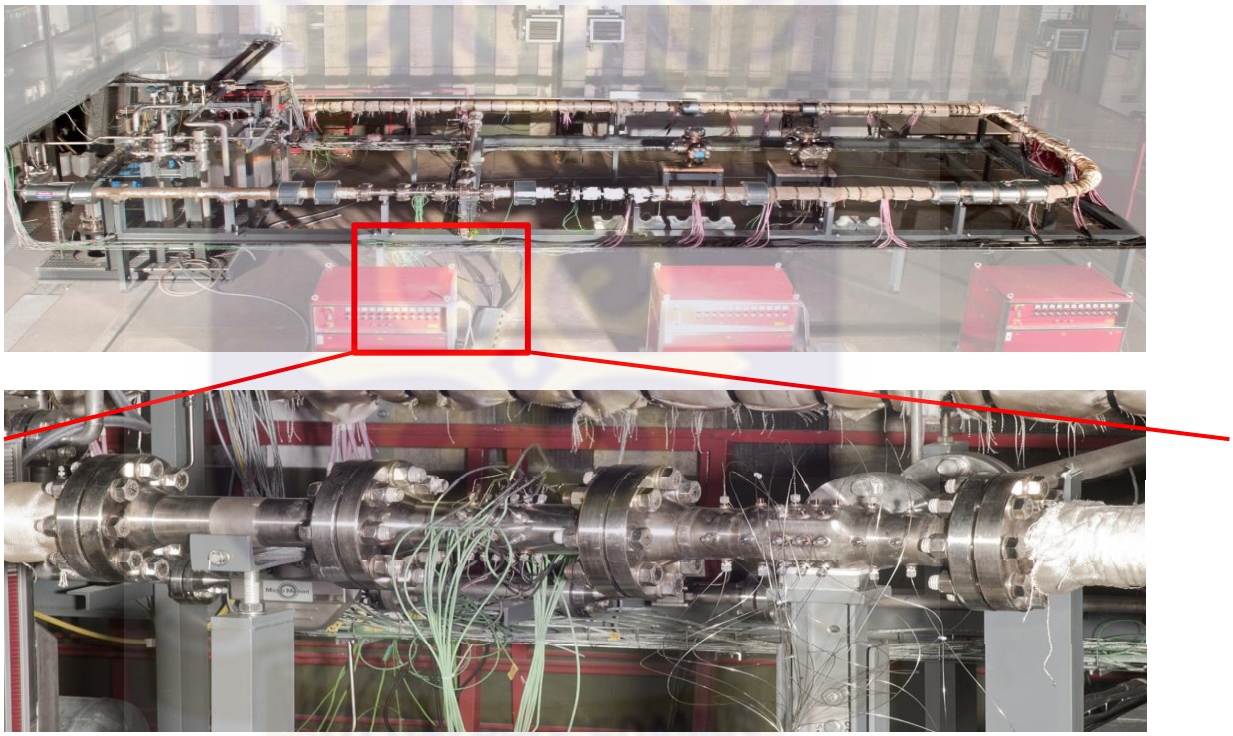

Figure 3.2: Photograph of the FSI test facility (top), magnified view of T-branch and a module equipped with TCs (bottom)

The facility can be operated in two operational modes. During the quasi-stationary tests (steady state thermal conditions and constant mass flow rates) the control values are left unchanged to keep the boundary conditions constant. While in the transient tests the mass

flow rate of the branch pipe *Mb* is altered from 0 kg/s to the nominal flow rate 0.1 kg/s and the main pipe flow rate *Mm* remains at constant level and requested temperature.

3.2.4 Material Properties.

The active pipping was made of Austenitic steel 1.4550 (X6 CrNiNb 18-10) AISI 347, the properties of Austenitic Steel used in both the experimental and simulations cases is summarized in table 3.1 while that of the water used is presented in table 3.2.

Table 3.1: Material properties of the Pipe

Property	**Symbol**	**Value**
Density	ρ	8000 kg/m^3
Thermal conductivity	*K*	16.1 W/mK
Specific heat capacity	Cp	500 J/kgK
Thermal expansion coefficient	A	16.6x10-6 K^{-1}

Table 3.2: Water Properties

Continuum Properties	
Properties	**Values**
Temperature	20^{0}C, 280C
Density	994.06 kg/m^3
Specific Heat	4179.1 J/kgK
Thermal Conductivity	0.62335 W/mK
Turbulent Prandtl Number	0.9
Dynamic Viscosity	7.1932 × 10^{-4} J/kgK

3.3 PHASES 2 AND 3

The second and third phases of this work were reported alongside. The major activity to be conducted is the numerical solution of the research problem by using computational fluid dynamics (CFD) code, the STAR-CCM+. The solution was then monitored and steered until convergence. Finally, data obtained was plotted using various visualization techniques and vivid analysis of trends was presented.

3.3.1 STAR-CCM+: Simulation of Thermal Mixing

Star-CCM+ code were employed in this research. The code provides comprehensive engineering physics simulation of flow problems by application of computational fluid dynamics (CFD).

3.3.2 Geometry Modelling

The geometry used was modeled and generated using the Three Dimensional-Computer Aided Design (3D-CAD) features in STAR-CCM+.

The test section was modeled using the sketch, extrude and extrude cut tools available in STAR-CCM+ to form figure 3.4a while figure 3.4b is the corresponding transparent view of the designed geometry. The sketch was transformed into structure solids using the extrude and extrude cut feature. The dimensions of the computational flow domain considered is shown in Figures 3.3 for both cases.

Design dimensions.

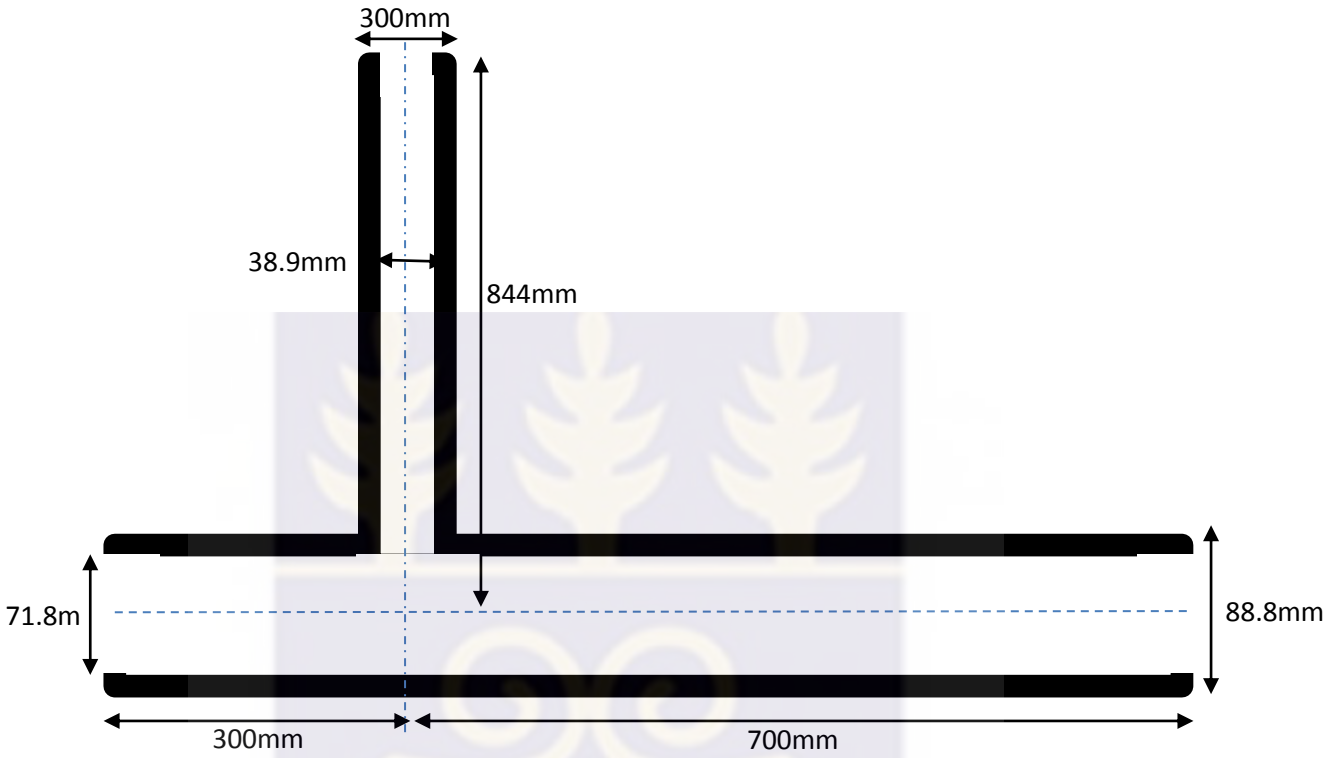

Figure 3.3: Dimensions of the computational flow domain using experimental data

Table 3.3 Design Parameters

	Inner Diameter (mm)	Thickness (mm)	Length (m)
Main Line:	71.8	8.5	0.3 upstream, 0.7 downstream
Branch Line:	38.9	4.7	0.5

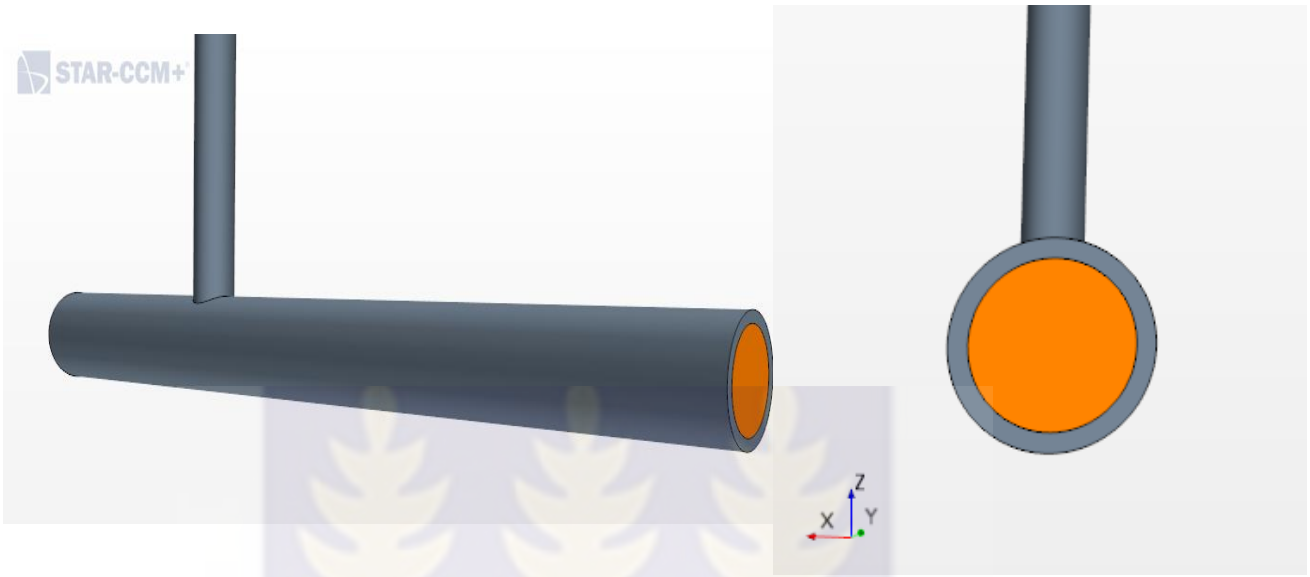

Figure 3.4a: Modeled Geometry

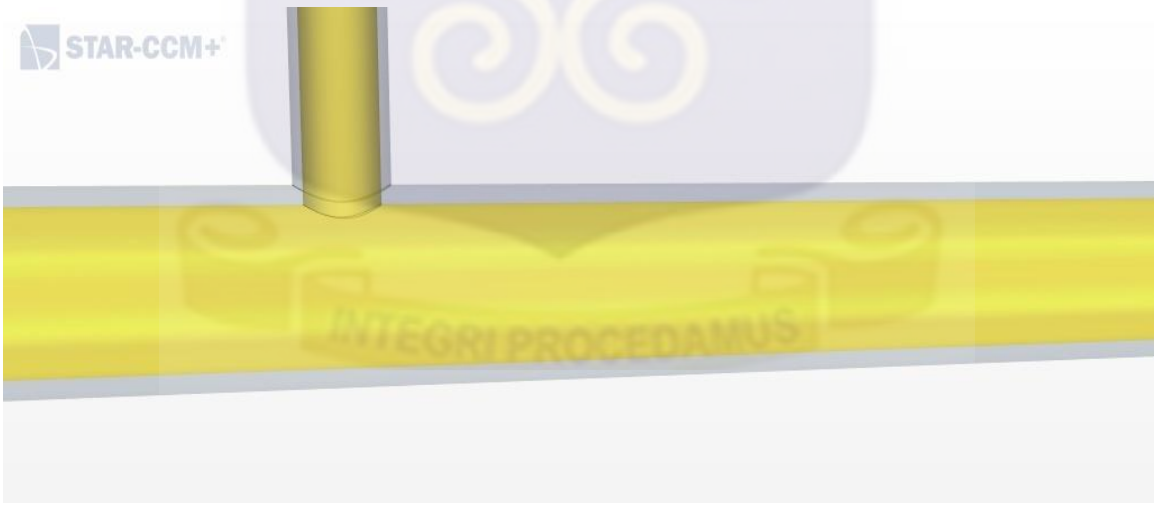

Figure 3.4 b: Transparent View of the Geometry

3.3.3 Meshing Models

In this study, the domain was discretized by the application of surface re-mesher (so as to re-meshe the initial surface and produce a good discretized mesh which is suitable for CFD and due to the fact that it is used to re-triangulate the surface based on a target edge length supplied and can also omit specific surfaces or boundaries preserving the original triangulation from the imported mesh) [77] and polyhedral meshing model (to generates a volume mesh which comprise of polyhedral-shaped cells. Numerically, it is more stable, less diffusive and more precise than the similar tetrahedral mesh. Besides, polyhedral mesh contains almost five times fewer cells than a tetrahedral mesh for the starting surface)[77].

After several attempt to arrived at the best and allowable number of cells considering the capability of the processing computer that will give a better output, 2.77Millions cells was chosen at 1.7mmBH interval. This representation of the computational domain shown in various view in figure 3.5 a, b and c is what the physics solvers use to provide a numerical solution. Various meshing tactics exists, and each one has its advantages and disadvantages with each particular strategy suitable for one or other applications depending on the area of interest.

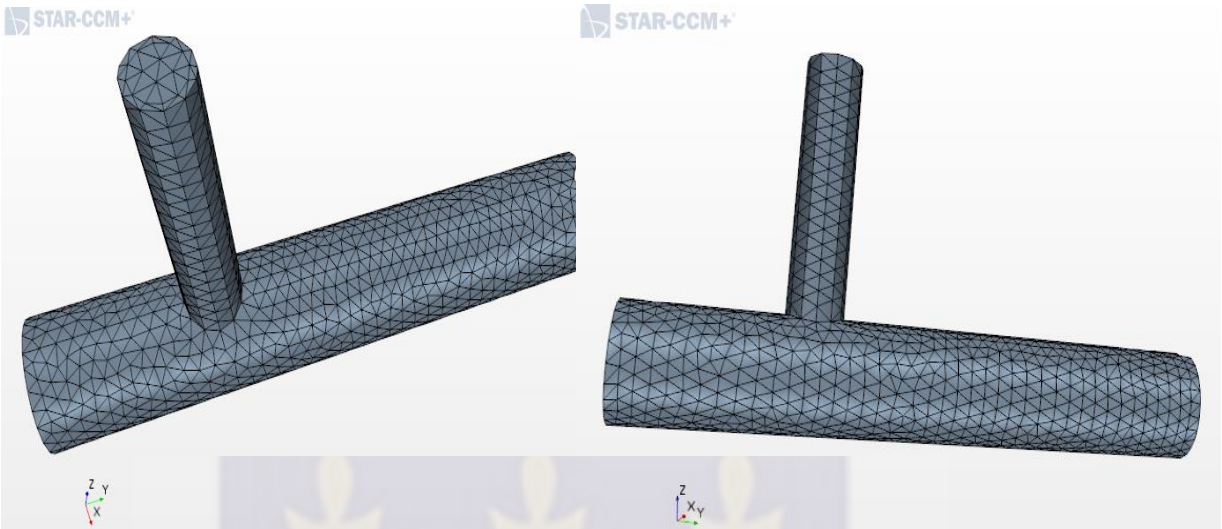

A B

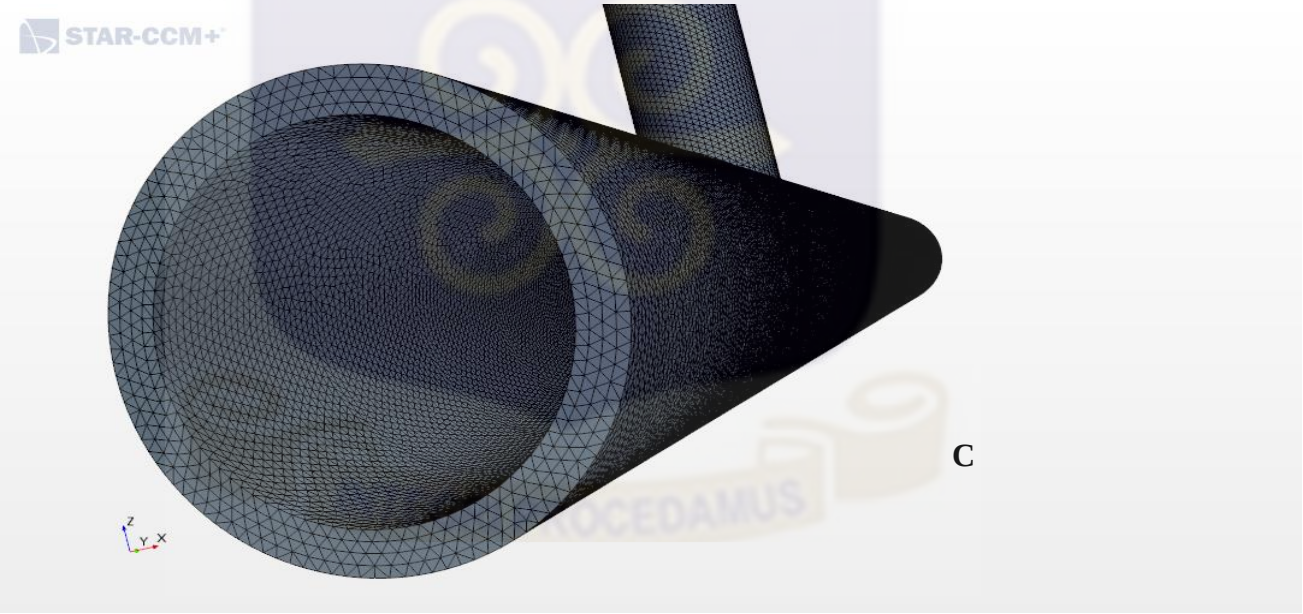

C

Figure 3.5a, b and c: Discretization of the domain

3.3.4 Physics Models Set Up

Appropriate models used for solving both mean and turbulent flow properties for the problem considered were selected from a list of models available in STAR-CCM+. Thermal striping is intrinsically unsteady and hence not accessible to steady state simulation approaches such as steady state Reynolds-averaged Navier-Stokes (RANS) models. Table 3.4 shows the physics models that were applied for the flow problem considered in this study.

Consequently, unsteady RANS was considered. Turbulence modelling is one of the significant factors prompting the reproduction of the temperature fluctuation instigated by the vortices downstream from a T-junction and as such, a turbulence sensitivity analysis was performed to arrive at an appropriate turbulence model that would accurately predict the experimental data. The two turbulence models to be considered for the URANS models were k-epsilon model and k-omega models.

Table 3.4: Applied Physics Model

MODEL	MODEL SPECIFICATION
Space Model	3-Dimensional
Time Model	Implicit Unsteady
Energy of State Model	User Defined EOS
Flow Model	Segregated Flow
Energy Model	Segregated Fluid Temperaturel
Viscous Regime Model	Turbulent
Turbulent Model	SST K-Omega
Wall Function	All y + wall Model
Convection Scheme	2nd Order Upwind

3.3.5 Initial Conditions

Table 3.5, shows the initial conditions of the various parameters.

Table 3.5: Initial conditions of both simulations

	CASE 1 SIMULATION	CASE 2 SIMULATION
Temperature of (^{o}C): Main Line Branch line	280 20	20 280
Pressure (Mpa)	7.08	7.08
Mass flow rate (kg/s): Main line Branch line	0.4 0.1	0.4 0.1
Velocity (m/s): Main line Branch line	0.1 0.12	0.1 0.12

3.4 Probes Insertion

The probes (simulation case) and thermocouple equipped (experimental work) T-junction are used to investigate the extent of the motivated thermal mixing. In this study, probes were inserted in different positions for both phases to extract data for validation and to analyze the temperature variation and other parameters downstream both in the fluid and in the solid structure.

3.4.1 Measurement Points for First Phase Simulation

The validation points where data was extracted in the simulation were calculated so as to reflect the same position where data was taken for the experiment result. Probes were

correctly placed at axial location of X/Dm = 1 for the downstream position and X/Dm = -1 for the upstream positions, as shown in figure 3.6 Left

Point probes were used since the temperature is with respect to time and not with distance but at the same radial position in the simulation as the experimental (Figure 3.6, Right)

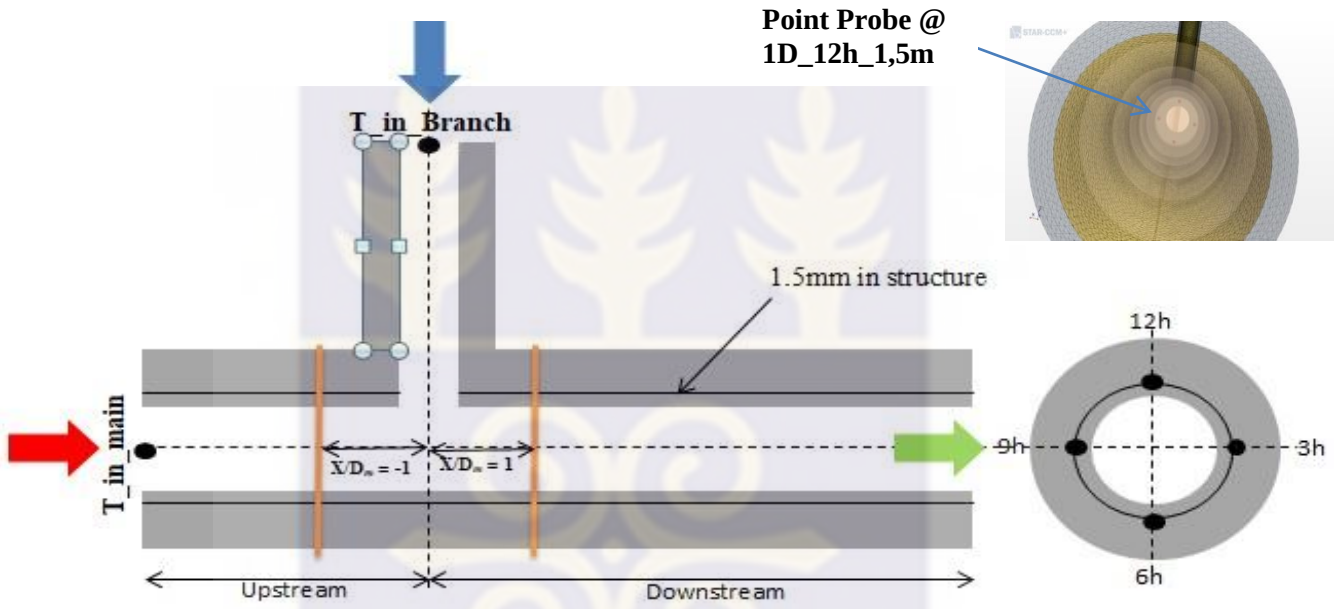

Figure 3.6 Axial (Left) and Radial (Right) Probes Locations

3.4.2 Measurements Points of the Second Simulation

In order to get important output from the simulation and to capture the relevant temperature variations that may cause damage. Temperature were recorded at various positions downstream of the mixing junction at the wall (facet average from the nearest computational cell wall), in the fluid and the solid.

For further analyses, line probes were derived to cut thru the 6 – 12hr of the structure-fluid-structure at seven (7) different locations downstream so as to detect the extent of

heat intensity being transferred to the solid structure via conduction and also extended downstream on each layer in the upper sections of structure from the mixing point where susceptible to stress. Each point in the line probes helps to plot the profiles and in-depth analysis conducted. Figure 3.7 shows the specific segments where the data was retrieved by the aid of Line probes. Data was extracted at 0.5Dm, 1Dm, 2Dm, 3Dm, 4Dm, 5Dm, 6Dm and 7Dm along the mixing tube.

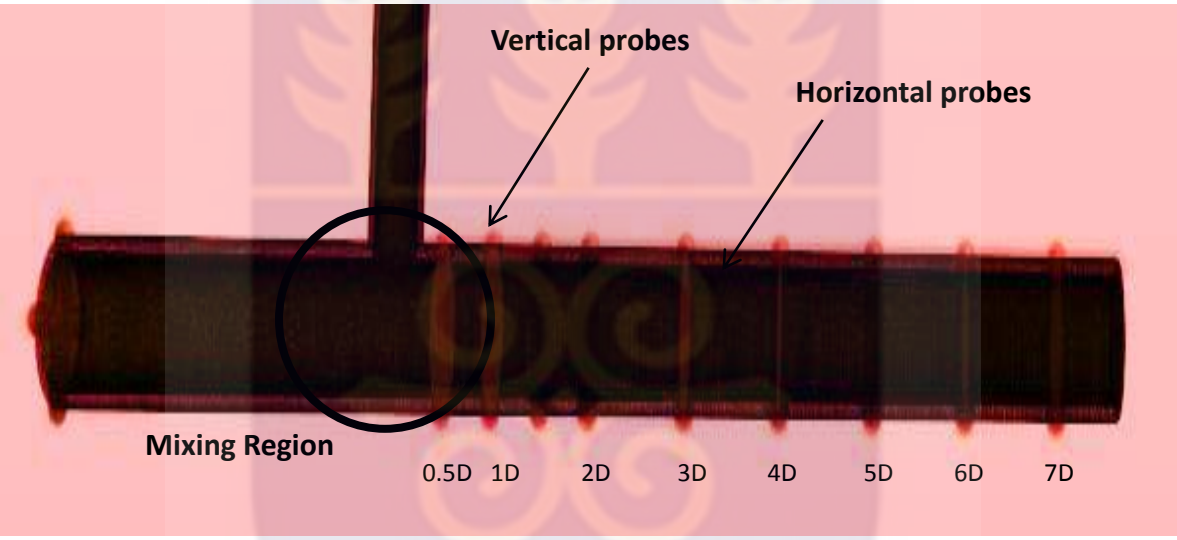

Figure 3.7 Measurements Points

3.4.3 Validation of Experimental Results

To elucidate the validation, the data from the experimental result was extracted with the aid of ***PlotDigitizer*** software so as to record data for each curve at the following locations and time of the experiment readings, This result was recorded at various axial and radial positions of temperatures trends of the T-junction wall (inner pipe surface offset 1.5mm) in upstream and downstream this includes, -1D_6h_1.5mm, 1D_9h_1.5mm,

1D_6h_1.5mm, 1D_12h_1.5mm and initial temperatures at both inlets, T_in_main, T_in_branch).

The curves at these locations were re-plotted with the simulation result to allow for clearer observation of both trends and magnitude. For each curve, the experimental result was plotted alongside the same parameter from the simulation; this was followed by analyses of the trend. For the validation, data were collected at the physical time of 15.8 seconds to 16.8 seconds.

Comparing simulation result to the experimental findings, results are display in a plot for clearer visualization to aid easy understanding. To achieve this, the exact point where reading where taking in the experimental was replicated in the simulation.

3.5 Governing Equations

The Governing equation employed by Star CCM+ Computation Fluid Dynamics are stated as follows:

Continuity equation

$$\frac{\partial}{\partial x}(pU)+\frac{1}{r}\frac{\partial}{\partial r}(prV)=0 \qquad (3.1)$$

Where: $\frac{\partial \rho}{\partial t}$ –change in density with time

$div(\rho u)$- Convective term, describes net flow of mass out of the element across its boundaries

X- Component of momentum equation

$$\rho \frac{Du}{Dt} = \frac{\partial(-\rho+\tau_{XX})}{\partial x} + \frac{\partial \tau_{xx}}{\partial y} + \frac{\partial \tau_{zx}}{\partial z} + S_{Mx} \quad \text{.....(3.2)}$$

Where: 1st three terms at the RHS- total force in the *x*-direction on the element due to surface stresses

S_{Mx}- Source of *x*-momentum per unit volume per unit time.

Y- Component of momentum equation

$$\rho \frac{Dv}{Dt} = \frac{\partial \tau_{xy}}{\partial x} + \frac{\partial(-\rho+\tau_{yy})}{\partial y} + \frac{\partial \tau_{zy}}{\partial z} + S_{My} \quad \text{..... (3.3)}$$

Where: 1st three terms at the RHS- total force in the *y*-direction on the element due to surface stresses

S_{Mx}- Source of *y*-momentum per unit volume per unit time.

Z- Component of momentum equation

$$\frac{Dw}{Dt} = \frac{\partial \tau_{xz}}{\partial x} + \frac{\partial \tau_{yz}}{\partial y} + \frac{\partial(-\rho+\tau_{zz})}{\partial z} + S_{Mz} \quad \text{..... (3.4)}$$

Where: 1st three terms at the RHS- total force in the z-direction on the element due to surface stresses

S_{My}- Source of *y*-momentum per unit volume per unit time.

Equation (5)

Energy equation (enthalpy based)

$$\frac{\partial}{\partial x}(pUH)+\frac{1}{r}(prVH)=$$

$$\frac{\partial}{\partial x}\left[\left(\frac{\mu}{pr}+\frac{\mu_T}{\sigma_T}\right)\frac{\sigma H}{\sigma x}\right]+\frac{1}{r}\frac{\partial}{\partial r}\left[r\left(\frac{\mu}{pr}+\frac{\mu_T}{\sigma_T}\right)\frac{\partial H}{\partial r}\right] \quad \ldots\ldots\ldots\ldots\ldots\ldots\ldots\ldots\ldots\ldots\ldots\ldots \quad (3.5)$$

Energy equation (temperature based)

$$\frac{\partial}{\partial x}\left(pC_pUT\right)+\frac{1}{r}\frac{\partial}{\partial r}\left(pC_prVT\right)=$$

$$\frac{\partial}{\partial x}\left[C_p\left(\frac{\mu}{\Pr}+\frac{\mu_T}{\sigma_T}\right)\frac{\partial T}{\partial x}\right]+\frac{1}{r}\frac{\partial}{\partial r}\left[rC_p\left(\frac{\mu}{pr}+\frac{\mu_T}{\sigma_T}\right)\frac{\partial T}{\partial r}\right] \quad \ldots\ldots\ldots\ldots\ldots\ldots\ldots\ldots\ldots\ldots\ldots\ldots \quad (3.6)$$

In both expression of energy equations σ_T is the turbulent Prandtl number, assigned to a value of 0.9 , as suggested by common practice in fluids.

Turbulence Kinetic Energy equation (k)

$$\frac{\partial}{\partial x}(pUK)+\frac{1}{r}\frac{\partial}{\partial r}(prVK)=$$

$$\frac{\partial}{\partial x}\left[\left(\mu+\frac{\mu_T}{\sigma_k}\right)\frac{\partial k}{\partial x}\right]+\frac{1}{r}\frac{\partial}{\partial r}\left[r\left(\mu+\frac{\mu_T}{\sigma_k}\right)\frac{\partial k}{\partial r}\right]+P_k+G_k-p\varepsilon-pD \quad \ldots\ldots\ldots\ldots\ldots\ldots\ldots \quad (3.7)$$

Dissipation rate ε

$$\frac{\partial}{\partial x}(pU\varepsilon)+\frac{1}{r}\frac{\partial}{\partial r}(prV\varepsilon)=\frac{\partial}{\partial x}\left[\left(\mu+\frac{\mu_T}{\sigma_\varepsilon}\right)\frac{\partial \varepsilon}{\partial x}\right]+\frac{1}{r}\frac{\partial}{\partial r}\left[r\left(\mu+\frac{\mu_T}{\sigma_\varepsilon}\right)\frac{\partial \varepsilon}{\partial r}\right]$$

$$+C_{\varepsilon_1 f_1}\frac{1}{T}(p_k+G_k)+C_{\varepsilon_2 f_2}\frac{p_\varepsilon}{T}+pE \quad \ldots\ldots\ldots\ldots\ldots\ldots\ldots\ldots\ldots\ldots\ldots\ldots\ldots\ldots\ldots\ldots \quad (3.8)$$

Shear Production

$$p_{k=\mu_T}\left[2\left\{\left(\frac{\partial U}{\partial x}\right)^2+\left(\frac{\partial V}{\partial r}\right)^2+\left(\frac{v}{r}\right)^2\right\}+\left(\frac{\partial U}{\partial r}+\frac{\partial V}{\partial x}\right)^2\right] \quad \text{.....} \quad (3.9)$$

Gravitational production

$$G_k=-pug_x=\frac{\beta\mu_T}{C_{1t}}\left(\frac{k}{\varepsilon}\right)\left(\frac{\partial V}{\partial r}+\frac{\partial V}{\partial x}\right)\left(\frac{\partial T}{\partial r}\right)g_x \quad \text{.....} \quad (3.10)$$

3.6 The Two Equation Turbulent Transport Models

The two equation turbulence model is the most extensively used equation model in engineering application. It provides transport modeling equations for both turbulence and turbulent kinetic energy [78]. These models which are categorized under the class of eddy viscosity are equations which are derived to describe the transport of two scalars. The Reynolds stress tensor is computed by applying an assumption which relates the Reynolds stress tensor to the velocity gradient and an eddy viscosity [79].

One fundamental assumption that is common among most of the two-equation models is the assumption of local equilibrium which equates turbulent production to dissipation. This therefore seeks to mean that the measure of turbulence is locally proportional to the level of the mean flow; therefore most of the two-equation models will be in error when applied to non-equilibrium flows. The first assumption of the two-equation is that the turbulent fluctuations $u', v' and\ w'$ are locally isotropic. This assumption is however valid for smaller eddies at high Reynolds because the large eddies are in a state of

anisotropy as a result of the strain rate of the mean flow though $u', v' and\ w'$ are almost of the same magnitude [78].

The second conjecture is called the local equilibrium assumption. This assumption accounts for the production and dissipation terms in the k-equation which are locally equal. This assumption was deduced from the fact that the Reynolds stress must be estimated at every point in the flow field. In order to permit the calculation of the Reynolds stresses using the local scales, most two equation models assume that production equals dissipation in the k-equation which is defined mathematically as;

$$\tau_{ij}S_{ij} = \rho\varepsilon \quad \text{.......................................(3.11)}$$

where $\tau_{ij}$is the turbulence stress tensor.

The eddy viscosity can be estimated based on the dimensional reasoning by applying either turbulent or mean scale since the turbulence and mean scales are proportional. This indicates that for the k-ε model

$$\mu_t \propto \frac{\rho k^2}{\varepsilon} \quad \text{.......................................(3.12)}$$

for the k-ω model

$$\mu_t \propto \frac{\rho k}{\omega} \quad \text{.......................................(3.13)}$$

If there is an imbalance between production and dissipation locally then the ratio of the Reynolds stresses to the mean strain rate will not be locally constant and the μ_t will be a function of both turbulent and mean scales. The types of two-equation models are discussed in the next section

3.6.1 The k-Epsilon (k-ε) Model

Various calculations involving turbulent mean flow in engineering applications have been performed with the Reynolds Average Navier-Stokes (RANS) equation in association with the k-epsilon turbulence model [80]. Originally proposed by Launder and Spalding in 1972, the standard k-epsilon turbulence model consists of the transport equation for the *k* and ε. The k-epsilon model which is the most widely used two equation model consists of the turbulence kinetic energy *k* and ε for the rate of dissipation [81]. The effects of curvature, non-isotropic turbulence and buoyancy were later factored into the model by Rodi in 1972 and Pantankar in 1980. Though the *k*-ε model is generally good in turbulence modeling, its range of validity is limited [81].

The transport equation for the *k* and ε are derived from the exact equation and the application of physical reasoning respectively [82]. The high number of unknowns and the multiple correlations of unstable velocities and pressure informed the derivation of the ε from physical reasoning [79].

The modeled equations for *k* and ε are respectively given as,

$$\frac{\partial(\rho k)}{\partial t} + div(\rho k U) = div\left[\frac{\mu_t}{\sigma_k} grand\ k\right] + 2\mu_t E_{ij} - \rho E \quad \text{.....(3.14a)}$$

$$\frac{\partial(\rho \varepsilon)}{\partial t} + div(\rho \varepsilon U) = div\left[\frac{\mu_t}{\sigma_\sigma} grand\ \varepsilon\right] + C_{1\varepsilon}\frac{\varepsilon}{k}2\mu_t E_{ij}E_{ij} - C_{2\varepsilon}\rho\frac{\varepsilon^2}{k} \quad \text{.....(3.14b)}$$

where the terms on the right-hand side of equation 2.8 (a and b) represents the production, dissipation and wall terms respectively. The closure coefficients are given as

$C_{1\varepsilon} = 1.44$, $C_{2\varepsilon} = 1.92$, $\sigma_k = 1.0$ and $\sigma_\sigma = 1.3$

Though the constants do not change in calculations, they need to be altered to accommodate modifications in Reynolds number and curvature [81]. In order to model the ε equation, the properties of the flow is simplified in stages. These stages are isotropic decay, homogenous shear flow and constant stress layer near solid walls.

The eddy viscosity is defined as a function of the turbulent kinetic energy, *k*, and the dissipation rate, ε, as [83],

$$\mu_f = \frac{c_\mu f_\mu \rho k^2}{\varepsilon} \quad \text{(3.15)}$$

The near wall damping functions are

$$f_\mu = \exp(-3.4/(1 + 0.002Re_t)^2) \quad \text{(3.16a)}$$

$$f_2 = 1 - 0.3\exp\left(-Re_t{}^2\right) \quad \text{(3.16b)}$$

$$Re_t = \frac{\rho k^2}{\mu\varepsilon} \quad \text{(3.16c)}$$

The explicit wall terms are

$$\Phi_k = 2\mu\left(\frac{\partial\sqrt{k}}{\partial y}\right)^2 \quad \text{(3.17a)}$$

$$\Phi_\varepsilon = 2\mu\frac{\mu_t}{\rho}\left(\frac{\partial^2 u_s}{\partial y^2}\right)^2 \quad \text{(3.17b)}$$

where u_s is the flow velocity parallel to the wall.

The boundary conditions at no-slip surfaces with integration to the wall are given by the following simpler relationships:

k= 0 and ε = 0

when the above wall terms are included in equation 2.11 and the effective dissipation rate is expressed as $\frac{\varepsilon-\phi_k}{\rho}$. Zero-gradient conditions are applied at symmetry.

The range of practicality of the k-epsilon model has been extended by introducing a number of correction terms aimed at introducing additional turbulence physics to the model. Examples of correction terms are the Pope correction [7] for three dimensional jet application and Sarkar and Lakshmanan correlation for the application use in high flow convective Mach number [80].

The k-epsilon model is relatively simple to implement which results in easy convergence and reasonable predictions for many flows. However, it is specifically poor at predicting swirling and rotating flows, flows with strong separation and fully developed flows in non-circular ducts. It is also only valid for fully turbulent flows and it over predicts turbulence in highly strained flow

Also in the k-epsilon model, there is the absence of a natural boundary condition for the ε near a solid surface. However, the dissipation rate is set at zero, similar to the turbulent kinetic energy and turbulent viscosity. The zero turbulent quantities are set near a viscous surface due to the near-wall damping functions [84].

3.6.2 The Standard k-Omega (k-ω) Model

To overcome the limitations of the k-epsilon model, many alternative models have been modeled [88]. With respect to both accuracy and robustness, the k-omega model from

Wilcox has been one of the most successful. The k-omega model came after the k-epsilon model and similar to the k-epsilon model however it solves the omega which represents the specific rate of dissipation of kinetic energy. The relation between the ω and ε is given by

$$\omega \propto \frac{\varepsilon}{k} \quad \text{.....(3.18)}$$

The modeled turbulent kinetic energy equations by Wilcox as expressed by [85] is given as

$$\frac{\partial \rho k}{\partial t} + \frac{\partial \rho u_j k}{\partial x_j} = P_k - \beta^* \rho \omega k + \frac{\partial}{\partial x_j}\left[(\mu + \sigma_{k1}\mu_t)\frac{\partial k}{\partial x_j}\right] \quad \text{.....(3.19a)}$$

$$\frac{\partial \rho \omega}{\partial t} + \frac{\partial \rho u_j \omega}{\partial x_j} = \gamma_1 P_\omega - \beta_1 \rho \omega^2 + \frac{\partial}{\partial x_j}\left[(\mu + \sigma_{\omega 1}\mu_t)\frac{\partial \omega}{\partial x_j}\right] \quad \text{.....(3.19b)}$$

The closure coefficients are defined by Menter [41] as,

$$\sigma_{k1} = 0.5\,,\ \sigma_{\omega 1} = 0.5\ \ \beta_1 = 0.0750,\ \beta^* = 0.09\,,\ \gamma_1 = \frac{\beta_1}{\beta^*} - \sigma_{\omega 1} k^2/\sqrt{\beta^*}$$

The k-omega model takes ω instead of ε as an independent variable. The turbulent kinetic energy and its specific dissipation rate are specified either by the pre-calculated distributions in the channel flow or by the following equations

$$k_{in} = 1.5\,(I_{in} u_{in})^2 \quad \text{.....(3.20a)}$$

$$\varepsilon_{in} = c_D k_{in}^{3/2}/I_{in} \quad \text{.....(3.20b)}$$

$$\omega_{in} = \frac{c_\mu \epsilon_{in}}{\alpha^* k_{in}} = \gamma \frac{\sqrt{k_{in}}}{I_{in}} \quad \text{.....(3.20c)}$$

The turbulence length scale at the inlet, l_{in}, is usually set as a fraction of the whole inlet height and c_D is a constant. Inlet conditions are specified by equations 12.14 when computing the flow in two-dimensional confined enclosure. In the outlet, the streamwise derivatives of the flow variables are zero at the outlet. The ω-equation has an exact solution in the immediate proximity of a wall surface where the viscous diffusion balances the destruction. With a refined grid in near-wall regions, the asymptotic solution is used to calculate the specific dissipation rate ω at the first node close to the wall surface. In present calculations, at least one node is required below $y^+ = 5$. This makes it possible to integrate the solution of the k-omega model directly into the viscous sublayer without using the conventional wall functions or low-Reynolds-number corrections as a bridge. In such an extended-to-wall method, a zero value can be imposed at the wall for the velocity components and turbulent kinetic energy, ie.

$u = v = 0,\ k = 0$ ……(3.21)

The exact limit for ω is

$$\omega \to \frac{6v}{\beta y^2} \text{ as } y \to 0 \quad \text{……..(3.22)}$$

In engineering application, the wall-function method is often preferred to avoid a highly refined grid near the wall. The wall functions used with k-omega can be derived by simplifying the model equations in the logarithmic layer of a boundary flow as

$$\frac{\partial}{\partial y}\left(v_t \frac{\partial u}{\partial y}\right) = 0 \quad \text{……(3.23a)}$$

$$v_t \left(\frac{\partial u}{\partial y}\right)^2 - \beta^* \omega k + \frac{\partial}{\partial y}\left[\left(\frac{v_t}{\sigma_k}\right)\frac{\partial k}{\partial y}\right] = 0 \quad \text{……...(3.23b)}$$

$$\alpha\alpha^{*}\left(\frac{\partial u}{\partial y}\right)^{2}-\beta\omega^{2}+\frac{\partial}{\partial y}\left[\left(\frac{v_t}{\sigma_\omega}\right)\frac{\partial\omega}{\partial y}\right]++c_\omega\frac{v_t}{k}\left(\frac{\partial k}{\partial y}\frac{\partial\omega}{\partial y}\right)=0 \quad \text{.....(3.23c)}$$

The velocity profile is assumed to obey the logarithmic law. The k-omega model has superior advantage over the k-epsilon model under hostile pressure-gradient conditions and also its simplicity of its formulation in the viscous sub layer. Unlike the k-epsilon model, the k-omega does not employ damping functions which leads to an advantage in numerical stability over the k-epsilon [84].

Aside the fact that the k-omega model has difficulty in converging, it is also delicate to initial guess at the solution. The k-omega model has two variations; these are the standard k-omega model and the SST model. The standard k-omega and the SST models similarly apply the k and omega equations however the SST, in the inner region of the boundary layer changes from the standard k-omega to the k-epsilon model in the outer part of the boundary layer. Also SST model accounts for the transport effects of the principal turbulent shear stress by including a modified turbulent viscosity equation [83].

The differences between the variations of the k-omega model, present transport equations and the method of solving for turbulent viscosity as well as all the constants are explained in the following sections.

3.6.2.1 The Shear Stress Turbulent (SST) K-Omega Model

Developed by Menter in 1994, the SST k-omega is a two-equation eddy model aimed at effectively combining the k-omega and k-epsilon models. The objective is to utilize the robust and precision of the k-omega model in the near-wall region and the free-stream

independence of the k-epsilon models in the far field. It does not use functions and tends to be most accurate when solving the flow near the wall [85].

To achieve the objective stated by Karim *et al.* [85], the k-epsilon is written in terms of omega and the standard k-omega model and the transformed k-epsilon model are both multiplied by blending function. Both functions are later added together. The blending function F_1 is zero (leading to the standard k-omega model) and the inner edge of a turbulent boundary layer and blend to a unitary value (corresponding to the standard k-epsilon) at the outer edge of the layer.

The SST modeled equations 1s given:[86]

$$\frac{\partial \rho k}{\partial t} + \frac{\partial \rho U_j k}{\partial x_j} = \widetilde{P_k} - \beta^* \rho \omega k + \frac{\partial}{\partial x_j}\left(\Gamma_k \frac{\partial k}{\partial x_j}\right) \quad \text{..... (3.24a)}$$

$$\frac{\partial \rho \omega}{\partial t} + \frac{\partial \rho U_j \omega}{\partial x_j} = \frac{\alpha}{v_t}\widetilde{P_k} - \beta^* \rho \omega^2 + \frac{\partial}{\partial x_j}\left(\Gamma_\omega \frac{\partial k}{\partial x_j}\right) + (1 - F_1) 2\rho\sigma_{\omega 2} \frac{1}{\omega}\frac{\partial k}{\partial x_j}\frac{\partial \omega}{\partial x_j} \quad \text{.....(3.24b)}$$

where the blending function F_1 is calculated from

$$F_1 = \tanh(arg_1^4) \quad \text{.....(3.25a)}$$

$$arg_1 = min\left(max\left(\frac{\sqrt{k}}{\beta^* \omega y}; \frac{500v}{y^2 \omega}\right)\frac{4\rho\sigma_{\omega 2} k}{CD_{k\omega} y^2}\right) \quad \text{.....(3.25b)}$$

$$CD_{k\omega} = max\left(2\rho\sigma_{\omega 2}\frac{1}{\omega}\frac{\partial k}{\partial x_j}\frac{\partial \omega}{\partial x_j}; 1.oe^{-10}\right) \quad \text{..... (3.25c)}$$

with the constant a_1= 0.31 and the blending function F_2 obtained from

$$F_2 = \tanh(arg_2^2) \quad \text{..... (3.26a)}$$

$\arg_2 = \max\left(2\frac{\sqrt{k}}{\beta^* \omega y}; \frac{500\nu}{y^2 \omega}\right)$ ……(3.26b)

The coefficients, φ of the model are functions of F_1: $\varphi = F_1\varphi_1 + (1\text{-}F_1)\,\varphi_2$, where φ_1, φ_2 stand for the coefficients of the k-omega and the k-epsilon respectively:

$\sigma_{k1} = 1.176$, $\sigma_{\omega 2} = 2.000$, k= 0.41, $\alpha_1 = 0.5532$, β_1= 0.0750, β^*= 0.09, c_1= 10

$\sigma_{k1} = 1.000$, $\sigma_{\omega 2} =$, k= 0.41, $\alpha_2 = 0.4403$, β_2= 0.0828, β^*= 0.09

The SST model does not always converge to the solution quickly, so the k-ε or k-ω models are solved first to give good initial conditions [85].

As explained earlier, to overcome the limitations of the k-epsilon model, with respect to both accuracy and robustness, the k-omega model from Wilcox which has been one of the most successful was adopted in this work. A recent study by Boatema (2015), recommend the k-omega model as given a better prediction.

CHAPTER FOUR

DISCUSSION OF RESULTS

4.0 Introduction

This chapter concentrate on the flow characteristics and analysis of thermal load present in the T-junction. Validation of Simulation results with the studied experiment presented, thereafter analysis carried out in two major categories; Heat Transfer from Fluid to Solid and Heat Transfer within the Solid (wall downstream).

To visualize the important physical phenomena associated with turbulent mixing, snapshots of the temperature and velocity field have been presented. A more quantitative description can be found in subsequent sections where effects of other parameters are discussed. Two fluid streams accelerate in the mixing zone and together they form a jet-like structure, which results to a decreasing temperature difference along the main channel from mixing joints downstream. Further downstream as mixing tend toward thermal equilibrium; parameters under investigation experienced a drop or fall which leads to less effect of thermal stress on those locations. Turbulent flow is observed with a high flow variability, which mixes hot and cold fluid streams.

4.1 Pre-Mixing Phenomena

As a means to overcome the limitation of the code to capture the entire length of the pipes and in order to ensure a fully developed flow that was injected into both inlets of the simulated T-junction, a separate simulation was conducted for two straight pipes in both cases (horizontal and vertical tubes) representing hot inlet and cold inlet which was

named Pre-Mixing Main DN 80 and Pre-mixing Branch DN40 respectively with fluid (water) properties synonymous to the conditions being modelled

The output parameters generated from the pre mixing were then coupled to the designed T-Junction simulation as initial conditions.

Mass flow boundary conditions were imposed at both cold and hot inlet of the mixing-junction and a pressure boundary condition imposed at the outlet. Adiabatic condition was imposed on the wall surfaces. A non-slip condition was adopted for all the walls. The fluid properties were carefully derived attached to the simulations.

This was repeated also for the second simulation but with exchange of flow rate at both hot and cold inlet from that applied in validation case.

The results from the well-developed fluids at the exit of the Branch (vertical) tube and main (horizontal) tube prior to mixing as shown in Figure 4.1 were extracted and imposed as inlets conditions for the main 90 degree T-junction flow geometry for onward simulation.

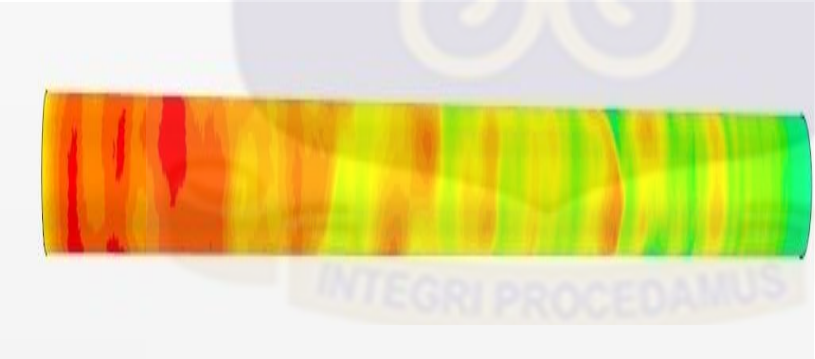

(a) Main Pipe

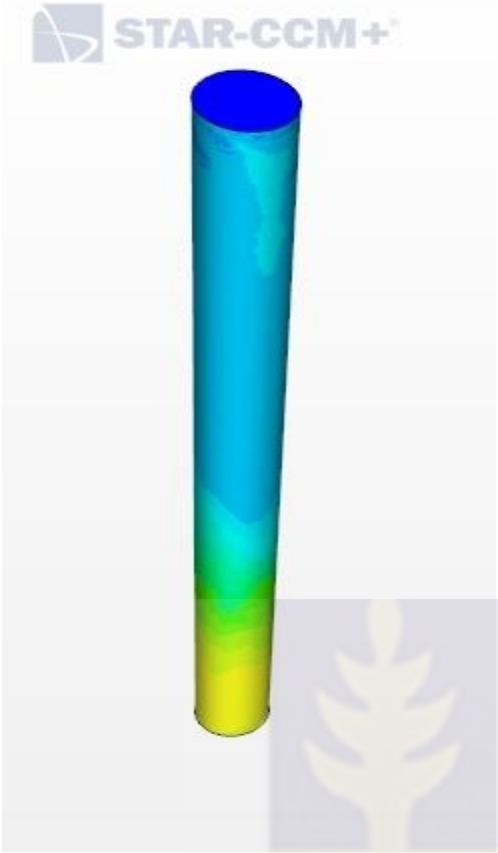

(b) Branch Vertical Pipe

Figure 4.1: Temperature Fields of Pre-Mixing Pipes.

4.2 Validation of Results

Since this phase of the research was to perform a simulation replicating a reported experiment, all result gotten from this present work was validated with that from the experiment which includes the inlet result, results at points 1D_6h_1.5mm, 1D_9h_1.5mm and -1D_12h_1.5mm. This points were already shown in figure 3.6 and the results of the experiments is shown in appendix IV.

The visible difference in all trend and magnitude can be attributed to the number of cells the designed geometry was meshed into which is dependent on the processing power of the computer systems that was used for the simulation.

Higher computer processing power and speed will enable more number of meshed cells which will narrow each cells and thus limit computational error.

In this work, considering the system capacity, we were able to get two million, seven hundred million meshes of the geometry, this can be increased to Five million with a higher system processor.

The trend of temperature of both the simulation shows good agreement with the experimental at the main and branch inlets which confirms the qualitative ability of the model used in predicting the trend as shown in figure 4.2. However, the approximately 20^{o}C difference at the Main inlet can be linked to a downside in terms of the quantitative power. The Branch inlets temperatures gave a more perfect similarity in both trend and magnitude, thus, the inlets temperature can be said to be successfully validated.

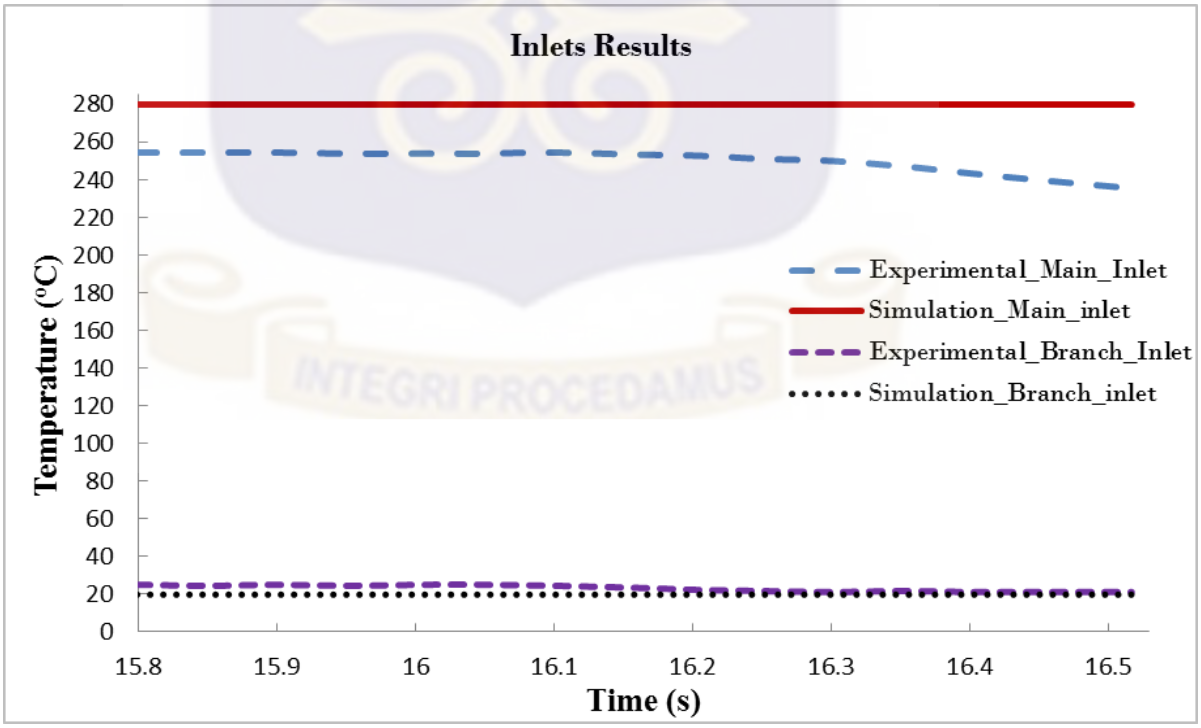

Figure 4.2 Plot of Inlets temperature of Main and Branch Pipes.

The shape of both curve of temperature distribution in the pipe wall look similar at the ***1D_6h_1.5mm*** for both results as seen in figure 4.3 which also confirms the qualitative prediction of the computation model employed. Temperature of the experiment at 15.8 seconds was at 222.6^{o}C which was maintained but slipped at about 16.1 seconds and continues the fall till the 16.5 seconds. But a little lower temperature of 205.6^{o}C of the simulation trend at the same commencement time of 15.8Seconds was noticed though was unsteady till it exceed the 16.1 second and a noticeable drop was then recorded at about 16.25, which translate to a 0.15 seconds later than the experimental curve. This disparities can be attributed to the iterations time step employed which can contribute to the longer time required per iteration and thus the delay experienced, However, 0.15 margine Seconds can be accepted as its within the truncation error as stated previously. Putting this stated factors in consideration, it can be said that the temperature distribution at the 1D_6h_1.5mm location is successfully validated with the experimental plot.

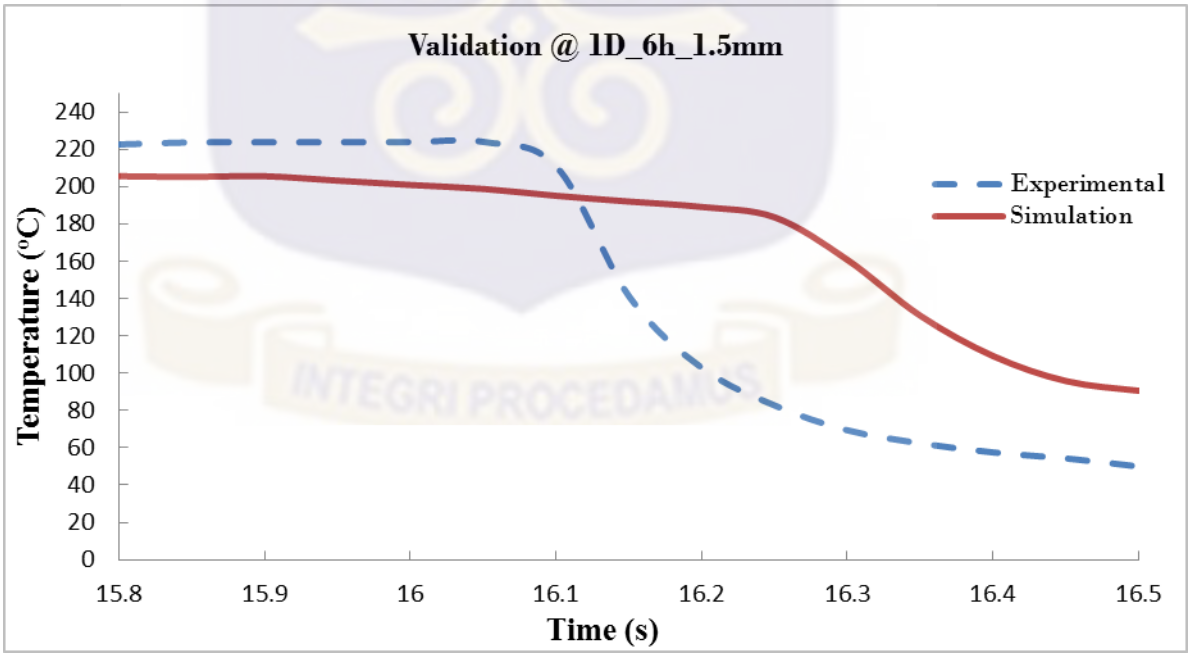

Figure 4.3 Temperature trend at 1D_6h_1.5mm

Similar to the validation case at the 1D_6h_1.5mm location, the experimental curve of 1D_9h_1.5mm again sustained its temperature till 16.1seconds before a sharp drop but unlike the previous validation case the simulation temperature began at a much closer temperature as the experiment but began a gradual drop all through to the 16.1 and experience a sharper drop from the 16.2 seconds and continue the fall further as presented in figure 4.4.

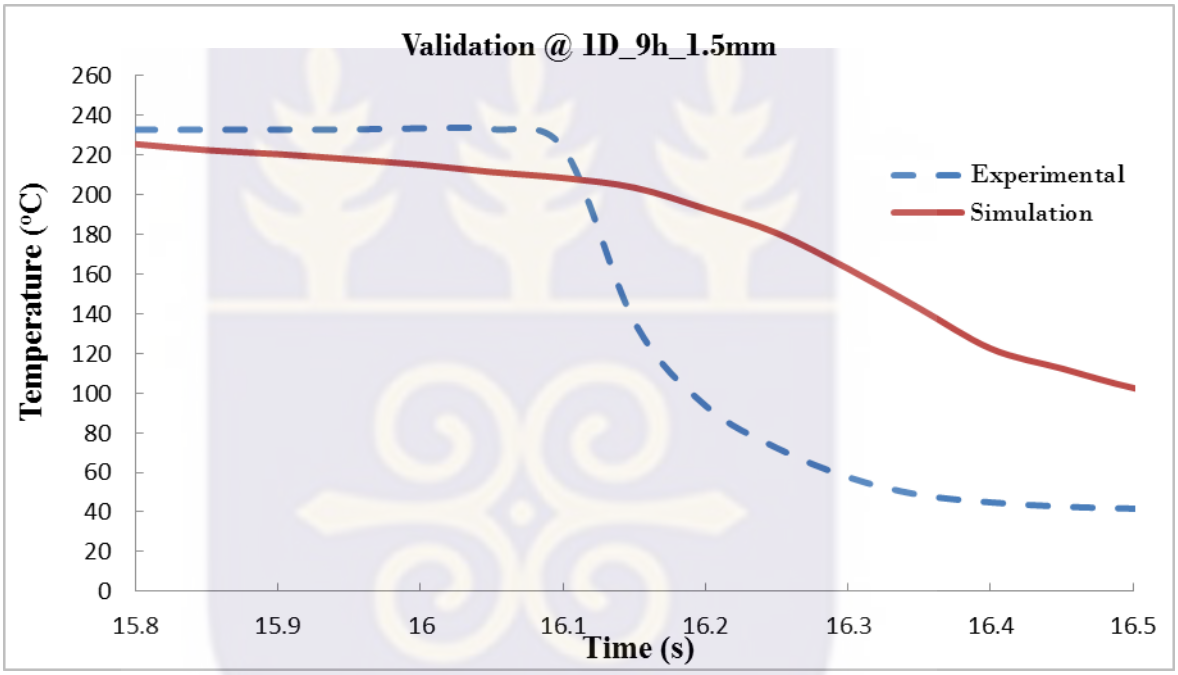

Figure 4.4 Temperature trend at 1D_9h_1.5mm

From the validation, the 9h-position in the experimental case appeared to be more affected by the cooling than the 6h-position on the very downside. This effect is discernible because the temperature at 9h decreases a little steeper than the temperature at 6h. A possibile reason could be a slight direction change of the cold flow when it already flows in the main pipe after it is turned round by the main pipe flow. From the

Experimental Setup of FSI test facility described in sub-section 3.2.1, it was stated that a split of flow occurred which was recycled back to the main flow. This phenomena was not captured in the simulation and thus could result to the gradual and longer period for a drop of temperature to occur as compared to the case in the experiment.

Turbulent K-Omega model has been used for validation thus applying same for further simulation will give to a large extend the true representation and solution of other flow scenarios, thus leads us to the next simulation case presented in section 4.5.

For the validation of results from the -1D_12h_1.5mm locations within the simulated time, there appeared a remarkable resemblance of both shape and magnitude of the upstream temperature results and this depicts agreement with the experiment as can also be seen in figure 4.5. The visualization from the 15.8seconds althrough to the 16.5seconds, the disparity between both plots can be related to the mesh sizes, the time step, and the quantitative computing accuracy of the adopted model.

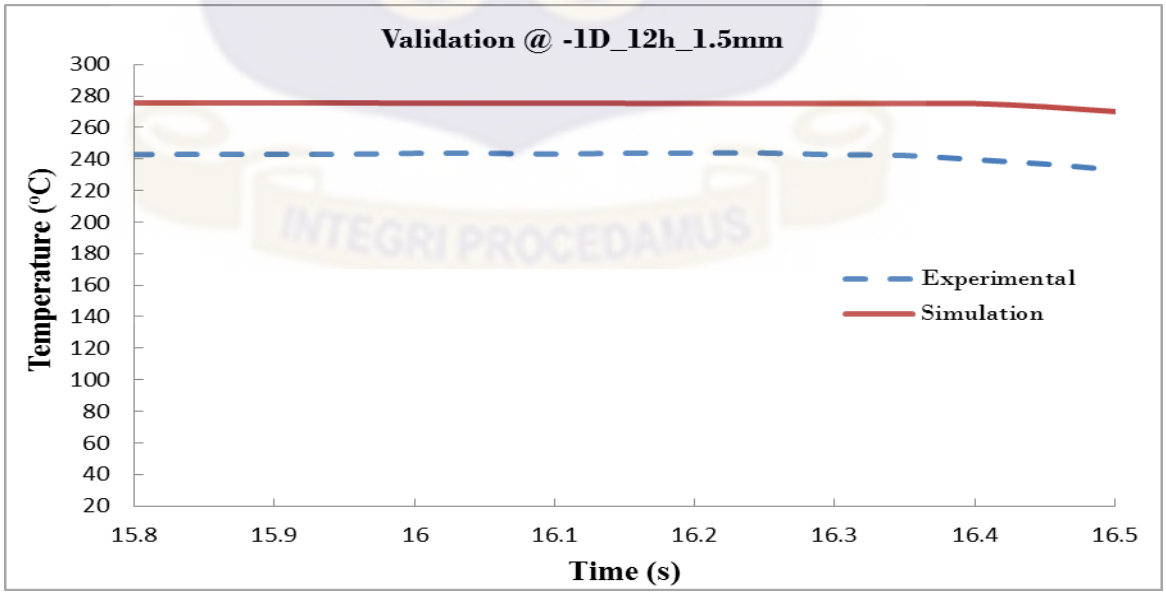

Figure 4.5 Temperature trend at -1D_12h_1.5mm

4.3 Simulation Flow Characteristics

Figure 4.6 reveal the flow pattern of the simulation in terms of temperatures distribution. The Hot flow from the main line with larger volume as compare to it mass flow rate experience stratification at the upstream prior to mixing with the vertical branch flow thus a temperature drop will be experienced just before mixing. Turbulence set s in after mixing leading to increase velocity and pressure with much kinetic energy which affect mixing at th e 1D location, but as the mixing goes further downstream more effective mixing was noticed at the tail end of the pipe. The thermo-fluid dynamics simulations also presume the back-flow effect of the branch flow for main pipe flow temperatures which is seen as a part of the branch pipe flow seems to flow in upstream direction.

The downstream flow is characterized by turbulence mixing movement and temperature movement induced by lateral momentum of the cold flow.

The distinct nature of the flow regimes was made possible by the already determined T-junction's mean temperature distribution. Thus, depending on the temperature differences of the mixing streams and the mass flow rate ratio of both the main and branch pipe, a penetration of hot fluid into the cold branch line of the T-junction can be observed.

Again, the upstream could also experience an inflow of stratified cold fluid from the branch line but not pronounce in the simulation .

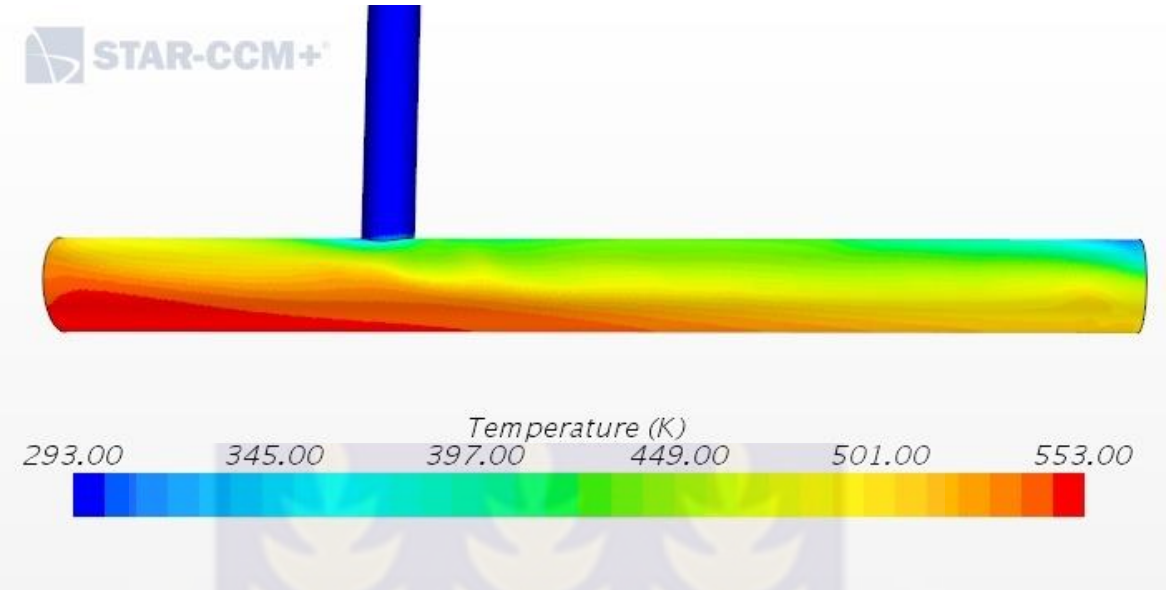

Figure 4.6: Temperature Profile of the T-junction for Case 1

4.4 SIMULATION ANALYSIS: CASE 2

For thermal fatigue, the main objective is to predict fluctuation of flow variable near to the wall boundary. SST K- ω turbulent model prediction in the neighborhood of the wall boundary observed was appreciable in relation to the experimental observation thus after a successful validation was carried out, another simulation was conducted where the hot fluid is now loaded in the branch pipe and cold flow channeled via the main pipe, this interchange or reorientation was necessary so as to further investigate another possible reactor scenario. The Liquid Scene at a point during the iteration is displayed in figure 4.7

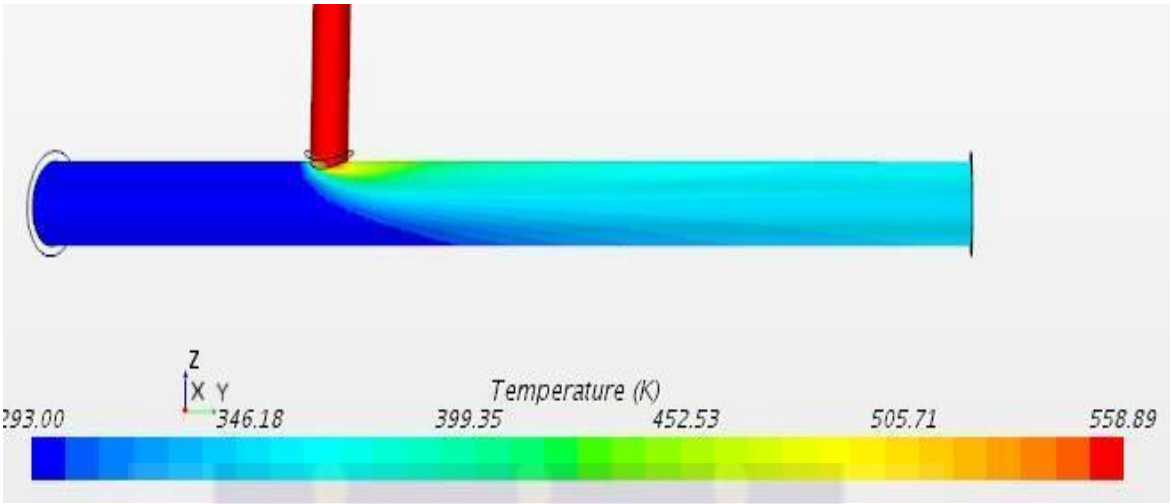

Figure 4.7 Temperature Profile of the T-Junction for Case 2

From the case 2 simulation, two category of analysis was performed, namely:

- Heat Transfer from Liquid to solid,
- Heat Transfer within the pipe.

4.4.1 Heat Transfer from Fluid to Solid

Fluid temperature fluctuation caused by mixing are transported to the structure when mixing happen near the pipe wall boundary and this detail is important in fatigue analysis. Figure 4.8 shows temperature distribution from the fluid body to the solid structure obtained at various positions downstream the pipe. In these locations the flow appeared stratified as it was observed that the cold fluid flows on the bottom of the pipe while the hot water flows above it but higher percentages at the mixing regions as compared to other part meaning intense heat was transferred to the solid at the mixing region (locations 1D and 2D) and decreases as compared to other location downstream. This implies that much stress will act on the mixing region that experienced the temperature flunctuation coused by the mixing of hot and cold..

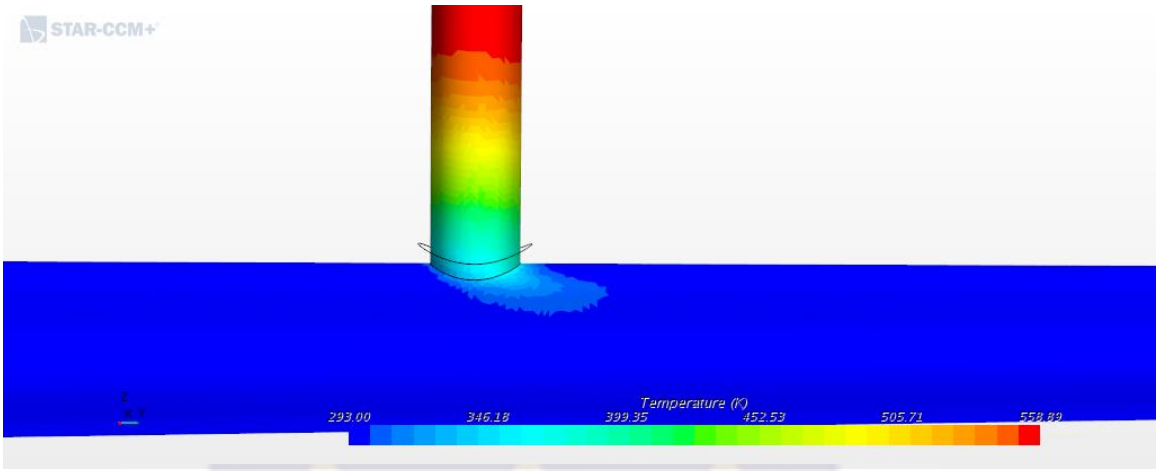

Figure 4.8 Flow pattern at onset of hot stream

At the onset of hot fluid from the branched pipe shown in Figure 4.8, the hot fluid was swept by the cold fluid towards the upper boundary of the horizontal pipe downstream especially at 1D location of the mixing zone. At this zone, the upper boundary registered a higher temperature than what was observed at the bottom of the tube. This implied more effective flow mixing along the channel due to the mass flow rate of the main pipe.

The maximum and minimum temperatures detected by Probes at the 1D and 7D points in the fluid were about 39°C, 170°C and 69°C, 82°C respectively, this can be visualize in Figure 4.9b. This temperature difference at the mixing points where there is no uniformity of temperature distribution in the pipe, the uneven temperature distribution may generate thermal stress at the mixing region.

Comparing the mixing profile (Figure 4.9a) and plots of temperature distribution (Figure 4.9b) for the 1D to that at 7D shows clearly the differences in the heat transferred.

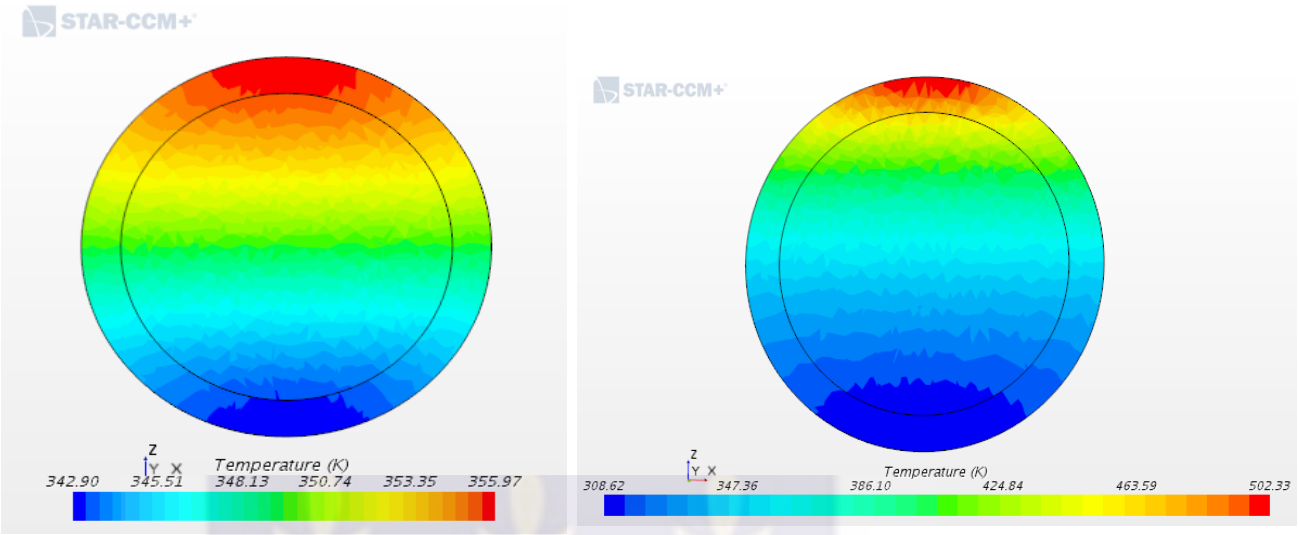

Figure 4.9a Profile of Temperature Distribution at (a) 1D (b) 7D

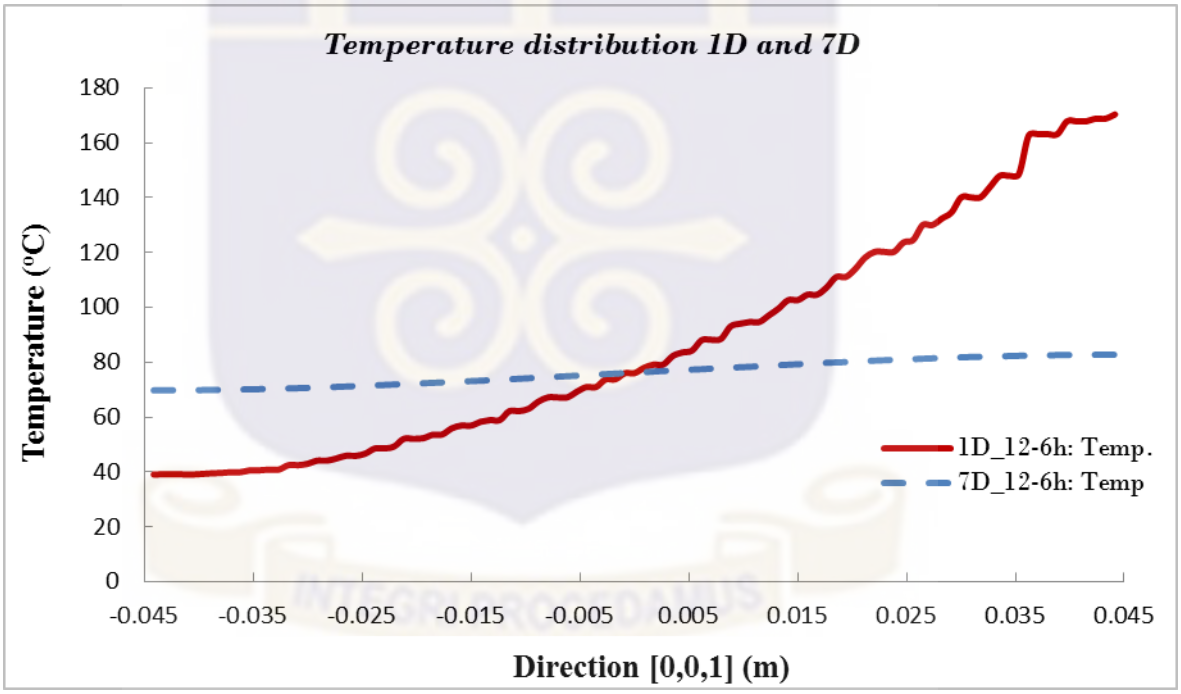

Figure 4.9b Plot of temperature distribution at both the 1D and 7D (6-12h) Location

Position 1D is the point just after the branch flow touches the main flow while position 7D is the last point where probe is inserted at the tail end of the downstream pipe for measurement as mixing tends to uniformity. All trends and profile of temperature variations in other locations downstream are presented in ***Appendix II.*** The temperature at 1D location rises from value close to the inlet temperature at the bottom of the pipe and rise appreciably to the center and a further increase to the upper section of the pipe this reveal the high temperature difference of about 130^{o}C. Downstream at the 7D location, the minimal temperature at the bottom was close to what was experience at the upper section of the pipe with just about 15^{o}C, which confirms that effective mixing took place towards the exit of the main flow channel.

4.4.2 Heat Transfer within Structure

To clearly understand the thermal load induced in the solid structure, the Upper section of the pipe under consideration was divided into layers with the first 5layers closer to the inner wall while the second group of 5layers termed the outer wall. For each layer probes was inserted from the pipe intersection downstream as shown in Figure 4.10.

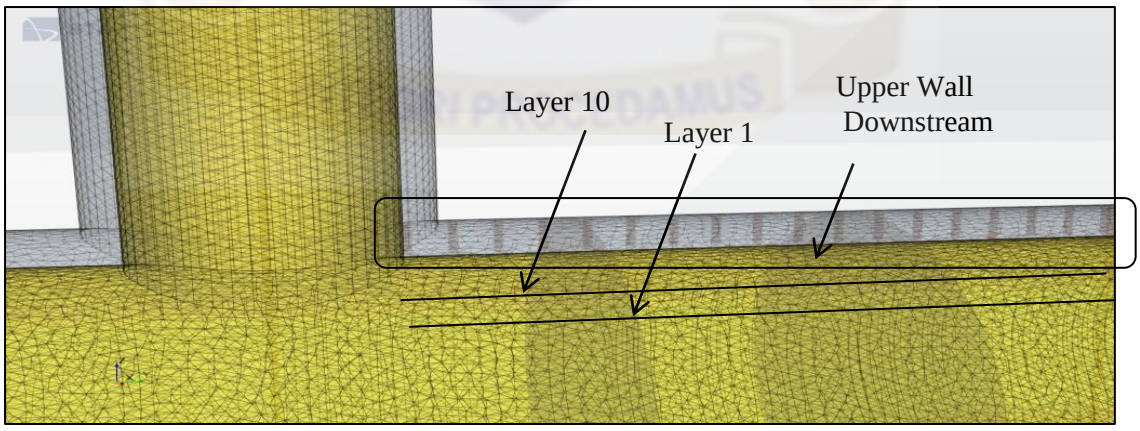

Figure 4.10 Upper wall divided into layers

A comparatively high temperature was recorded at the upper section of the pipe (layer10) closer to the out wall which was as a result of heat transfer by conduction from the high temperature of the incoming branch fluid to the solid structure met and not the effect of temperature fluctuation in the mixing channel. This high temperature recorded at the layer closer to the outer wall as can be deduced from comparing both plots (layer 1, layer 10) will over time narrows down to maintain thermal equilibrium along the wall. Plots of the entire temperature variation within the layers in the structure can be seen in ***Appendix III.***

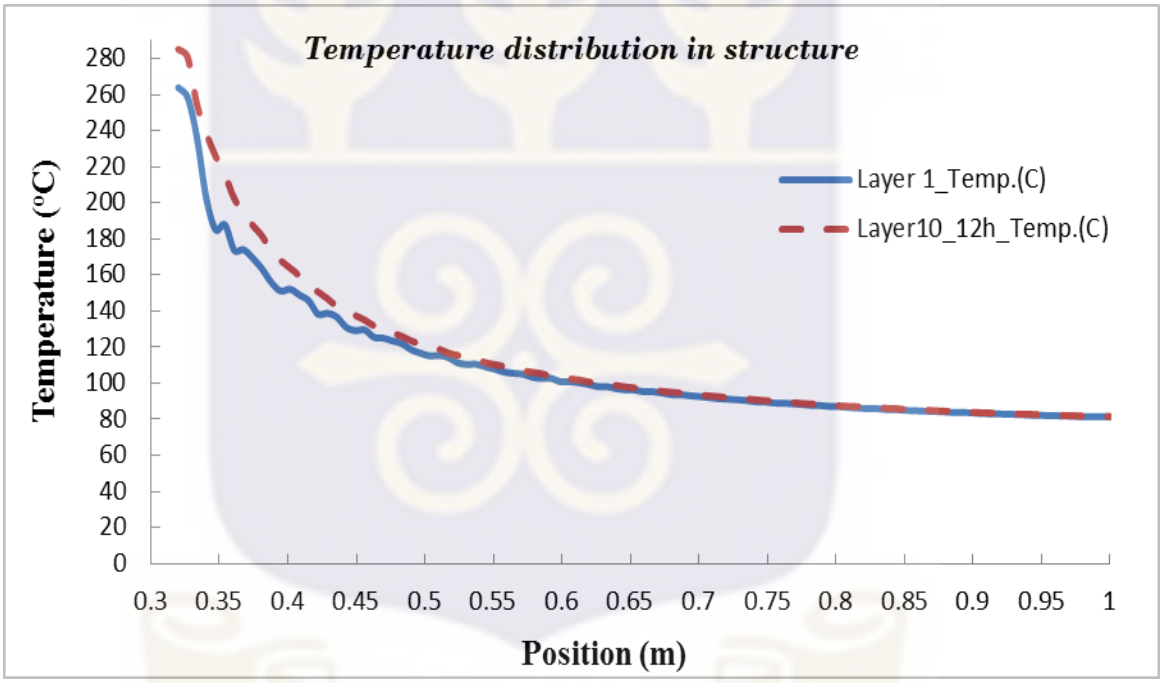

Figure 4.11 Plot of Temperature distributions at inner and outer wall

From the plot shown in Figure 4.11, it could be said that at the mixing region, there is a temperature difference between the inner and outer layer. The inner wall was exposed to a higher temperature as compared to the outer wall. Overtime, this temperature difference between the layers narrows down to confirmed that there exist gradual transfer of heat within the structure. Further downstream, not much of this phenomenon is noticed which

was as a result of thermal equilibrium at which the mixing is tending to which leads to reduced temperature difference.

4.5 Effects of Other Parameters

There are various other factors contributing to thermal fatigue such as Velocity of fluid, Mass flow rate, Pressure Distribution. These factors were also investigated and analyzed.

4.5.1 Velocity Distribution

The simulation results were visualized and the fluid velocity distribution downstream the mixing junctions are shown in Figures 4.12a

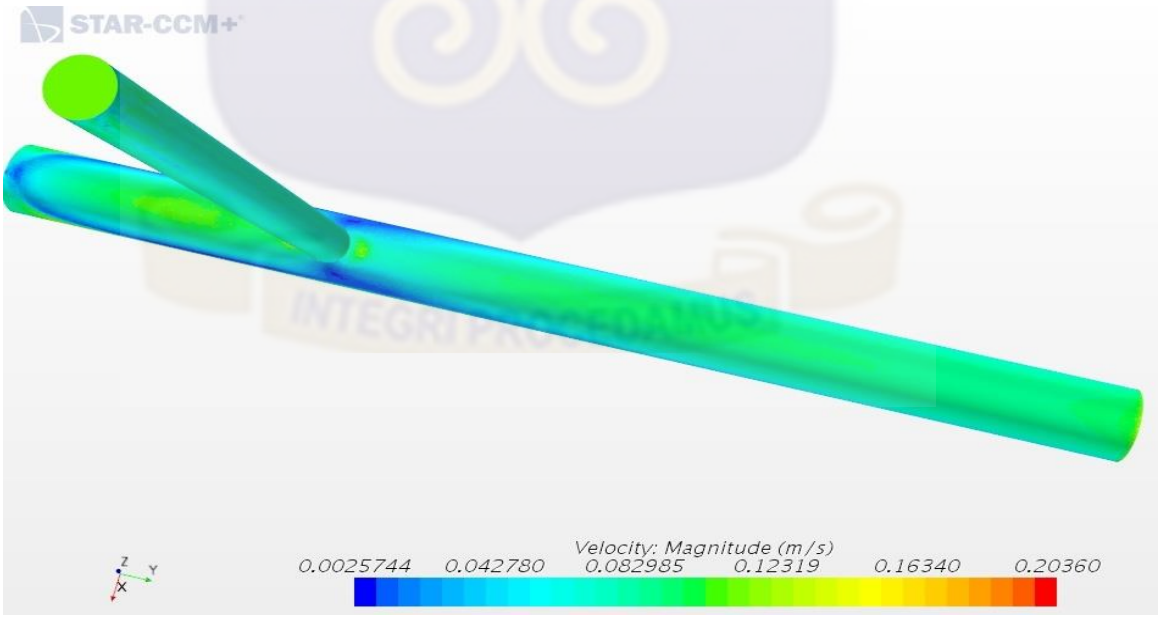

Figure 4.12a Velocity Profile of the T-junction

It can be deduced that, rapid velocity is seen at the upper wall in the 1D location this leads to faster heat transfer towards the pipe wall generating temperature buildup in this location than the 7D location also rapid mixing takes place in the main flow and heat transfer from the hot fluid to the cold fluid will be effective leading to the attainment of thermal equilibrium and hence reduced buildup of temperature at the wall boundary

At the mixing region, the influence of the mixing phenomena was also seen as velocities were of higher magnitude compared to velocity magnitudes at positions further downstream the flow channel.

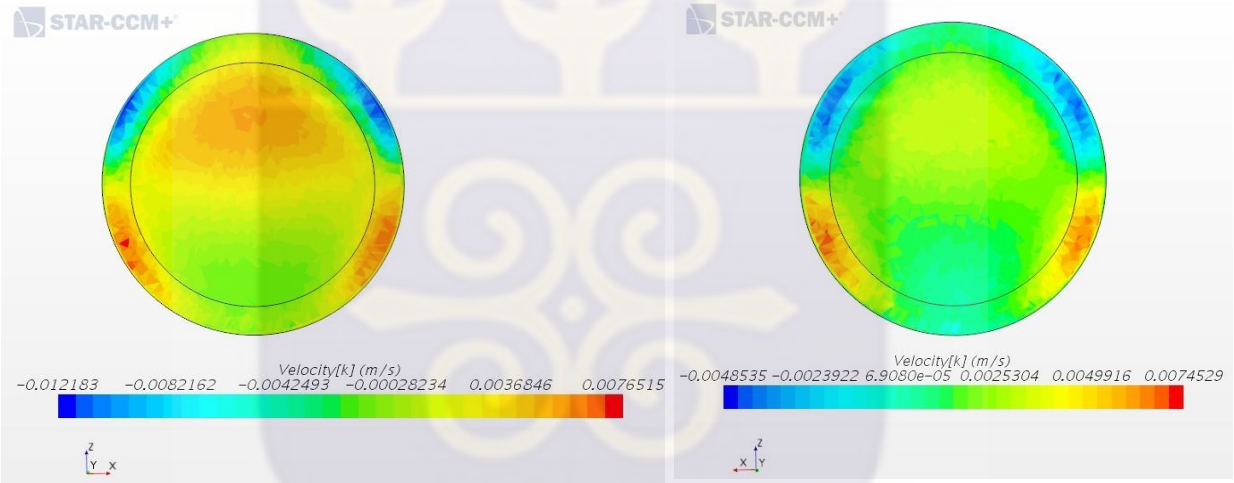

Figure 4.12b Velocity Profile @ 1D and 7D

It is shown in figure 4.12b and (as well as ***Appendix III***) that for the simulations, moving downstream the mixing junction, the velocity magnitude decreased and the highest velocity shifted from the wall boundary towards the main flow thereby leading to uniform mixing in the bulk flow. Thus, the higher velocities at the wall boundary in the velocity profile of figure 4.15a means an increase in the heat transfer from the main fluid flow to the wall boundary especially for the 1D_6-12h location (Figure 4.12b), the flow

streams will not have sufficient time to mix and there will be higher temperature buildup at the wall boundary. The longer the time for impeccable mixing to uniformity to occur the more temperature flunctuation will be experience and subsequently the more stress generated that will lead to thermal fatigue.

4.5.2 Pressure Distribution

In order to analyze the mechanism of thermal fatigue, the pressure distributions downstream the mixing junction of the simulations were studied. Figure 4.13a is the comparison of pressure distributions along the centerline in the main flow direction from the mixing junction to the main outlet. The pressure profiles were obtained in the simulations at 1Dh and 7Dh axial distance of the main flow channels.

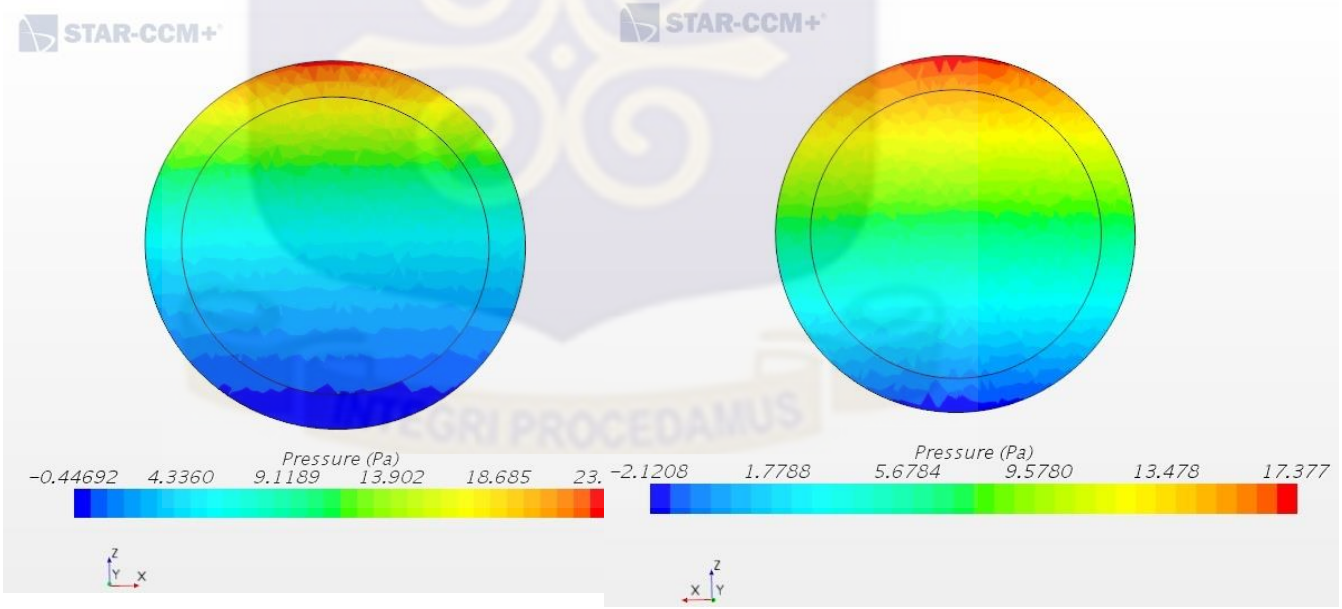

Figure 4.13a Pressure profile @ 1D and 7D

The profile indicates that higher pressure of both streams was recorded at the mixing junction and drops further downstream. The pressure drop in the mixing process are as a result of momentum exchange, friction and heat exchange. The quality of mixing reflects the interaction intensity between the two flows and is related to the pressure drop, the better the mixing effect, the higher the pressure drop. Confirming Kockmann (2007) observation that effective mixing is achieve by the magnitude of the drop in the pressure of the mixing fluid in the tube. It can be inferred that, the branch flow made remarkable effect in pressure and energy loss as shown in the plot of Figure 4.13b recording about -30MPa of pressure drop reason because the liquid velocities entering the main channel was constant prior to mixing . The intensity of mixing decreases as the liquid flows downstream and the pressure along the centerline begins to stabilize.

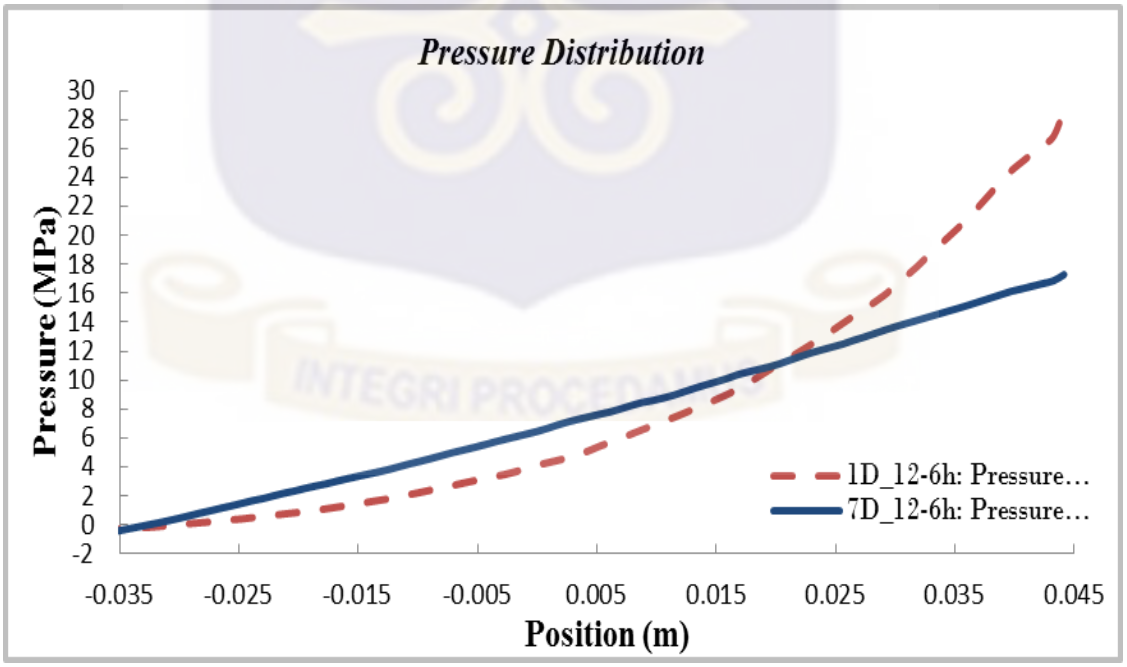

Figure 4.13b Plot of pressure distribution at 1D and 7D

4.5.3 Turbulent Kinetic Energy

The turbulent mixing of hot and cold water was characterized by fast and highly irregular fluid movements. These fluctuations raises the energy transfer rate at the mixing region as compare to the last (7D) measured position. Turbulence is linked with irregular fluctuations and the fluid motion takes place on several length scales.

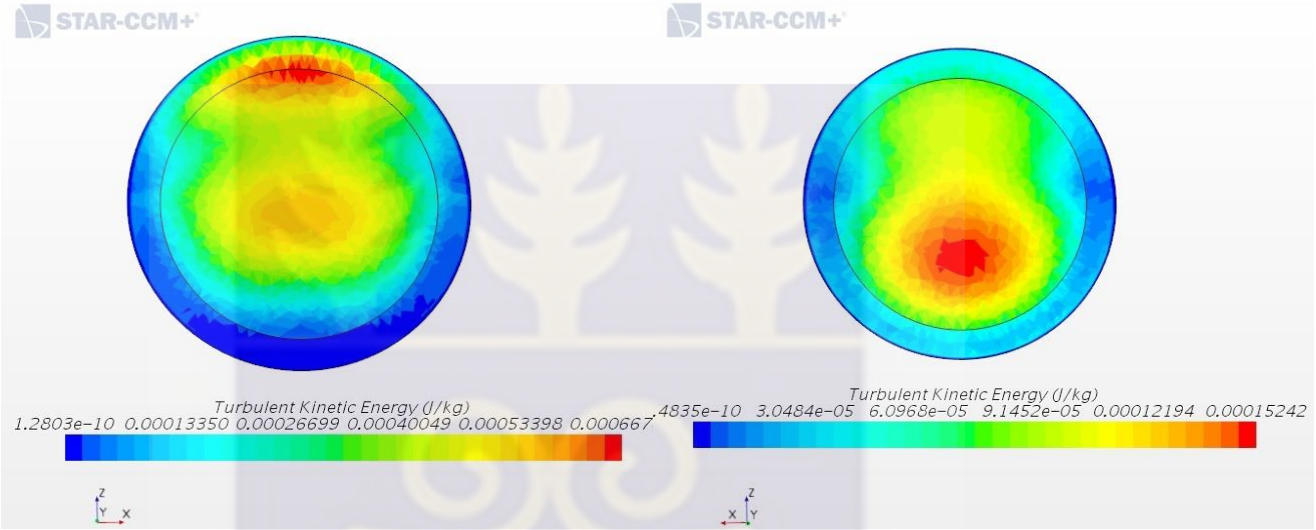

Figure 4.14a TKE profile @ 1D and 7D

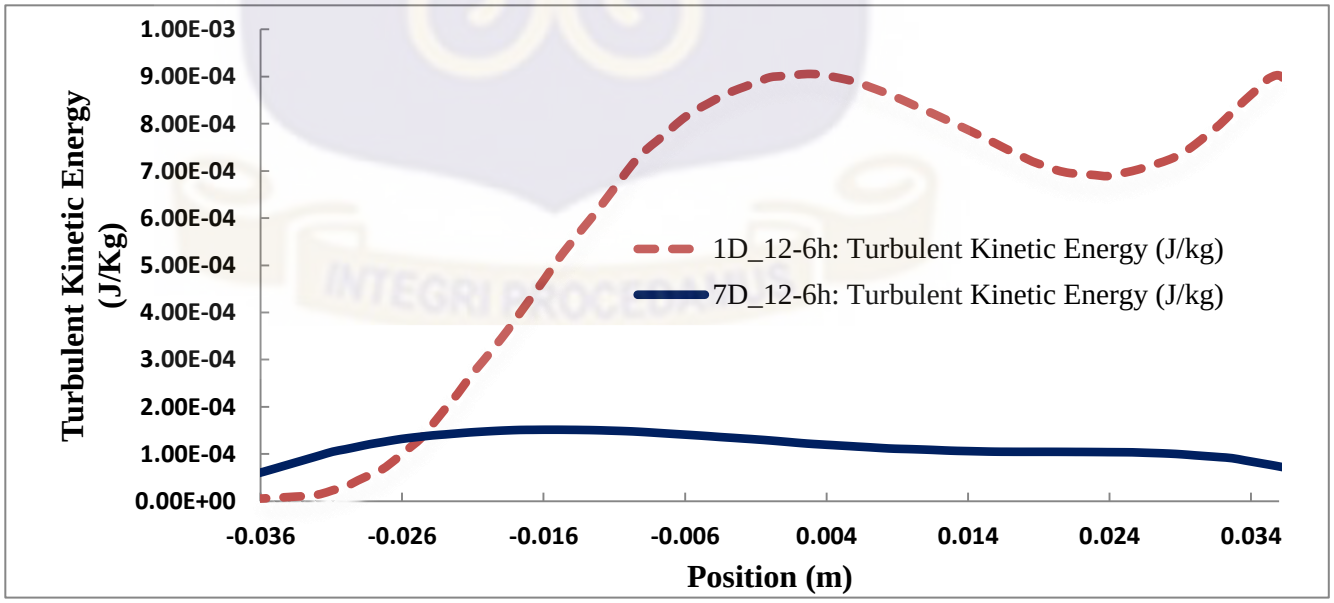

Figure 4.14b Plot of Turbulent Kinetic Energy at 1D and 7D

From the visualization in Figure 4.14a and 4.14b, it is seen that turbulent kinetic energy is experience at the 12h of the 1D location thus the very high difference in turbulence kinetic energy agrees that more heat moved rapidly from the fluid at the lower wall boundary towards the upper wall boundary as visible in the 1D_12-6h location as compare to the 7D_12-6h location. With the high difference in TKE experience at the mixing region (1D_12-6h location), it can be said that more stress will act at this location compare to other location in the pipe.

4.5.4 Density Difference

Another safety relevant issue is higher density differences which causes longer mixing lengths because longer piping sections are affected by intensely inhomogeneous temperature distributions. The differences in density (between main and branch fluids) results in a weakly or completely unmixed fluids in high concentrations much closer to the mixing region.

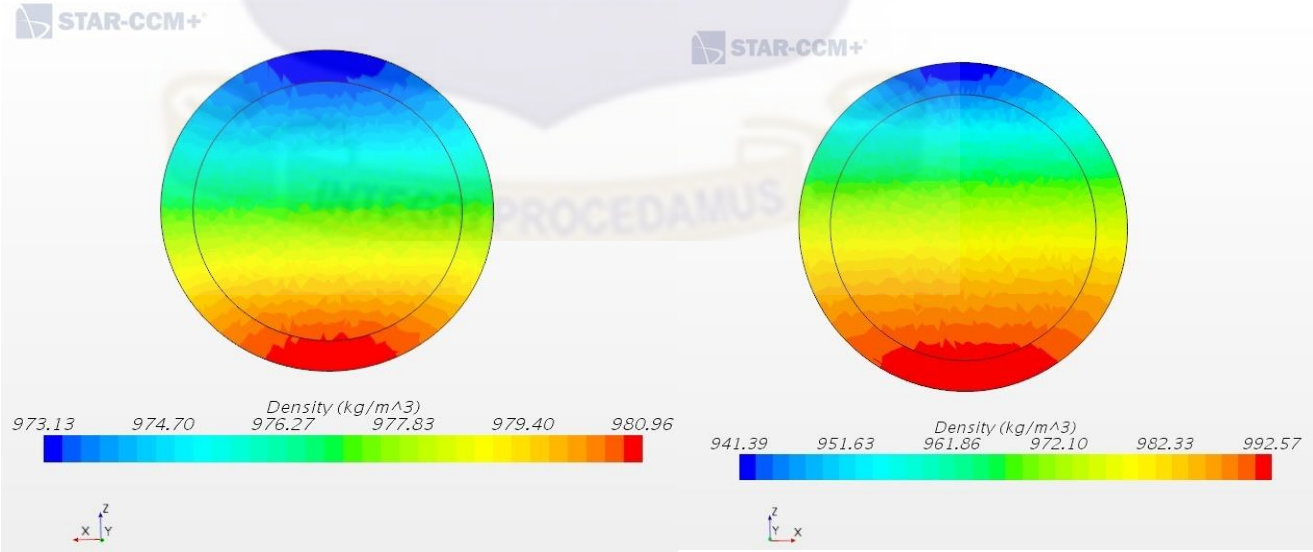

Figure 4.15a Density profile at 1D and 7D

Density trend from Figure 4.15a indicates that the 1D location experience a drop of flow density from the bottom of the pipe through the center to the upper part which implies that the thermal fluctuation in this location will be easily sweep towards the much denser point thus accumulation of heat at the upper wall boundary is eminent. This phenomenum, similar to the velocity distribution discussed earlier causes the flow streams not to have sufficient time to mix, and the more time it takes to mix the more temperature flunctuation will be experience and subsequently the more stress generated that will lead to thermal fatigue. Figure 4.15b shows the correspond plot of density variation at 1D and 7D location

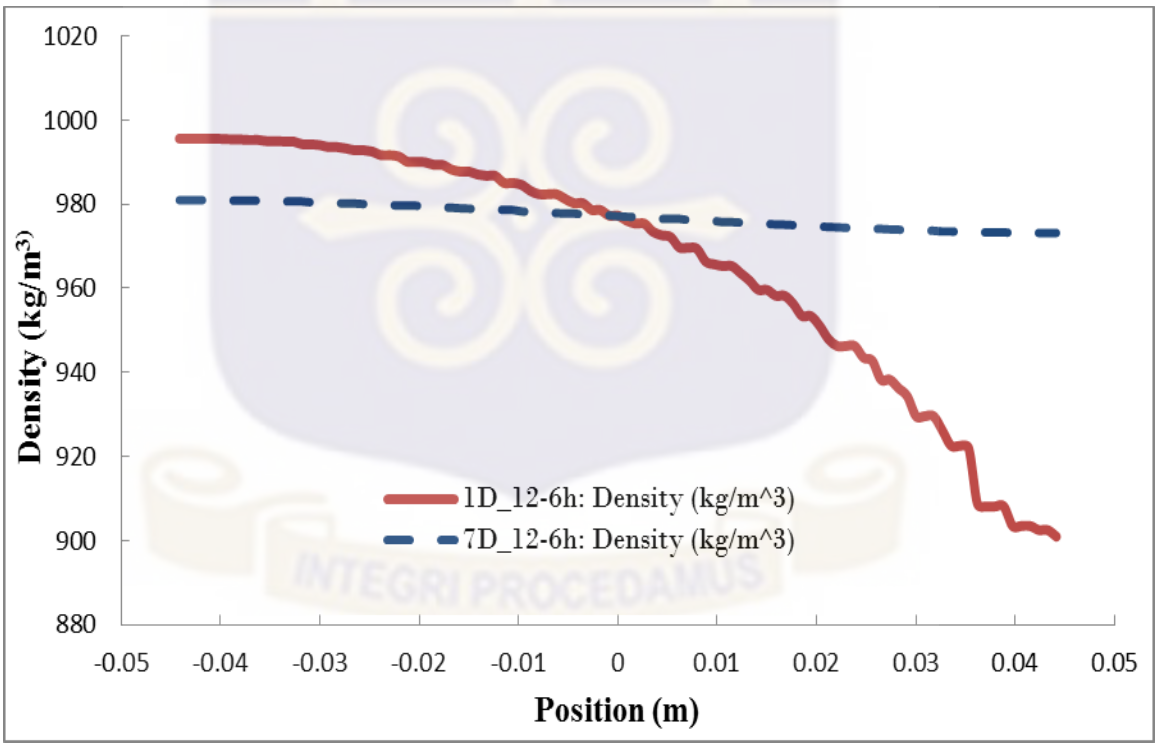

Figure 4.15b Plot of Density Variation at 1D and 7D

4.5.5 Thermal Conductivity

The rate at which heat passes through the pipe material in the 1D location is significantly greater than what was obtainable at the last location within this study, this shows that the extent of heat that runs through the structure per unit time through a unit area with a temperature gradient of one degree per unit distance as a result of thermal mixing within the simulation time is high enough to induce more stress at the 1D location than locations downstream. In as much as this is a normal situation this section is to confirm the effect of thermal conductivity in the flow channel and from the profile and corresponding plots of this difference is shown in figure 4.16a and 4.16b, this disparity was clearly shown.

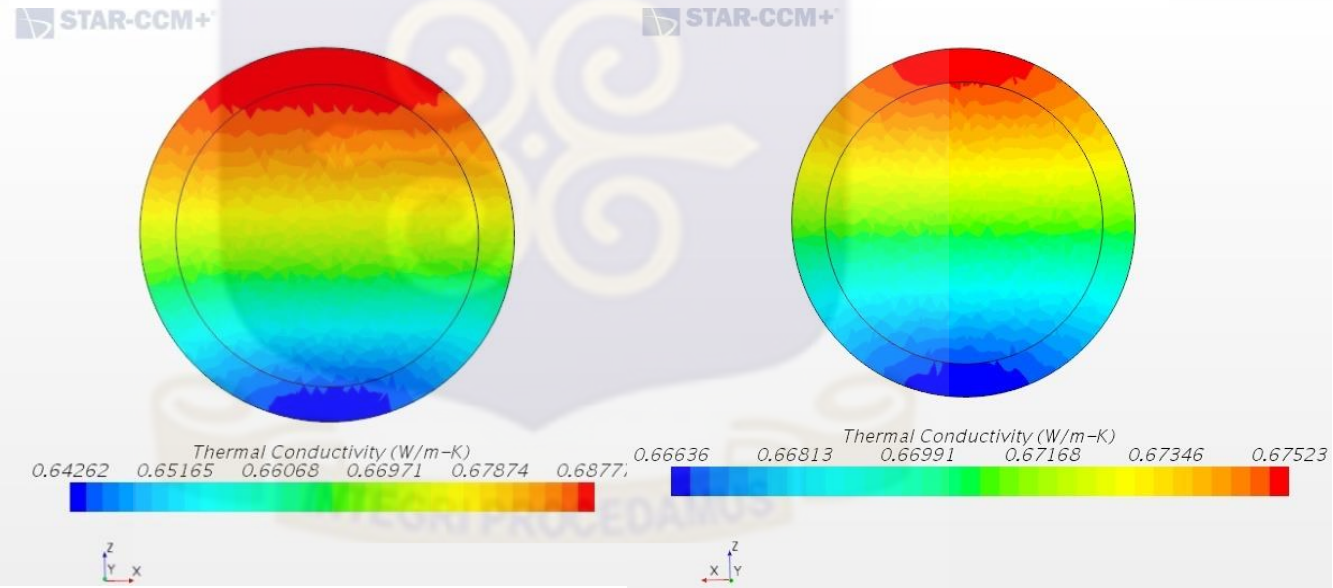

Figure 4.16a Thermal conductivity profiles @ 1D and 7D

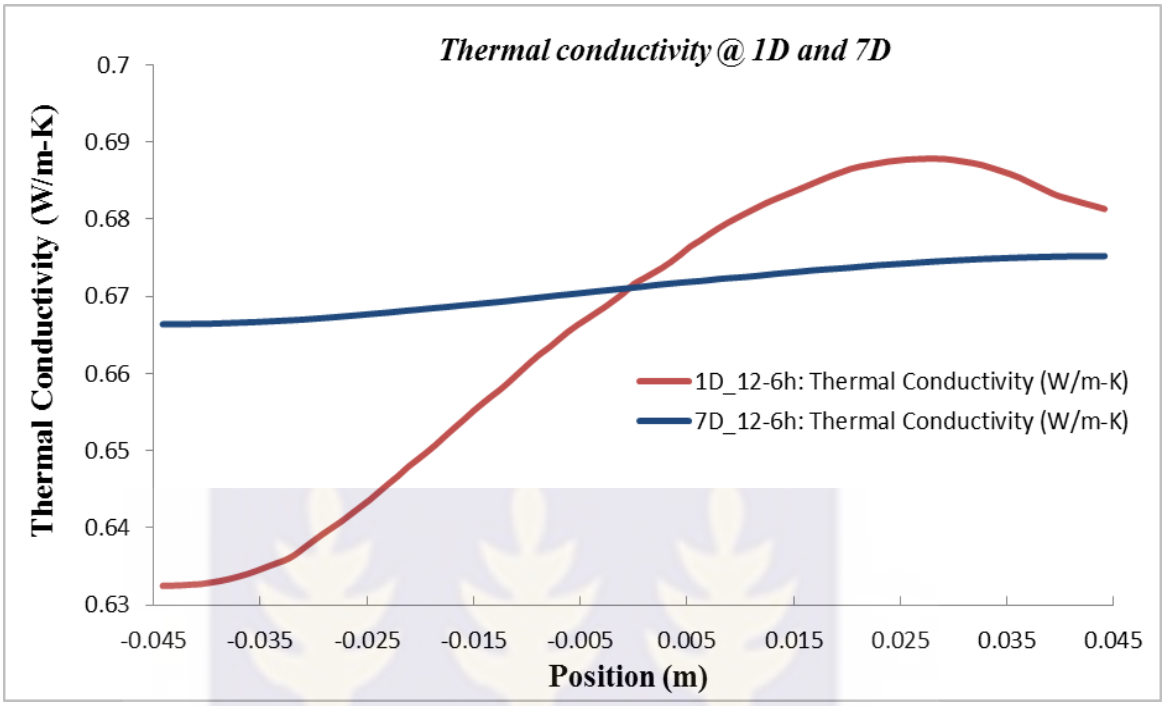

Figure 4.16b Plot of thermal conductivity at 1D and 7D

CHAPTER FIVE

CONCLUSIONS AND RECOMMENDAIONS

5.1 Conclusions

In conclusion, the numerical simulations of thermal analyses of fluid – solid interaction contributing to thermal fatigue in mixing junctions of vertical branch pipe and validation of results with experiment studied was carried out. The simulations were conducted using SST k-omega turbulence model in STAR-CCM+. The following conclusions were drawn:

- Experimental review and numerical simulation (thermo-fluid dynamics simulations) of thermal mixing of Hot and Cold liquid flows in a T-junction / piping configuration was carried out. The fluid-structure interactions test facility FSI (closed flow loop) for thermal fatigue investigations of thermal mixing of fluid in a T-junction was successfully implemented. The special features of the test facility are that the design is oriented on typical geometrical dimensions and thermo-hydraulic operating condition of nuclear power plants (main / branch line piping diameters DN80 / DN40, maximum pressure 75 bar, maximum temperature 280°C.

- The CFD simulations visualized results show that the thermo-fluid dynamical modeling of a T-junction mixing flows with the SST K-Omega turbulent model is feasible and suitable to describe adequately the thermal fluctuation phenomena of mixing flows and the fluid-structure interactions. The general findings of the

experiments could be confirmed. Therefore, the simulation results are very helpful as input data for thermal fatigue analyses in structural mechanics studies.

- The comparison of the Temperature distribution near the wall indicates that the heat transfer to the wall boundary in the mixing region (0.5D, 1D and 2D) as a result of temperature fluctuation caused by thermal mixing is much higher than that in other location downstream pipe. This implies that effective mixing of cold and hot fluid which led to reduced and uniform temperature field at the pipe wall boundary, were achieved towards the 7D position of main flow pipe, hence lower stress levels could be observed in the structural material of the pipe and the wall at the mixing region will be more liable to structural degradation.

- There is greater pressure drop at the point where two fluid streams meet, the higher the pressure drop the better the mixing effect because more energy is consumed in the process. The quality of mixing reflects the interaction intensity between the two flows and is related to the pressure drop. The mixing phenomena at the mixing zone causes differences in pressure and energy loss because, the liquid velocities entering the main channel was constant for both simulations while pressure drop decreases downstream which lead to effective mixing. Effective mixing that was attained lead to reduced and uniform temperature field at the pipe wall boundary and hence lowers thermal stress levels in the structural material downstream.

- The 1D location recorded the highest velocity magnitude in the main flow indicating that, rapid mixing takes place in the main flow and heat transfer from the hot fluid to the cold fluid is effective thereby leading to the attainment of thermal equilibrium towards the 7D location and exit of the pipe. The effect of higher velocity gradient near the wall boundary of the horizontal (main) pipe is highest thus leading to temperature buildup at the wall boundary. This is due to insufficient time for the different flow streams to mix

- Result of analysis carried out proved that the parameters analyzed (Pressure, Velocity, Turbulent Kinetic Energy, Thermal Conductivity, Mass flow rate) all contribute to thermal fatigue and their effects is directly proportional.

- Star-CCM+ provides a very useful technique for modeling of fluid-structure interactions and for validation purposes thus capable of further simulations in thermal fatigue studies related to flow stratification effects with unsteady heat transfer phenomena.

5.2 Recommendation

- For determination of stresses induced in the solid material as a result of the temperature fluctuation, it will be recommended that Finite Element Mechanics feature in STAR-CCM+ be harnessed and implemented to bring finality to this research.

- A structural mechanics code such as Reactor Vessel Code and ASME Boiler can as well be acquired by the Nuclear Engineering Department to facilitate further study of the gradual degradation mechanism.

- This research though considered two different orientations of fluid inlets in a T-Junction, other possible layout or setup may be considered. And further work on other mixing joints of reactor cooling system can be carried out.

- Though a much higher temperature was considered in this research, temperatures of other PWR and BWR especially the operating temperatures relating to the upgraded VVER-1200 (Version 491) reactor and the supercritical reactors can also be investigated.

REFERENCES

[1] Walker, C., Simiano, M., Zboray, R., Prasser, H. M., 2009. Investigations on mixing phenomena in single-phase flow in T-junction geometry. Nuclear Engineering and Design 239, 116 – 126.

[2] Nakamura, A., Utanohara, Y., Miyoshi, K., & Kasahara, N. (2015). A Review of Evaluation Methods Developed for Numerical Simulation of the Temperature Fluctuation Contributing to Thermal Fatigue of a T-junction Pipe, 6, 118–130.

[3] Prawoto, Y. (2013). *Solid Mechanics for Materials Engineers* - Principles and Applications of Mesomechanics. Lulu.com. Retrieved from https://books.google.com/books?id=Z98HBgAAQBAJ&pgis=1

[4] W. Häfner and J. H. Spurk, "Formation of Waves in Thermal Stratified Flow," In: Proc. of the International Conference on Physical Modeling of Transport and Dispersion, Cambridge, U.S.A., (1990).

[5] Velusamy, K., Natesan, K., Selvaraj, P., Chellapandi, P., Chetal, S. C., Sundararajan, T., & Suyambazhahan, S. (2006). CFD Studies in the Prediction of Thermal Striping in an LMFBR. In Proc. *CFD4NRS Conference*, Garching, Munich, Germany.

[6] Batchelor, G. (2000). *Introduction to Fluid Mechanics*

[7] Eames, I.; Flor, J. B. (January 17, 2011). "New developments in understanding interfacial processes in turbulent flows". *Philosophical Transactions of the Royal Society A*. doi:10.1098/rsta.2010.0332.

[8] Jayaraju, S. T., Komen, E. M. J., & Baglietto, E. (2010). Suitability of wall-functions in large eddy simulation for thermal fatigue in a T-junction. Nuclear Engineering and Design, 240(10), 2544-2554.

[9] Hu, L. W., Kazimi, M. S., 2006. LES benchmark study of high cycle temperature fluctuations caused by thermal striping in a mixing tee. International Journal of Heat and Fluid Flow 27, pp. 54 – 64.

[10] Course 228 – Module 3 - Selection and Specification of Materials for Nuclear Applications.

[11] E. Paffumi, K.-F. Nilsson and N. G. Taylor, "Simulation of thermal fatigue damage in a 316L model pipe component," *International Journal of Pressure Vessels and Piping* 85, pp. 798–813 (2008).

[12] P. R. Huebotter, "Report of the National Task Force on Thermal Striping in LMFBRs," 1978.

[13] J. E. Brunnings, "LMFBR thermal-striping evaluation," 1982.

[14] S.Chapuliot, C. Gourdin, T. Payen, J. P. Magnaud and A. Monavon, "Hydro-thermal-mechanical analysis of thermal fatigue in a mixing tee," *Nuclear Engineering and Design* 235 (*5*), pp. 575-596 (2005).

[15] Peniguel, C., Sakiz, M., Benhamadouche, S., Stephan, J. M., Vindeirinho, C., 2003. Presentation of a numerical 3d approach to tackle thermal striping in a PWR nuclear T junction. ASME PVP

[16] B. Lydell and J. Riznic, "OPDE—The international pipe failure data exchange project," *Nuclear Engineering and Design* 238 (*8*), pp. 2115-2123 (2008).

[17] Aulery, F., Toutant, A., Monot, R., Brillant, G., & Bataille, F. (2010). Numerical simulations of thermal fatigue due to turbulent fluctuations in a mixing tee. In Proc. 16th *International Solar Paces Concentrating Solar Power Symposium* (pp. 21-24).

[18] Pasutto, T., Peniguel, C., Sakiz, M., 2005. Chained computations using an unsteady 3d approach for the determination of thermal fatigue in a tjunction of a pwr nuclear plant. International Congress on Advances in Nuclear Power Plants.

[19] Howard, R. J. A., Pasutto, T., 2009. The effect of adiabatic and conducting wall boundary conditions on LES of a thermal mixing tee. NURETH-13.

[20] Westin, J., Mannetje, C., Alavyoon, F., Veber, P., Andersson, L., Andersson, U. Eriksson, J., Henriksson, M., Andersson, C., 2008. High-cycle thermal fatigue in mixing tees. large eddy simulations compared to a new validation experiment. ICONE16.

[21] Nakamura, A., Oumaya, T., 2009. Numerical investigation of thermal stripping at a mixing tee using des. NURETH-13.

[22] L.-W. Hu and M.S. Kazimi. 2006. LES benchmark study of high cycle temperature fluctuations caused by thermal striping in a mixing tee. International Journal of Heat and Fluid Flow, 27(1):54–64

[23] V.S. Naik-Nimbalkar, A.W. Patwardhan, I. Banerjee, G. Padmakumar, and G. Vaidyanathan. 2010. Thermal mixing in T-junctions. Chemical Engineering Science, 65(22):5901–5911

[24] H. Ayhan and C.N. Sökmen. 2012. CFD modeling of thermal mixing in a T-junction geometry using LES model. *Nuclear Engineering and Design*, 253:183–191.

[25] S. Qian, S. Kanamaru, and N. Kasahara. 2015. High-accuracy CFD prediction methods for fluid and structure temperature fluctuations at T-junction for thermal fatigue evaluation. *Nuclear Engineering and Design*, 288:98–109.

[26] S. Qian and N. Kasahara, "Large Eddy Simulation Analysis of Fluid Temperature
Fluctuations at a T-junction for Prediction of Thermal Loading," *Journal of Pressure Vessel Technology* 137, (2015)

[27] H. Tinoco, A. Darelius, E. Bernerskog, and H. Lindqvist. 2009. Forsmark 3 – time dependent flow simulations of the mixing process between crud and bypass flows inside the control rod guide tube. Technical Report FT-2008-3425, Forsmark.

[28] B. L. Smith, J. H. Mahaffy and K. Angele, "A CFD benchmarking exercise based on flow mixing in a T-junction", Nuclear Engineering and Design 264, 80-88 (2013).

[29] X. Schuler, E. Laurien, K.H. Herter, S. Moogk, D. Klören, R. Kulenovic, and M. Kuschewski. 2012. Thermal fatigue: fluid–structure interaction at thermal mixing events. In *38th MPA Seminar:"Energieerzeugung und Energieeffizienz -Werkstoffe und Bauteilverhalten"*.

[30] A. Sakowitz, M. Mihaescu and L. Fuchs, "Effects of velocity ratio and inflow pulsations on the flow in a T-junction by Large Eddy Simulation," *Computers & Fluids* 88, pp. 374–3b (2013).

[31] H. Kamide, M. Igarashi, S. Kawashima, N. Kimura and K. Hayashi, "Study on mixing behavior in a tee piping and numerical analyses for evaluation of thermal striping," *Nuclear Engineering and Design* 239 (*1*), pp. 58-67 (2009).

[32] Assessment of Computational Fluid Dynamics (CFD) for Nuclear Reactor Safety Problems, NEA/CSNI/R(2007)13," O. N. E. Agency, 2008.

[33] J.P. Simoneau, J. Champigny and O. Gelineau, "Applications of large eddy simulations in nuclear field," *Nuclear Engineering and Design* 240 (*2*), pp. 429-439 (2010). 152

[34] Ayhan, H., & Sökmen, C. N. (2013). CFD Modeling of Thermal Mixing In T-junction: Effect of Branch Pipe Diameter Ratio. The 15th

International Topical Meeting on Nuclear Reactor Thermal - Hydraulics, NURETH-15, Pisa, Italy.

[35] G. Grötzbach and M. Wörner, "Direct numerical and large eddy simulations in nuclear applications," *International Journal of Heat and Fluid Flow* 20, pp. 222-240 (1999).

[36] L.W. Hu and M. S. Kazimi, "LES benchmark study of high cycle temperature fluctuations caused by thermal striping in a mixing tee," *International Journal of Heat and Fluid Flow* 27 (*1*), pp. 54-64 (2006).

[37] T. Lu, D. Attinger and S. M. Liu, "Large-eddy simulations of velocity and temperature fluctuations in hot and cold fluids mixing in a tee junction with an upstream straight or elbow main pipe," *Nuclear Engineering and Design* 263, pp. 32-41 (2013).

[38] T. Lu, S. M. Liu and D. Attinger, "Large-eddy simulations of structure effects of an upstream elbow main pipe on hot and cold fluids mixing in a vertical tee junction," *Annals of Nuclear Energy* 60, pp. 420-431 (2013).

[39] A. K. Kuczaj and E. M. J. Komen, "An Assessment of Large-eddy Simulation Toward Thermal Fatigue Prediction," *Nuclear Technology* 170, (2010).

[40] J. Galpin and J. P. Simoneau, "Large Eddy Simulation of a thermal mixing tee in order to assess the thermal fatigue," *International Journal of Heat and Fluid Flow* 32 (*3*), pp. 539-545 (2011).

[41] T. Ming and J. Zhao, "Large-eddy simulation of thermal fatigue in a mixing tee," *International Journal of Heat and Fluid Flow* 37, pp. 93-108 (2012).

[42] S. Kuhn, O. Braillard, B. Ničeno and H.-M. Prasser, "Computational study of conjugate heat transfer in T-junctions," *Nuclear Engineering and Design* 240 (*6*), pp. 1548-1557 (2010).

[43] D. Klören and E. Laurien, "Coupled Large-Eddy Simulation of Thermal Mixing in a T-Junction," In: Proc. of the 14th International Topical Meeting on Nuclear Reactor Thermal Hydraulics (NURETH-14), Toronto, Ontario, Canada, (2011).

[44] CEA, http://www-cast3m.cea.fr/, Accessed: 27.10.2014.

[45] B. L. Smith, J. H. Mahaffy and K. Angele, "A CFD Benchmarking Exercise Based on Flow Mixing in a T-Junction," In: Proc. of the 14th International Topical Meeting on Nuclear Reactor Thermal Hydraulics (NURETH-14), Toronto, Ontario, Canada, (2011).

[46] Y. Odemark, T. M. Green, K. Angele, J. Westin, F. Alavyoon and S. Lundström, "High-cycle Thermal Fatigue in Mixing Tees: New Large-Eddy Simulations Validated Against New Data Obtained by PIV in the Vattenfall Experiment," In: Proc. of the 17th International Conference on Nuclear Engineering (ICONE17), Brussels, Belgium, (2009).

[47] T. Frank, C. Lifante, H. M. Prasser and F. Menter, "Simulation of turbulent and thermal mixing in T-junctions using URANS and scale-resolving turbulence models in ANSYS CFX," *Nuclear Engineering and Design* 240 (*9*), pp. 2313-2328 (2010).

[48] K. El Omari and Y. Le Guer. 2010. Alternate rotating walls for thermal chaotic mixing. *International Journal of Heat and Mass Transfer*, 53(1-3):123–134.

[49] NUGENIA, http://s538600174.onlinehome.fr/nugenia/portfolio/mother-project/, Accessed: 27.10.2014.

[50] M. Kuschewski, R. Kulenovic and E. Laurien, "Experimental Setup for the Investigation of Fluid-Structure Interactions in a T-junction," In: Proc. of the 14th International Topical Meeting on Nuclear Reactor Thermal Hydraulics (NURETH-14), Toronto, Ontario, Canada, (2011). 151

[51] M. Kuschewski, R. Kulenovic and E. Laurien, "Experimental setup for the investigation of fluid–structure interactions in a T-junction," *Nuclear Engineering and Design* 264, pp. 223-230 (2013).

[52] D. Kloeren, M. Kuschewski and E. Laurien, "Large-Eddy Simulations of Stratified Flows in Pipe Configurations Influenced by a Weld Seam," In: Proc. of the CFD for Nuclear Reactor Safety Applications (CFD4NRS-4) Workshop, Daejeon, Korea, (2012). 153

[53] K. Selvam, R. Kulenovic and E. Laurien, "Large Eddy Simulation of Fluid Mixing at High Temperature Differences in a T-junction Piping System," In: Proc. of the International Congress on Advances in Nuclear Power Plants (ICAPP '14), Charlotte, U.S.A., (2014).

[54] M. Tanaka, H. Ohshima and H. Monji, "Thermal Mixing in T-Junction Piping System Related to High-Cycle Thermal Fatigue in Structure," *Journal of Nuclear Science and Technology* 47 (*9*), pp. 790–801 (2010).

[55] M. Igarashi, M. Tanaka, N. Kimura and H. Kamide, "Study on Fluid Mixing Phenomena for Evaluation of Thermal Striping in a Mixing Tee," In: Proc. of the 10th International Topical Meeting on Nuclear Reactor Thermal Hydraulics (NURETH-10), Seoul, Korea, (2003).

[56] A. Nakamura, H. Ikeda, S. Qian, M. Tanaka and N. Kasahara, "Benchmark Simulation of Temperature Fluctuation Using CFD for the Evaluation of the Thermal Load in a T-junction Pipe," In: Proc. of the The Seventh Korea-Japan Symposium on Nuclear Thermal Hydraulics and Safety (NTHAS7), Chuncheon, Korea, (2010).

[57] M. Kamaya and A. Nakamura, "Thermal stress analysis for fatigue damage evaluation at a mixing tee," *Nuclear Engineering and Design* 241 (*8*), pp. 2674-2687 (2011).

[58] H. D. Kweon, J. S. Kim and K. Y. Lee, "Fatigue design of nuclear class 1 piping considering thermal stratification," *Nuclear Engineering and Design* 238 (*6*), pp. 1265-1274 (2008).

[59] IAEA, "Assessment and Management of Ageing of Major Nuclear Power Plant Components Important to Safety: Primary piping in PWRs," IAEA IAEA-TECDOC-1361, Vienna, Austria, 2003.

[60] E. Paffumi, K. F. Nilsson and N. G. Taylor, "Thermal frequency response studies of a hollow cylinder subject to loads of different amplitude and shape," *Nuclear Engineering and Design* 240 (*6*), pp. 1355-1362 (2010).

[61] K. J. metzner, U. Wilke "European THERFAT project-thermal fatigue evaluation of piping system "Tee"-connections," Nuclear Engineering and Design, Volume 235, 2005, pp. 473-484

[62] S.T. Jayaraju[1], E.M.J. Komen[1], 1 and E. Baglietto[2] . "Large Eddy Simulations for Thermal Fatigue predictions in a T-Junction: Wall-function or Wall-resolve based les?" [1]*nuclear research & consultancy group, p.o. box 25, 1755 zg petten, the Netherlands,* [2]*cd-adapco, nuclear applications, 60 broadhollow rd, melville, new york.*

[63] M. Robert, "Corkscrew Flow Pattern In Piping System Dead Legs," In: Proc. of the 5th International Topical Meeting on Nuclear Reactor Thermal Hydraulics (NURETH-5) Salt Lake City, UT, USA, (1992).

[64] Zboray R., Manera A., Niceno B., Prasser H.-M.: "Investigations on Mixing Phenomena in Single-phase Flows in a T-Junction Geometry", The 12th Int. Topical Meeting on Nuclear Reactor Thermal Hydraulics (NURETH-12), Sheraton Station Square, Pittsburgh, Pennsylvania, U.S.A. September 30-October 4, 2007, Paper No. 71, pp. 1-20.

[65] Y. Utanohara, A. Nakamura and K. Miyoshi, "Numerical Simulation of Long-period Fluid Temperature Fluctuation Downstream from a Mixing Tee," In: Proc. of the 10th International Topical Meeting on Nuclear Thermal-Hydraulics, Operation and Safety (NUTHOS-10), Okinawa, Japan, (2014).

[66] Lifetime and ageing management of nuclear power plants: a brief overview of some light water reactor component ageing degradation problems and ways of mitigation. *International journal of pressure vessels and piping*, 66(1), 17-25.

[67] Saito, M., & Sawada, T. (2002). Advanced Nuclear Energy Systems Toward Zero Release of Radioactive Wastes, *Gulf Professional Publishing* (Vol. 40, No. 3-4).

[68] Roos, E., Herter, K. H., & Schuler, X. (2006). Lifetime management for mechanical systems, structures and components in nuclear power plants. *International journal of pressure vessels and piping*, 83(10), 756-766.

[69] Manera, A., Prasser, H. M., Lechner, R., & Frank, T. (2009). Toward the prediction of temperature fluctuations by means of steady RANS for the estimation of thermal 89 fatigue. In Proc. *13th International Topical Meeting* on Nuclear Reactor Thermal Hydraulics (NURETH-13) (Vol. 27).

[70] Hannink, M.H.C., Kuczaj, A. K., Blom, F. J. Church, J. M. and Komen, E. M. J. "A coupled CFD-FEM strategy to predict thermal fatigue in mixing tees of nuclear reactors".

[71] Jhung, M. J. [74(2013). Assessment of Thermal Fatigue in Mixing Tee by Fluid Structure Interaction Analysis. *Nuclear Engineering and Technology*, 45(1), 99-106.

[72] S. Taheri, L. Vincent and J.-C. Le-roux, "A new model for fatigue damage accumulation of austenitic stainless steel under variable amplitude loading," *Procedia Engineering* 66, pp. 575-586 (2013).

[73] M. Dahlberg, K.-F. Nilsson, et al.. Development of a European procedure for assessmentof high cycle thermal fatigue in light water reactors: final report of the NESC-thermal fatigue project. Technical Report EUR 22763 EN, Joint Research Centre, TheNetherlands, 2007.

[74] E. Paffumi, V. Radu and K. F. Nilsson, "Thermal fatigue striping damage assessment from simple screening criterion to spectrum loading approach," *International Journal of Fatig*

[75] V. Radu, E. Paffumi, N. Taylor and K.-F. Nilsson, "Assessment of thermal fatigue crack growth in the high cycle domain under sinusoidal thermal loading: An application – Civaux 1 case," 2007.

[76] J.H. Konrad. 1977. *An Experimental Investigation of Mixing in Two-dimensional Turbulent Shear Flows with Applications to Diffusion-limited Chemical Reactions*. PhD thesis, California Institute of Technology.

[77] CD-adapco (2008). Computational Fluid Dynamics (CFD) Basics. *Americas Agency Training Document.*

[78] Celik, I. B., Introductory Turbulence Modeling, West Virginia University, Department of Mechanical and Aerospace Engineering, Morgantown, 1999, pages

[79] Davidson, L., An Introduction to Turbulence Models, Chalmers University of Technology, Department of Thermo and Fluid Dynamics, Goteborg, September 6 2016, pages

[80] Tam, C. K. W., & Ganesan, A., Modified k-ε Turbulence Model for Calculating Hot Jet Mean Flows and Noise, AIAA Journal, 42(1), January 2004, pages 26–34.

[81] Mohammadi, B., Pironneau, O., Analysis of the K-Epsilon Turbulence Model, Research in Applied Mathematics, 1994, pages .

[82] Cable, M., An Evaluation of Turbulence Models for the Numerical Study of Forced and Natural Convective Flow in Atria, Department of Mechanical and Materials Engineering, Queen's University, Kingston, May 2009, pages

[83] Bardina, J. E., Huang, P. G.,Coakley, T. J., Turbulence Modeling Validation, Testing, and Development, Nasa Technical Memorandum, Issue: 110446, 1997, pages 8–20.

[84] Menter, F. R., Improved Two-Equation Turbulence Models for Aerodynamic Flows, NASA Technical Memorandum, Issue: 103975, October 1992, pages 1-2.

[85] Karim, M, Rahman,M,Alim,A, I. S., Two-Equation Eddy-Viscosity Turbulence Model for Computing Drag Force on Axisymmetric Underwater Vehicle Hull Form, WMTC, 2009, pages 1–7.

[86] Keshmiri, A., Analysis of Gas- Cooled Reactor, The Univeristy of Manchester, School of Mechanical, Aerospace and Civil Engineering, Manchester, July 2010, pages

APPENDIX I

Properties and Fatigue Limit of the Piping Material Used

Description: 1.4550/AISI 347 is an Austentic Chromium-Nickel Stainless Steel with titanium and niobium addition.

Standards	Material No.	EN Designation	AISI/SAE	UNS
0545245554	1.4550	X6CrNNb18-10	347	S34700

Special Properties: Good resistance to intergranular corrosion

Suitable Welding Filler Material: 1.4316, 1.4551, 1.4576

Chemical Composition

Carbon	0.08 max
Chromium	17 – 19
Iron	Balance
Manganese	2 max
Nickel	9 – 13
Niobium	Min:5 x C
Phosphorus	0.045 max
Silicon	1 max
Sulphur	0.03 max

Mechanical Properties

Elongation at break (%)	<60
Hardness - Brinell	160-190
Izod impact strength (J m^{-1})	20-136
Modulus of elasticity (GPa)	190-210
Tensile strength (MPa)	520-1100
0.2% Yield Strength R_n (N/mm^2)	205

Physical/Thermal properties

Density (g cm^{-3})	7.93
Melting point (C)	1400-1425
Specific Heat Capacity (J/kg K)	500
Electrical Resistivity (Ohm mm^2 /m)	0.73
Coefficient of thermal expansion @20-100C ($x10^{-6}$ K^{-1})	16-18
Maximum use temperature in air (C)	800
Thermal conductivity @100C (W m^{-1} K^{-1})	16.3

APPENDIX II

Profile/Plots of Parameters in the Flow Channel

Profile of Temperature Distribution at 2D, 3D, 5D, 6D

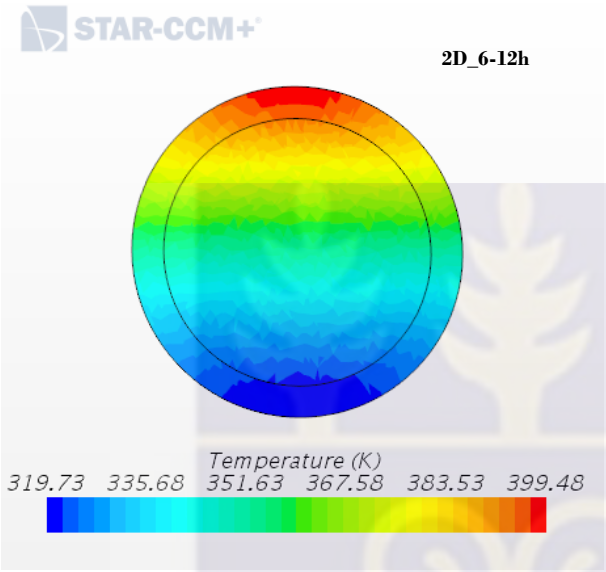

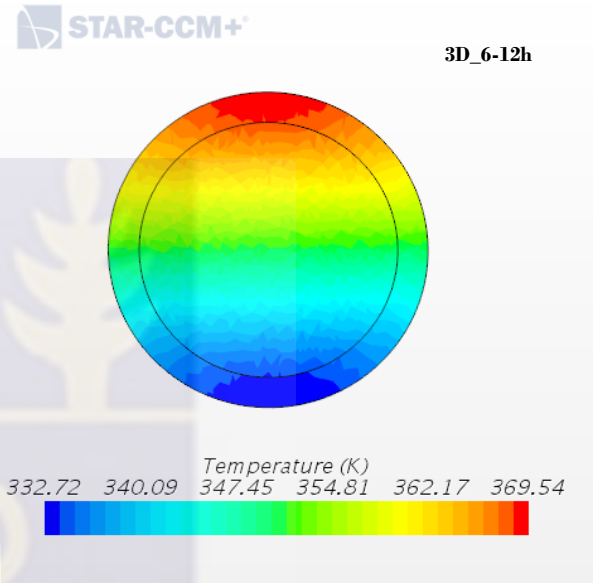

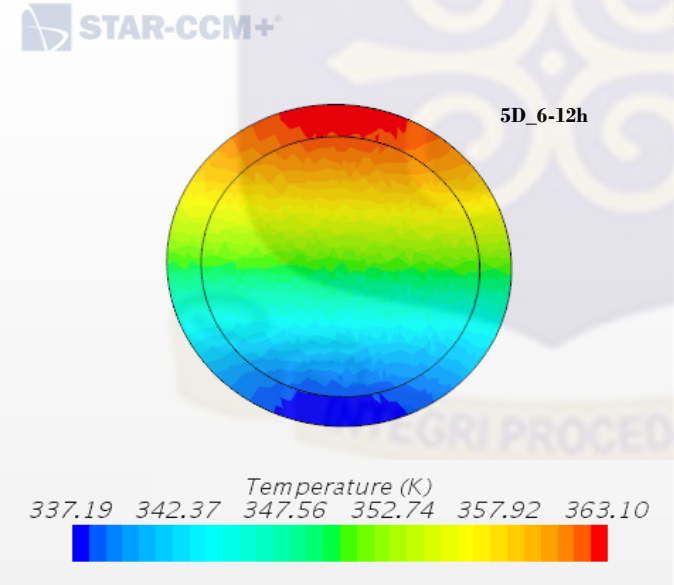

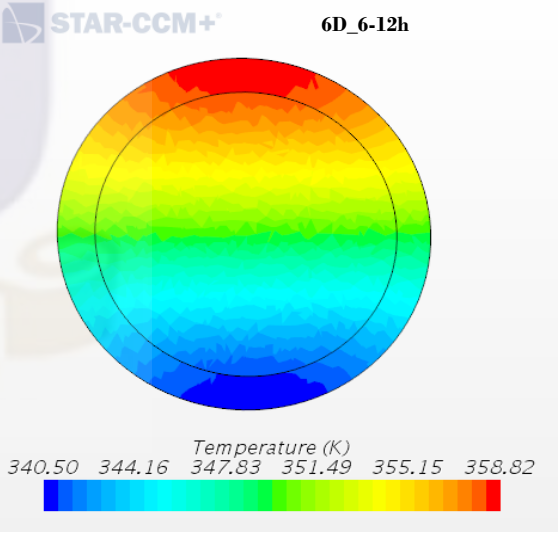

Plot of Temperature Distribution at 1D to 7D

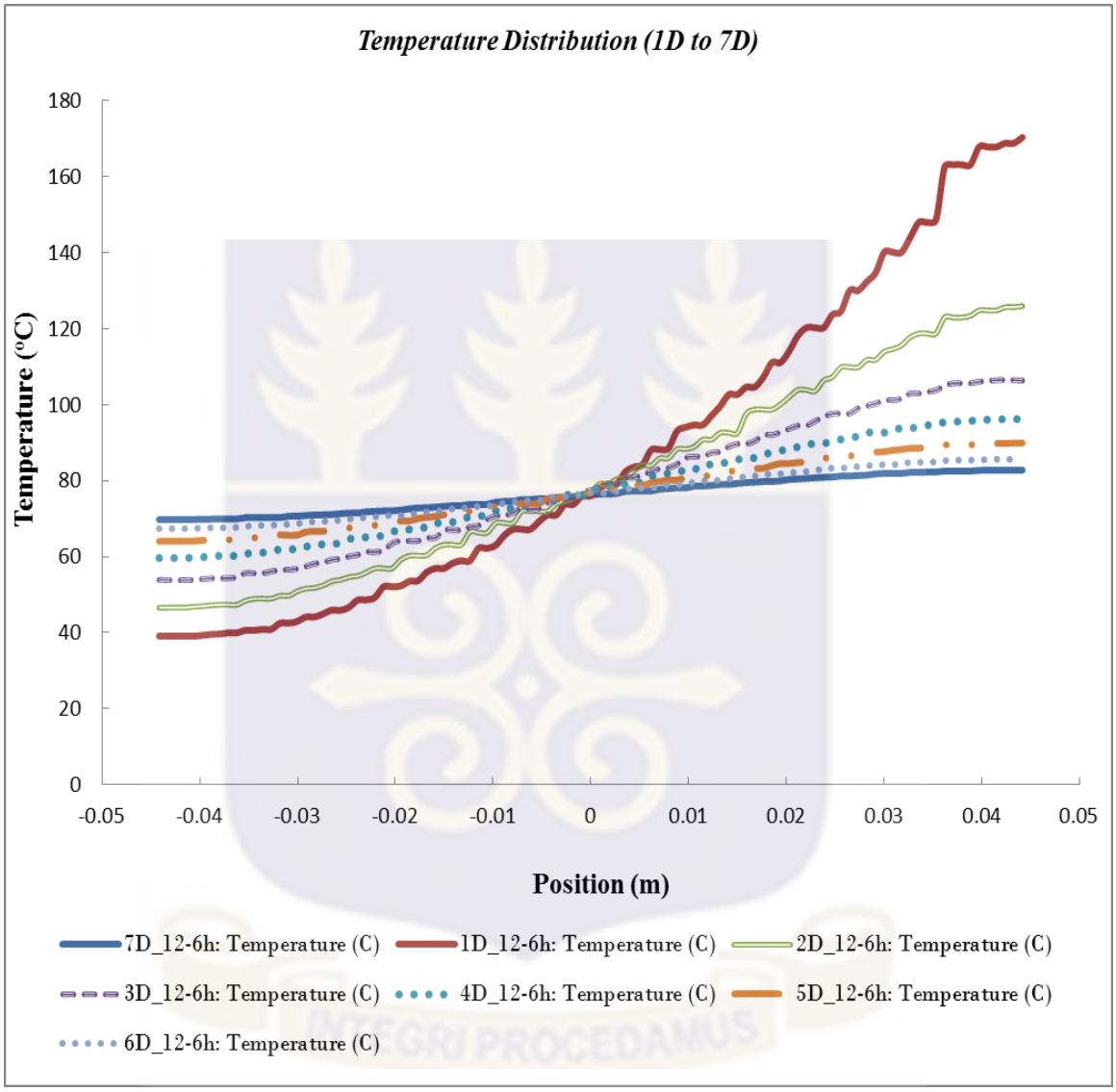

Velocity Profile at 2D, 3D, 5D, 6D

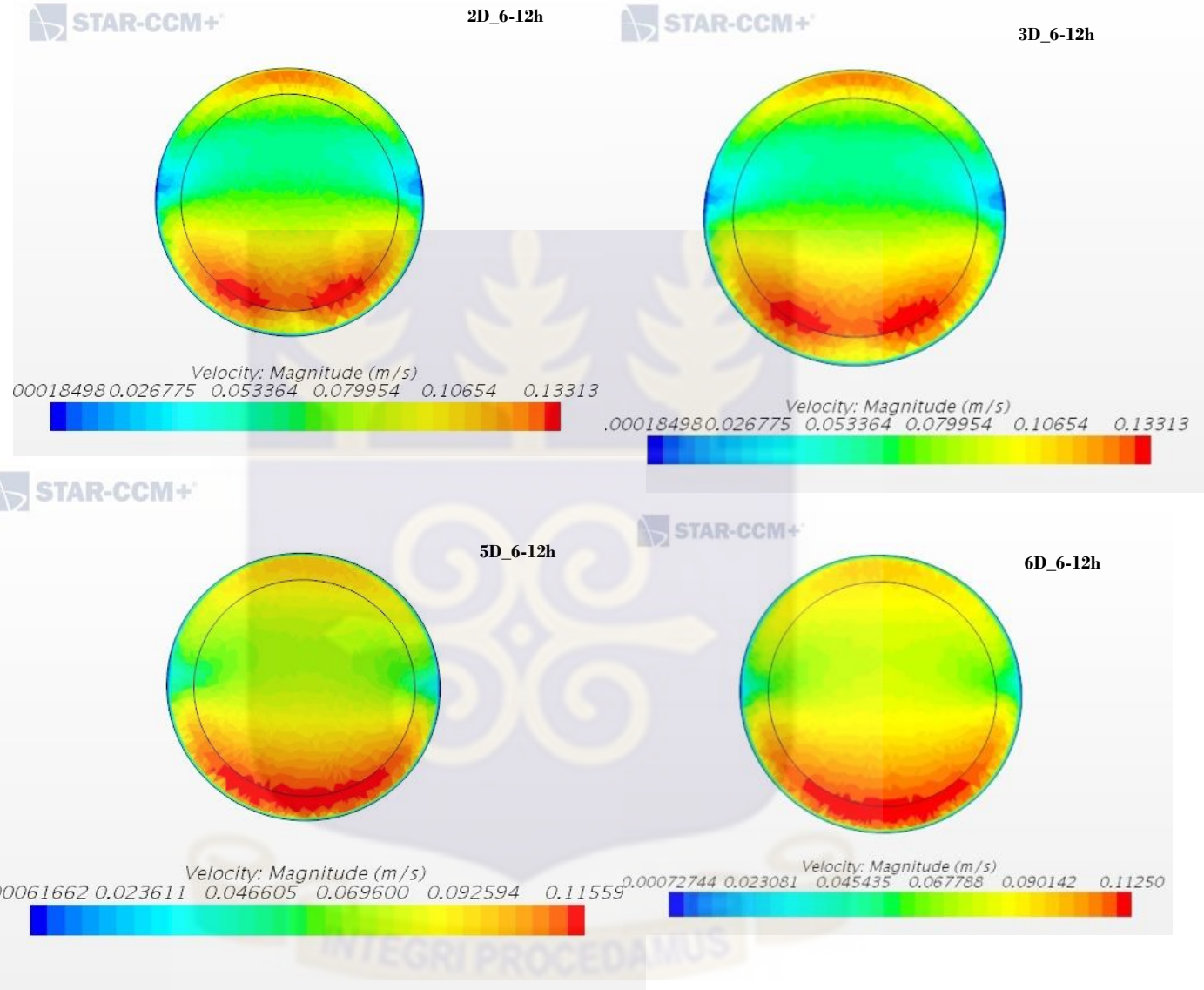

Plot of Velocity Distribution at 1D to 7D

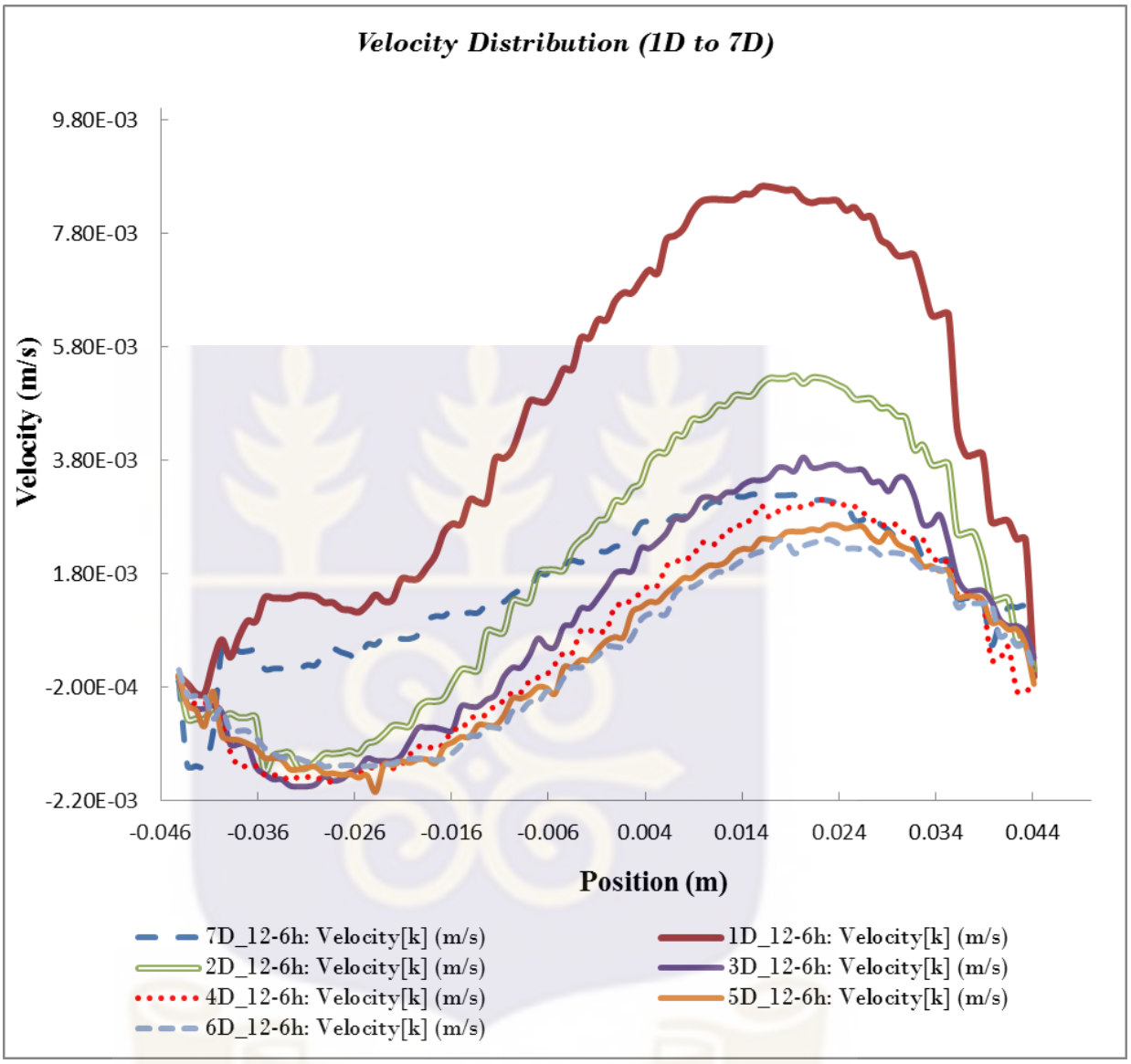

Density Profile at 2D, 3D, 5D, 6D

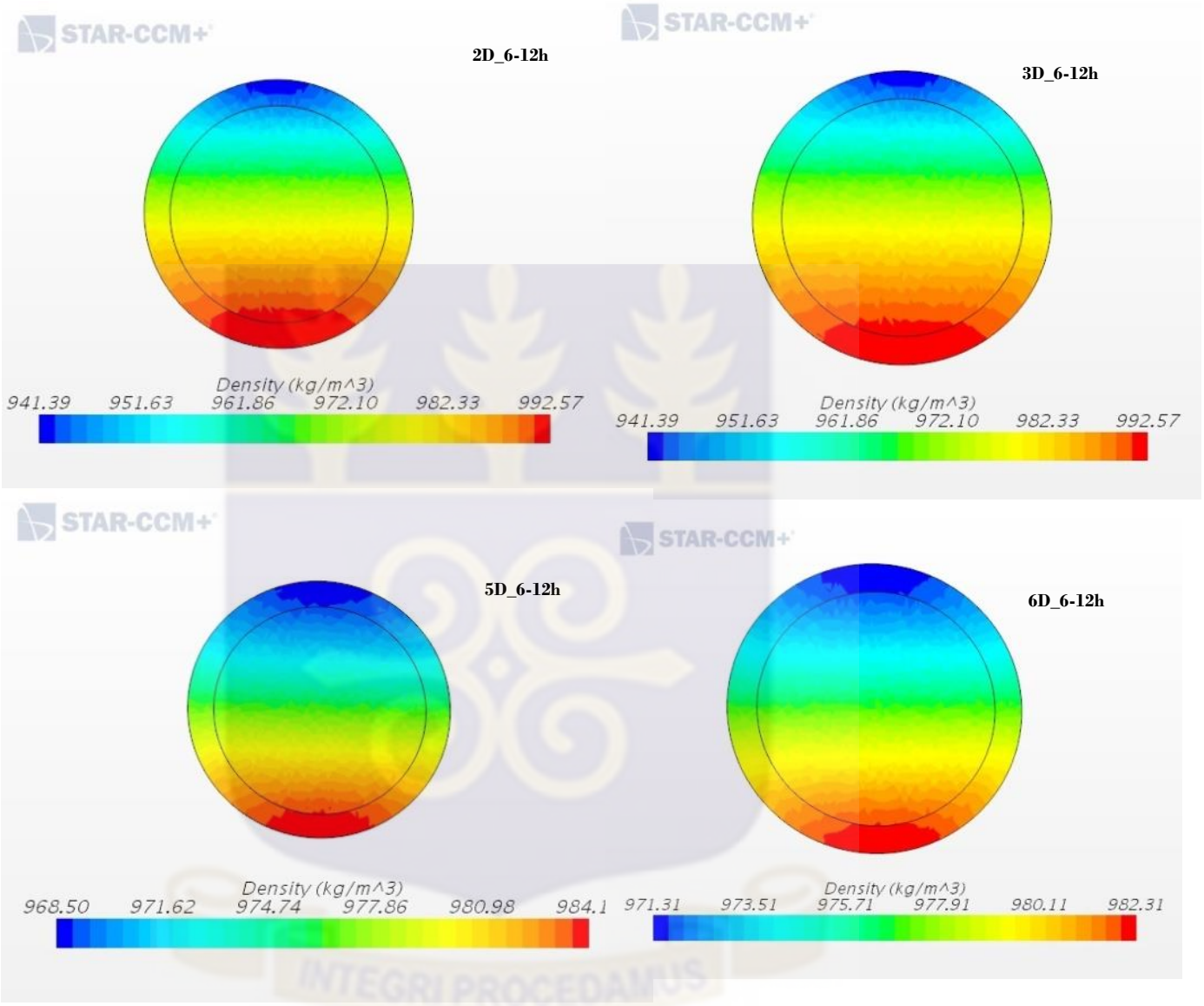

Plot of Density Distribution at 1D to 7D

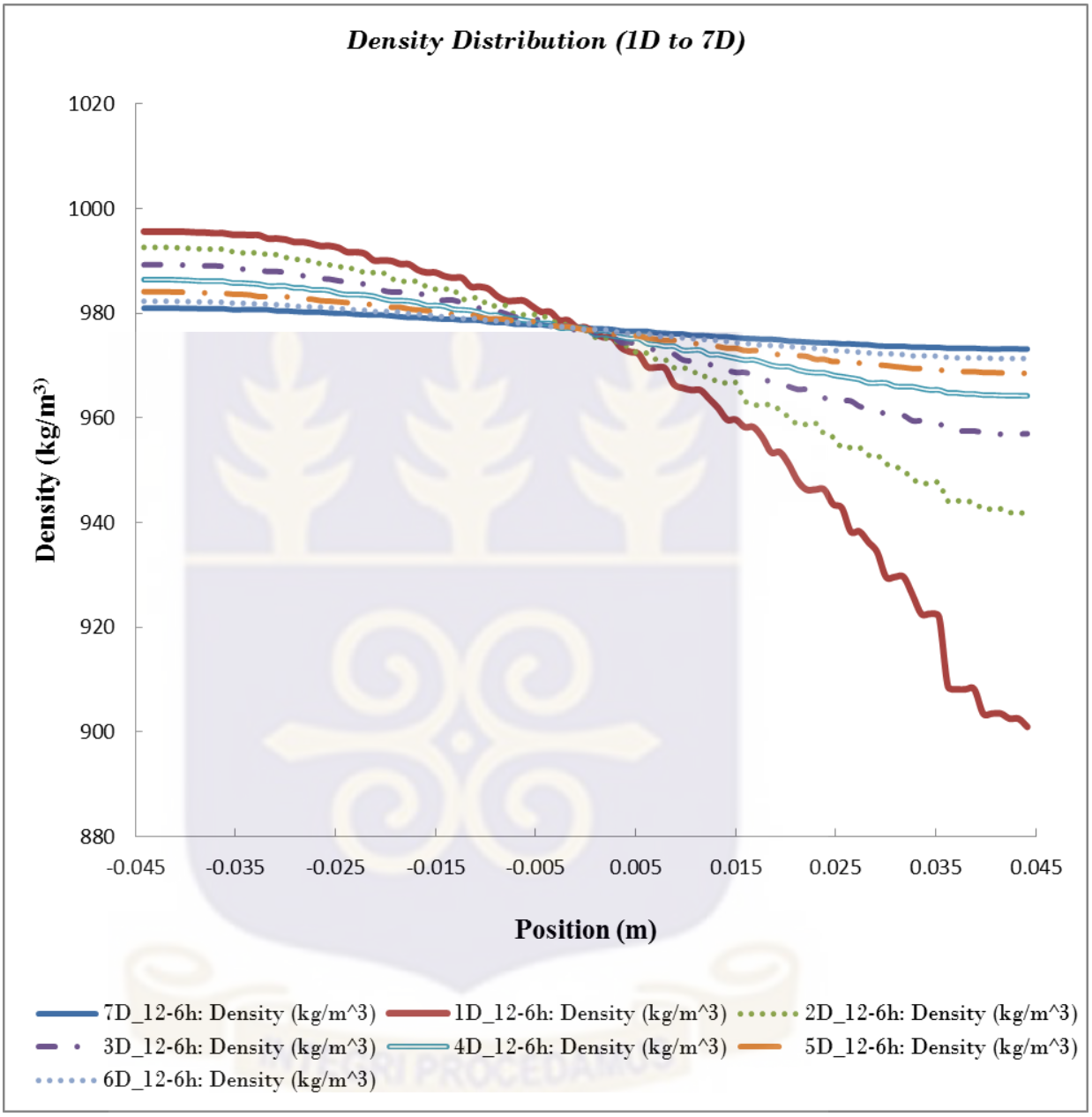

Thermal Conductivity at 2D, 3D, 5D, 6D

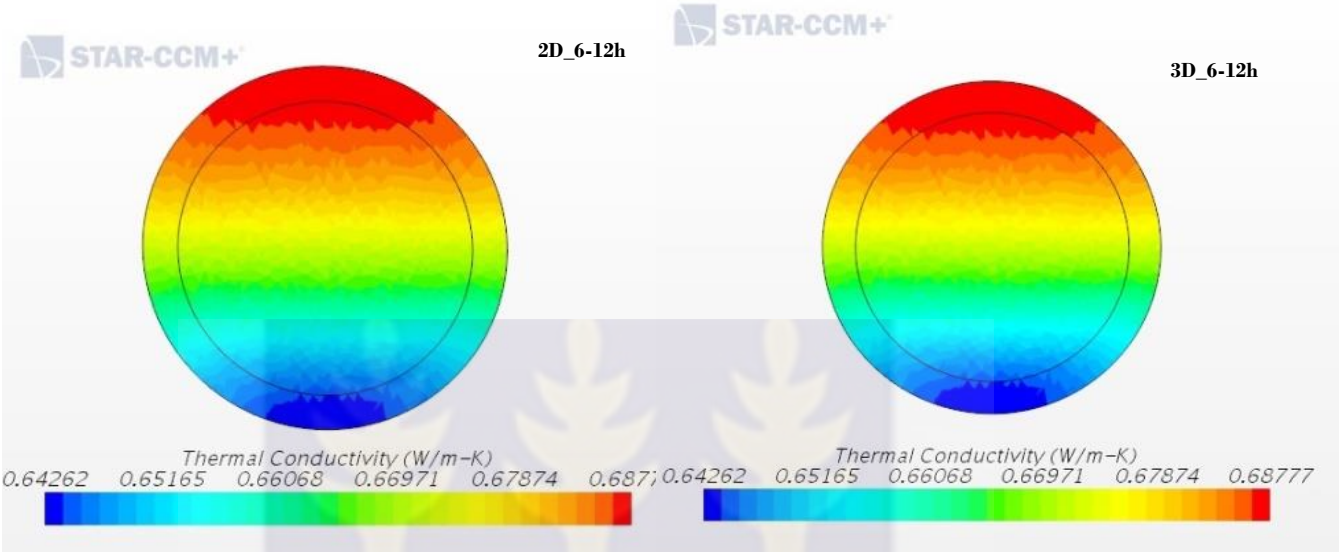

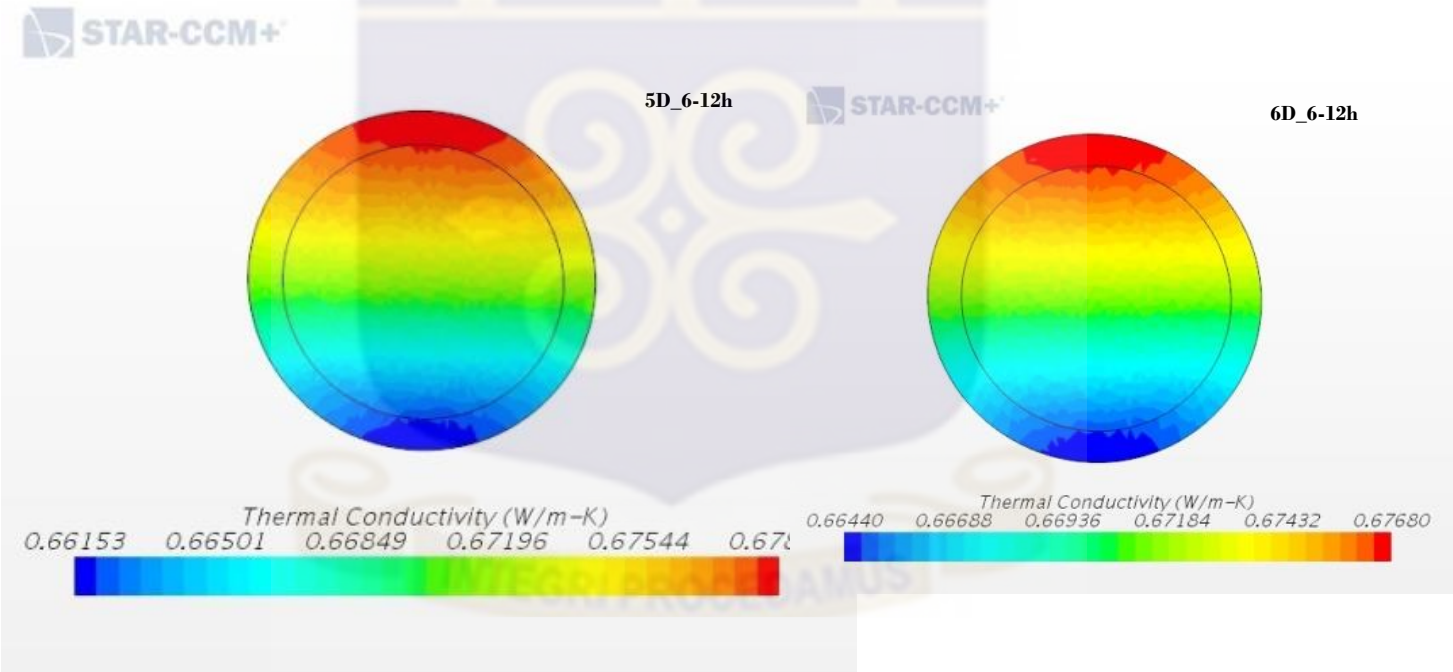

Plot of Thermal Conductivity at 1D to 7D

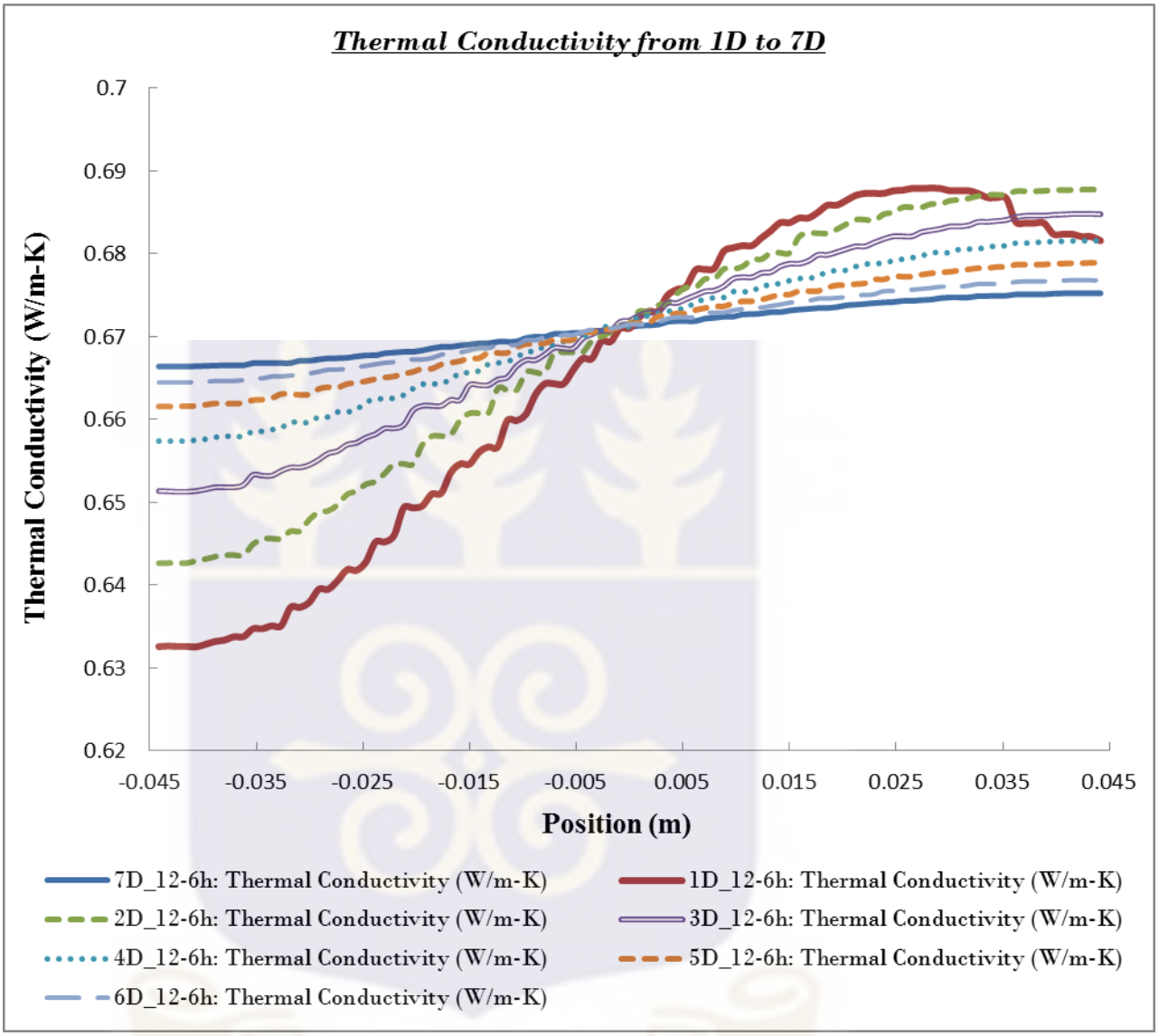

Turbulent Kinetic Energy at 2D,3D, 5D, 6D

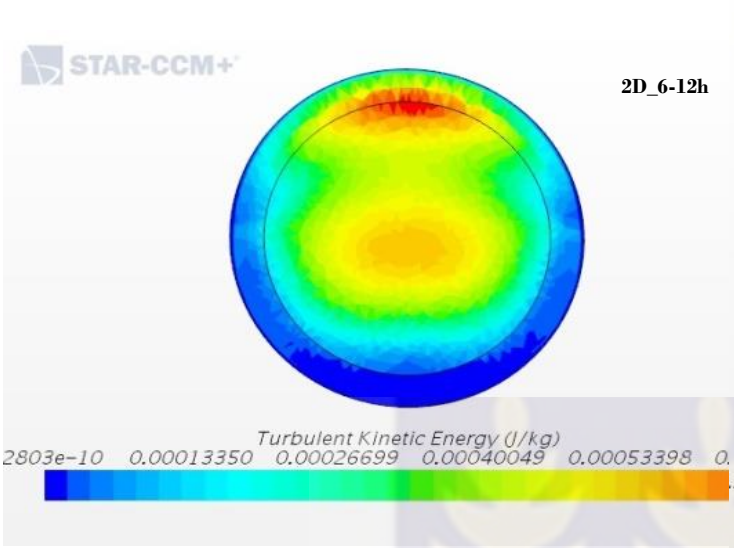

2D_6-12h

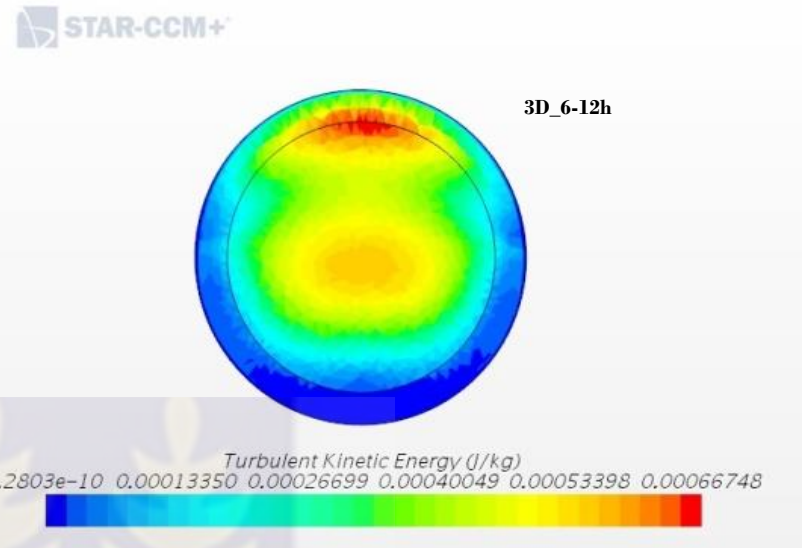

3D_6-12h

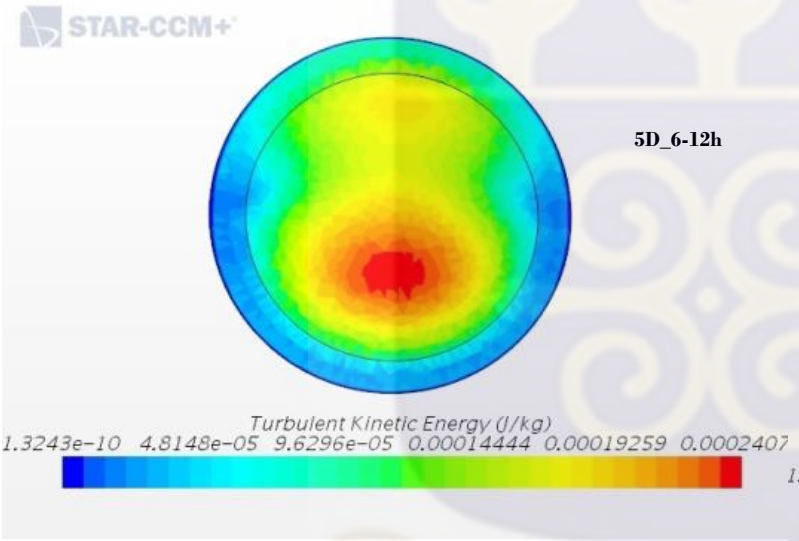

5D_6-12h

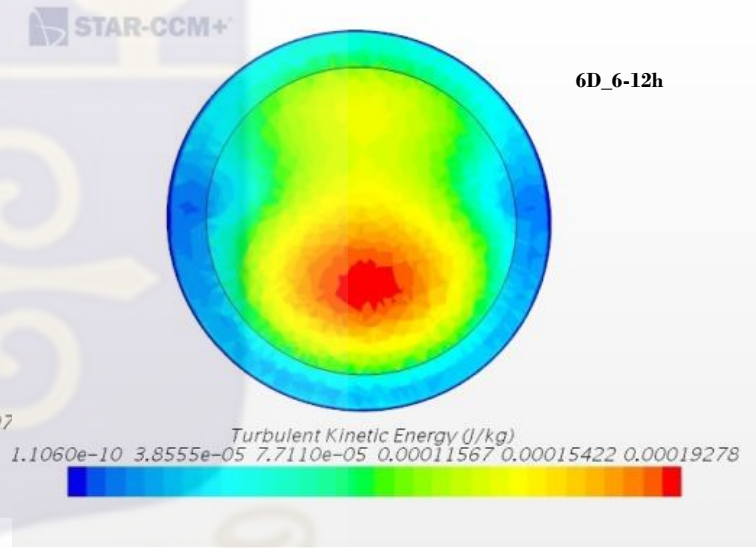

6D_6-12h

Plot of Turbulent Kinetic Energy at 2D, 3D, 5D, 6D

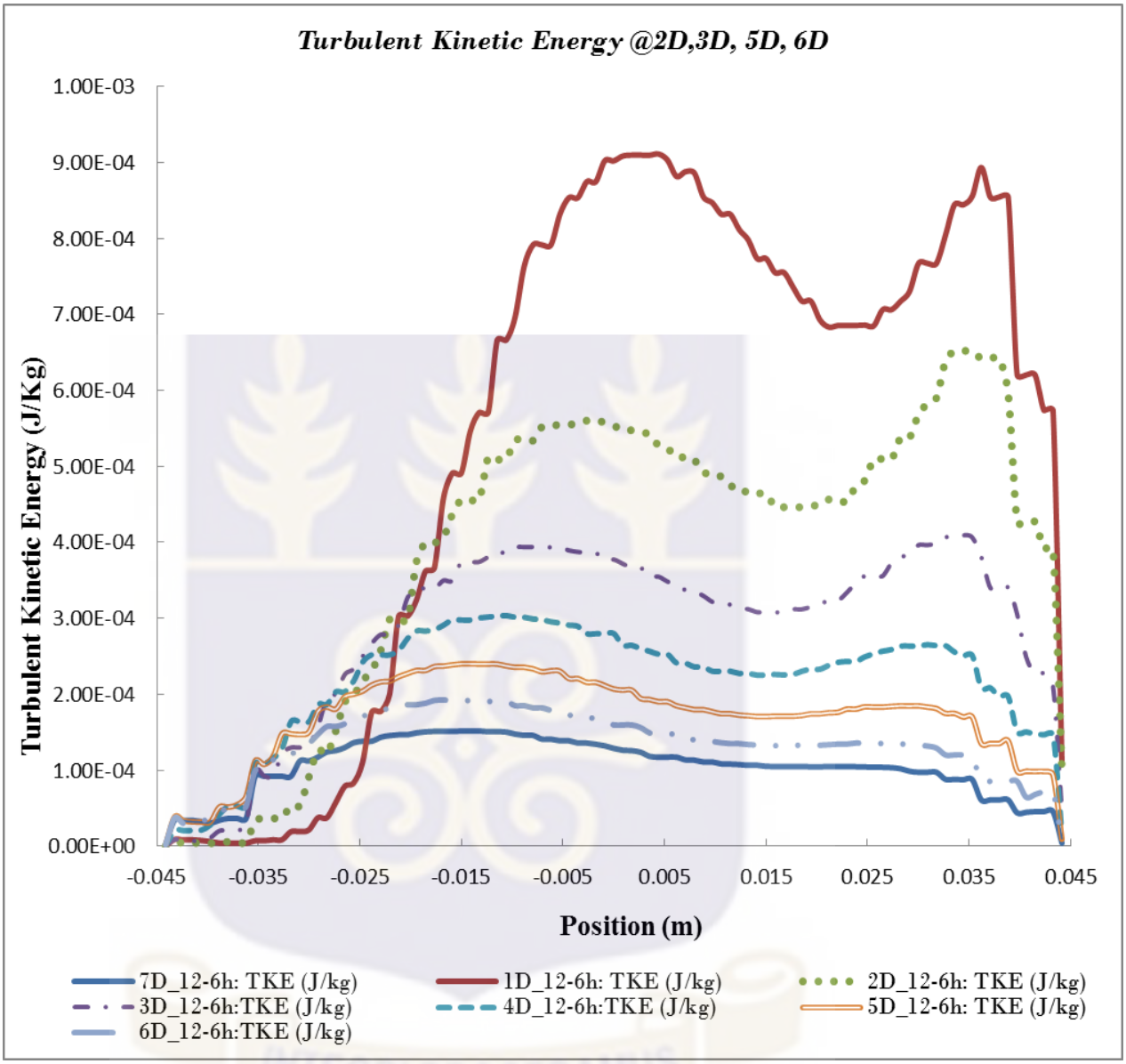

APPENDIX III

Temperature Distribution within Upper Structure

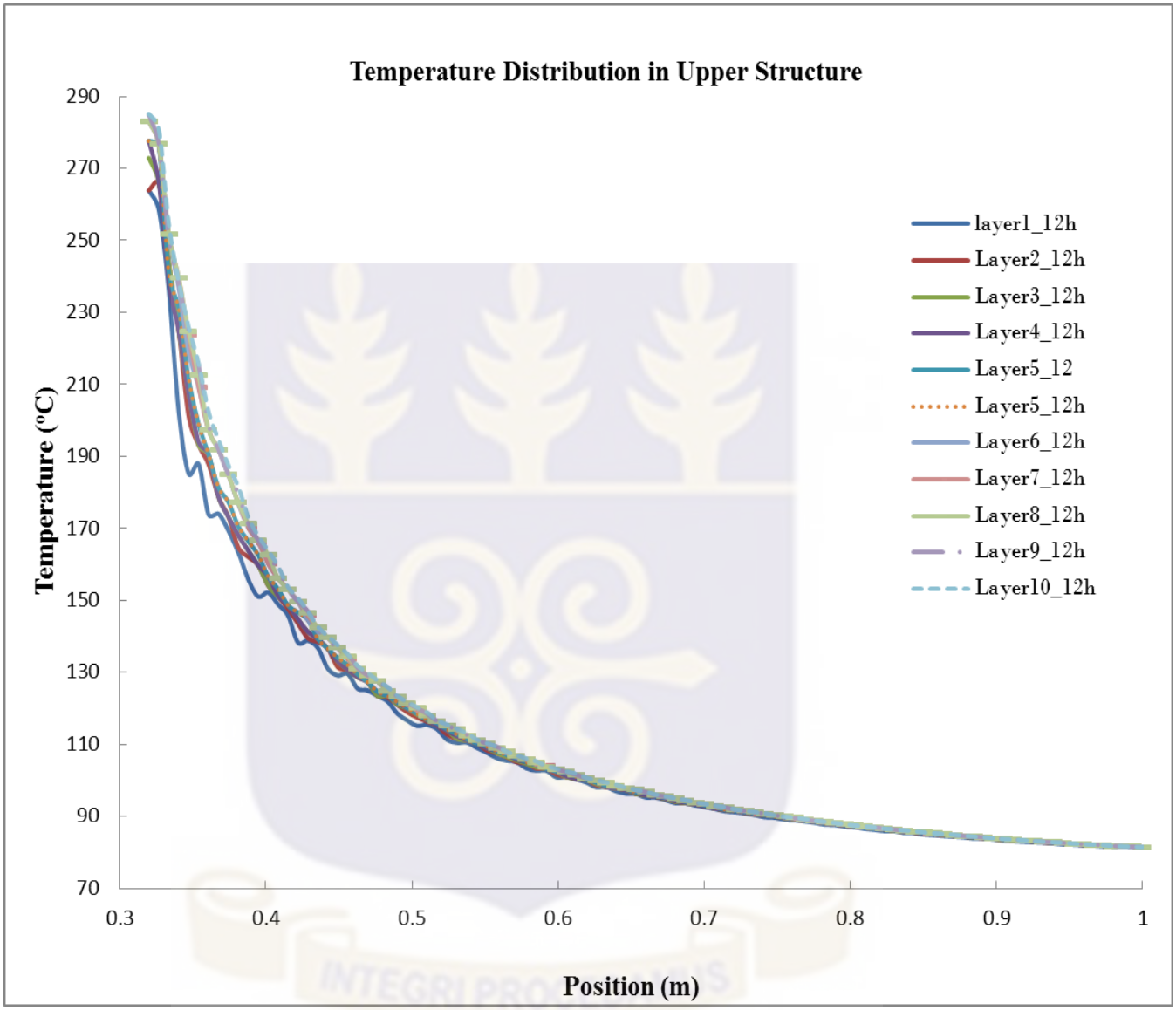

APPENDIX IV

Experimental Result